Three-dimensional printing of tablets – a potential approach to on-clinical-site extemporaneous formulation and personalized medicine

Inauguraldissertation

zur

Erlangung der Würde eines Doktors der Philosophie

vorgelegt der

Philosophisch-Naturwissenschaftlichen Fakultät

der Universität Basel

von

Marina Fanous

Basel, 2021

Genehmigt von der Philosophisch-Naturwissenschaftlichen Fakultät

Auf Auftrag von

Erstbetreuer	Prof. Dr. Georgios Imanidis
Zweitbetreuerin	Prof. Dr. Henriette Meyer zu Schwabedissen
Externer Experte	Prof. Dr. Abdul Basit

Basel, den 02. März 2021

Prof. Dr. Marcel Mayor

Dekan

The whole difference between construction and creation is exactly this: that a thing constructed can only be loved after it is constructed; but a thing created is loved before it exists.

Charles Dickens

Abstract

The oral route is the most common form of drug administration, being a safe and convenient, particularly for solid oral dosage forms. Current large-scale manufacturing techniques mostly result in fixed dose units and allow a limited choice of dosage strengths. In some cases, there is a need for dosage strength personalization, which include Narrow Therapeutic Index (NTI) medicines or concomitant drugs with pharmacodynamic/pharmacokinetic drug–drug interactions, pharmacogenetic variability of enzymes or transporters, as well as special populations including older adults, children and patients with renal /hepatic impairment. Tailoring the dose beyond the 1-3 available marketed strengths to an individual need arising from the patient's age, genetics, disease severity, concomitant treatments and other (patho)physiological factors may improve safety and/or efficacy of certain medications.

Industrial approaches supporting more flexible dosing include liquid and multiparticulate formulations. Dose individualization could be achieved by compounding or use of other routes of administration (e.g., parenteral), however these lack the same level of quality control as standard manufacturing and are less convenient/acceptable, respectively. An automated manufacturing of individualized solid oral forms of personalized strengths would address this need. Development of pharmaceutical three-dimensional(3D)-printing, which creates automatically the customized tablet in a layer-by-layer fashion based on computer-aided design (CAD) drawings, is one potential way to achieve personalized dosing. Besides individual dosing, 3D-printed tablets could potentially be used for dose escalation during early phase clinical trials, manufacturing on-demand for drugs with a short shelf-life and production of complex multi-drug tablet with different release profiles for personalized regimens. In particular, Fused Deposition Modeling (FDM), which involves extrusion of a thermoplastic filament via narrow heated nozzle and subsequent deposition to prepare solid objects, appears to be beneficial for on clinical site production as no loose powder is involved in the manufacturing process and post-processing can be avoided. Pharmaceutical application of FDM requires FDM-processable filaments manufactured by hot-melt extrusion (HME).

In this PhD work, pharmaceutical application of 3D-printing was explored with focus on Immediate Release (IR) formulation development. IR is the most common release profile required for oral dosage forms and simultaneously a significant challenge derived from intrinsic properties of 3D-printed tablets manufactured via hot-melt processes This work aimed to create options for a unique value proposition derived from FDM- and, alternatively direct powder printing (DPP)-specific aspects, which are fundamentally different from standard manufacturing processes (i.e., decentralized production and customizable tablet structures). Critical quality attributes (CQAs) set as success criteria for 3D-printed tablets included uniformity of content to deliver precision of dose (relative standard deviation of uniformity of content data), weight uniformity (in order to ensure content uniformity), dissolution profiles (targeting rapid release) and physico-chemical stability. Moreover, acceptable appearance and sizes of the developed 3D-printed dosage forms were considered.

One of the key goals of the work included the development of an industrially relevant formulation toolbox suitable for different APIs to develop scalable hot-melt extruded formulations with a range of drug loads. In the first study, combinations of selected excipients were explored to achieve rapid or very rapid dissolution from FDM-printed

tablets with a hydrophilic model compound. The effect of selected water-soluble polymers and hydrophilic dissolution/process aids on FDM-compatibility and, in combination with the effect of infill density, on quality attributes of the formulations (i.e., uniformity of weight and content, dissolution rate,) was studied. Hydroxypropyl-cellulose (HPC) SSL was chosen as hydrophilic polymer and caffeine with a drug load of 5-20% as thermally stable model drug. Poly-(vinyl pyrrolidone-vinyl acetate) copolymer (Kollidon VA64) and poly-(vinyl alcohol-polyethylene glycol) graft copolymer (Kollicoat® IR) were additional water-soluble polymers tested in combination with HPC. Xylitol and polyethylene glycol (PEG) 4000 were evaluated as hydrophilic plasticizers and PEG4000 and maltodextrin as pore formers. Formulations were hot-melt extruded using a scalable twin-screw extruder and 3D-printed into a honeycomb geometry solid dosage forms with high (100%) and low (80%) infill density. PEG4000 in combination with Kollidon VA64 demonstrated superior processability and significantly accelerated release properties of the matrix independently of infill density. Lowering caffeine content improved hot-melt extrusion processability for each formulation but prolonged dissolution. The use of Kollicoat® IR resulted in superior mechanical properties of the manufactured filaments, with easy handling and successful 3D-printing for drug load of 5 to 20%. For many of the investigated formulations, lowering the infill density of 3D-printed tablets yielded faster drug dissolution, consistent with other studies reported in the literature. It was found that the extent of the effect of infill density on the dissolution rate varied depending on formulation. Caffeine was present in the stable crystalline state in 3D-printed tablets. Printing temperature appeared to be critical for drug dissolution in-vitro. To conclude, filaments with the required mechanical properties to be 3D-printable and providing rapid/very rapid release dosage forms using safe materials (approved also for pediatric use) were developed for a hydrophilic model compound.

Formulation knowledge developed in the first study (HPC with or without Kollicoat® IR as matrix formers) was applied to develop FDM-processable filaments for the BCS class IV compound lumefantrine, for which the amorphous solid state is critical for the desired bioavailability. FDM 3D-printing technology was investigated in this study as a tool to achieve amorphous solid dispersion (ASD) at the point-of-care to guarantee bioavailability independently of the solid state of the intermediate product. Amorphous solid dispersions (ASDs) present a common formulation approach for dissolution/bioavailability enhancement of poorly soluble compounds, however the crystalline form of the drug is thermodynamically more stable leading to the risk of recrystallization during the shelf life. FDM-printing, which is a hot-melt technology by definition was explored to deliver ASD for near patient production, which requires shorter stability of the instable ASD system. Small grid-designed tablets with a size of size 9 x 5 x 4 mm, i.e., acceptable for children from 6 years old were successfully 3D-printed, demonstrating good uniformity of weight and assay for both 80% and 100% infill densities. Filaments (intermediate products) contained crystalline lumefantrine when tested two months after manufacturing. Following FDM-printing of the filaments it was possible to (re)create ASD, confirmed by Raman mapping which demonstrated that lumefantrine remained in the fully amorphous state in tablets for at least one month after manufacturing. The demonstrated feasibility to (re)create fully amorphous solid dispersions by FDM-printing on-demand, even when drug was present in crystalline form in the filaments, appears to be especially promising for manufacturing of personalized dosage forms with poorly soluble drugs.

In the third study, Immediate Release FDM-tablets with a poorly-soluble model compound were developed, and key structural parameters for the dissolution were detected using non-destructive accurate morphological analysis based on µCT. Basic butylated methacrylate copolymer (Eudragit® EPO) was used as matrix former as formulation approaches developed in 1st/2nd studies were not sufficient to meet IR criteria for lumefantrine tablets. A combination of a hydrophilic plasticizer xylitol and pore former maltodextrin was added and demonstrated to be a promising formulation approach to achieve fast dissolution rates. Tablets with 5% lumefantrine and corresponding placebo were printed, higher drug load as required for clinically relevant dosage strength however led to increased brittleness incompatible with FDM printing. Filaments with 30% drug loads were fully crystalline. For 5% drug load, highly sensitive Raman mapping technique showed that lumefantrine was present in amorphous state in the 3D-printed tablets as intended, however crystallinity traces in the corresponding filaments were detected. Grid-designed 3D-printed tablets with 65% infill density met rapid release criteria, while 80% and 100% showed slower dissolution. The critical structural characteristics of 3D-printed tablets with non-continuous surface such as accessible porosity, specific surface area by weight and by volume were quantified by an automated µCT- based methodology, and were confirmed to be critical attributes for the dissolution rate. Increase in accessible porosity, total surface area, specific surface area by weight and by volume and decrease in relative density appeared to impact the lumefantrine dissolution rate, whereas increase in closed pores volume did not increase the dissolution rate.

Although FDM-printing could be advantageous for on-clinical-site manufacturing as no powder or solvents are involved in the printing process, a significant challenge is achieving the required mechanical properties of the filament to allow FDM-processing. Hence, in the fourth study, direct powder (3D)-printing (DPP) of tablets was explored, which omitted the filament step to simplify fused deposition modelling (FDM). For direct 3D-printing, powder blends were loaded into a cartridge-like head and were successfully printed with honeycomb design following heating of the extrusion cartridge. This 1-step DPP with incorporation of in-built porosity providing higher surface area served as proof of concept for manufacture of rapid release dosage forms. Water soluble HPC SSL was chosen as matrix former and caffeine as model drug. The effect of PEG4000 as plasticizer/pore former and Kollidon® VA64 as rapidly dissolving polymer on DPP processability and dissolution rate was investigated. Directly 3D-printed tablets with low (30%) infill density showed rapid dissolution independently of the formulation, whereas for high (80%) infill density a combination of PEG4000 and Kollidon VA64 was required to achieve rapid release. The obtained tablets demonstrated good uniformity of percent drug content but had variable weight. Caffeine was present in crystalline state and in the stable polymorph in the tablets. Hence, Direct Powder Printing feasibility for immediate release dosage form manufacture was demonstrated. This technique might create an opportunity to avoid hot-melt extrusion allowing 3D-printing independently of mechanical properties of a filament and potentially prolonging product shelf life by reducing thermal stress.

Moreover, non-FDM-printable Eudragit® EPO-based formulations with 15% and 30% lumefantrine load examined in the second study, were shown to be DPP-printable. Hence, independence on mechanical properties of the filament would allow not only to shorten 3D-printed tablets manufacturing process but to expand formulations space and increase applicability across the portfolio.

In conclusion, this thesis demonstrated that FDM and DPP are promising 3D-printing technologies for flexible and personalized dosing, including IR drug products. Tablets were developed with sizes for both adults and children which met uniformity of content requirements to deliver precision of dose (relative standard deviation of uniformity of content data), weight uniformity, dissolution targets (rapid release) and physico-chemical stability. Morphological studies demonstrated, that for the future development of IR 3D-printed dosage forms, in addition to the suitable polymeric matrix selection, one could reduce closed pores volume, increase the open pore volume, as well as optimize the balance between shape/size and dissolution. The presented approaches of hydrophilic polymeric matrices combined with the CAD-designs, manufactured via FDM or DPP hold much promise in future pharmaceutical development of 3D-printed drug products. However, challenges which still should be overcome include diameter uniformity of filaments, accuracy and reproducibility of deposited mass, differences between designed and actual density, predictable final morphology and filaments' mechanical properties. In addition, there might be a need in a real-time monitoring of flow and viscosity of the molten mass during the 3D-printing process.

Contents

Acknowledgements

I would like to express my deepest gratitude to Prof. Georgios Imanidis for his most inspiring, patient and kindest academic supervision. Georg provided me with a once-in-a-lifetime opportunity to grow in the field of pharmaceutical sciences, and strengthen my scientific curiosity and capabilities.

Great appreciation goes to Dr. Joerg Ogorka, who made my PhD at Novartis Campus possible. Joerg always motivated me to thrive for success, push the restraints and make sure that sky's the limit. I am enormously grateful to amazing Dr. Sarah Gold and Dr. Stefan Hirsch and for their guidance and boost to thrive for perfection. Sarah and Stefan encouraged me to think critically and always ask more questions. Moreover, without them my PhD journey would not be so rich in learning and fun experiences.

Big "Thank You!" goes to my wonderful colleagues in Novartis. It is a shame I cannot have 50-pages space to describe in details great support and positive vibes of: Dr. Volker Moeckel, Hakan Topak, Dr. Malak Bitar, Dr. Adam Sobczuk, Jonny Kinzi, Dr. Erhan Altinoglu, Dr. Despina Solomonidou, Rafael Weiler, Jan Lenz, Janik Pfister, Juliane Mietz, Renate Pflugi, Olga Apryshkina, Dr. Jan Schlomach, Franzi Schneider, Dr. Ana Vidis, Dr. Stéphane Jonat, Dr. Reto Fischer, Dr. Allan MacLean, Manan Vora, Nicola Tulfilli, Maxime Thomas-Schrapp, Matthias Forschner, Patricia Seiler, Mohamed Raoui, Dr. Flavio Fabiani, Dr. Johannes Kluge, Dr. Toni Widmer, Séverine Serreau, Dr. Eric Brech, Allain Moyon, Christophe Nivill, Dr. James Pazdan, Pascal Haener, Mai-Loan Nguyen, David Oruc, Munisa Yuldasheva, Yulia Pogodina, Dr. Ingo Scholten, Dr. Julian Woelcke, Dr. Martin Lubej, Irina McNamara, Paolo De Marco, Dr. Márcia Duarte, Dr. Sarah David, Dr. Dee Stoneman, Dr. Alexei Karpov, Dr. Liz Martinez, Oliver Meier, Dr. Harry Tiemessen, Dr. Justin Wright, Dr. Farshad Ramazani, Dr. Marieta Duvnjak, Dr. Andrew Bryant, Hubert Ferry, Dr. Aaron Bickel, Dr. Ingo Muckenschnabel and Aldana Corizzo. I am endlessly grateful for their valuable time and efforts, as well as creating a truly joyful atmosphere.

Many thanks to Dr. Norbert Rasenack for being a kind and patient operational manager. Norbert enriched my industrial and cultural knowledge, as well as generously supported my scientific endeavors. My gratefulness goes to my cool team members Dr. Jati Langholz, Dr. Artur Reimer, Lorenzo Poloni, Patrick Tritschler, Dr. Fabian Weber, Massimo Moratto, Dr. Stefan Steigmiller, Dr. Hendrik Schneider, Dr. Johannes Nagel and Eric Husted.

Deep gratitude goes to Dr. Maurizio Gullo and Silvain Müller for the fantastic external collaborations and a pleasant company. Many thanks to Swiss AM Network colleagues Hendrik Holsboer, Prof. Hans-Florian Zeilhofer, Prof. Fritz Bircher, Dr. Uli Lösch, Beat Spirgi, Dr. Robert Kenzelmann, Dr. Dorothee Wandel and Prof. John van den Anker. They provided me a unique opportunity to explore real-world needs and dream about the future possibilities.

This PhD journey could not be possible without 24/7 support of my husband Dr. Joseph Fanous. Joe provided me a generous backup whenever my intensive schedule required, wrapping my soul in endless positivity and optimism. I am grateful to our daughters Maya and Rima for reminding me what really matters and keeping things in a proportion. Well, I would like to thank myself too. Doing a PhD is not easy as pie, especially with 2 small children in a foreign country. Way to go, Marina.

Introduction

1.1 Background

Oral drug administration presents the most common form of drug delivery route, being safe, convenient, and affordable in terms of goods and manufacturing [1, 2]. Traditional large-scale manufacturing techniques resulting in fixed dose units, limits possibilities for a personalization of drug dose(s). An option of tailoring release profile or drug combinations in one unit for the benefit of the specific patient belongs to the future.

In some cases (Fig 1.1) there is a need for a dose adjustment to an individual need derived from difference in human genotypes and phenotypes, as well as environment and lifestyles [3, 4]. About 20 years ago one study reported that 75-85% of adverse effects came from inappropriate dosing or dose combination [5]. Precision dosing would be beneficial for the patients belonging to special populations, such as children, patients with renal or hepatic impairment and older adults. Development of appropriate drug formulations for pediatric and older patients is complex in general due to the combined requirements of predictable and safe drug release in the patient together with an acceptable dosage form to ensure safety and adherence [6]. Safety and/or efficacy of certain medications could be improved by tailoring the dose beyond the 1-3 available marketed strengths based on the patient's age, genetics, disease severity, concomitant treatments and other (patho)physiological factors. Recent knowledge gathered with regards to genetic polymorphisms role in modulating activity in drug membrane transport and drug metabolism lead to the recognition of pharmacogenomics importance in dosing adjustments[7]. For instance, polymorphisms in CYP2D6/C19/3A4 enzymes or OATP1B1/NAT2 transporters are critical for the dose tailoring[8]. For medicines with a narrow therapeutic index (NTI) serious therapeutic failures and/or life-threatening adverse drug reactions could appear due to small differences in the drug concentration in the blood, therefore doses of such medications should be carefully adjusted [9]. In addition, the number of doses studied during clinical trials are limited due to mainly practical reasons, and inclusion/exclusion criteria lead to the homogenization of the populations studied [10]. Hence, an outcome is finding a safe and effective dose for the clinical study population as a whole, and not the best dose for an individual.

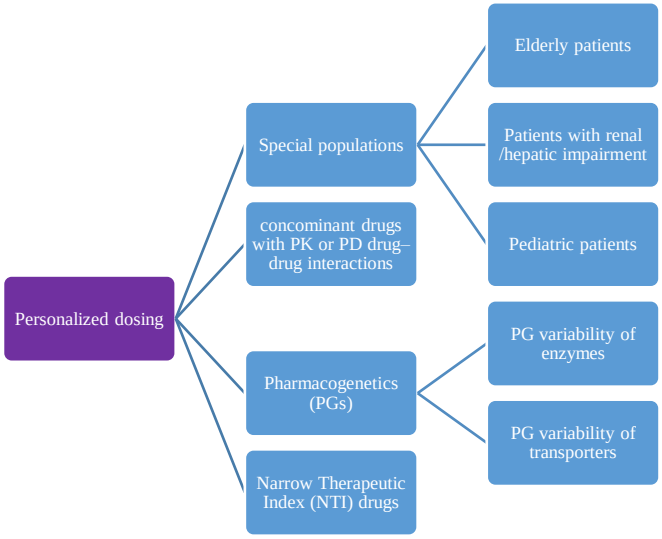

Fig.1.1. Clinical considerations relevant for the personalized dosing need

Industrial approaches supporting more flexible dosing include ready-to-use liquids or powders/granules for reconstitution, and multi-particulates. Currently only a single drug per product is incorporated. For the liquids palatability and dosage precision (i.e. errors with reconstitution carried out by inexperienced caregivers) considered to be major issues [6, 11]. Multi-particulate formulations could potentially allow greater drug product flexibility via combining particles with different drugs and/or with various release profiles [12], however precise dose accuracy is not in-built and dependent on the caregiver and specialized counting/dosing devices. Other approaches for dose individualization include compounding or development of a parenteral formulation, however these lack the same level of quality control as solid oral dosage forms manufacturing and are less convenient. On-clinical-site dose adaptations via crushing or extemporaneous modifications of marketed medications is often unlicensed and lacking dose accuracy, and might change bioavailability, toxicity and stability of the drug product [13]. An automated manufacturing of individualized solid oral forms of personalized strengths would address this need.

Development of pharmaceutical 3D-printing, which creates automatically a customized tablet in a layer-by-layer fashion based on computer-aided design (CAD) drawing, is a promising potential way to achieve personalized dosing [14]. The main approaches to 3D-print an object by consolidating materials into layers include photochemical and thermal transformation, as well as binding/adhesion[15]. Common steps for 3D-printing process include digital design, conversion of this design to the compatible format with 3D-printer, insertion of the starting material, 3D-printing itself and post-processing. Stereolithography (SLA), selective laser/heat sintering, inkjet-powder bed, fused deposition modeling (FDM), direct powder printing/extrusion, liquid inkjet and semi-solids extrusion are 3D-printing technologies explored for pharmaceutical applications[16-18]. Besides individual dosing, 3D-printed tablets present opportunities for on-demand production for drugs with a short shelf-life and production of complex multi-drug tablet with different release profiles for personalized regimens[19] [20], as well as dose escalation during early phase clinical trials and decentralized manufacturing.

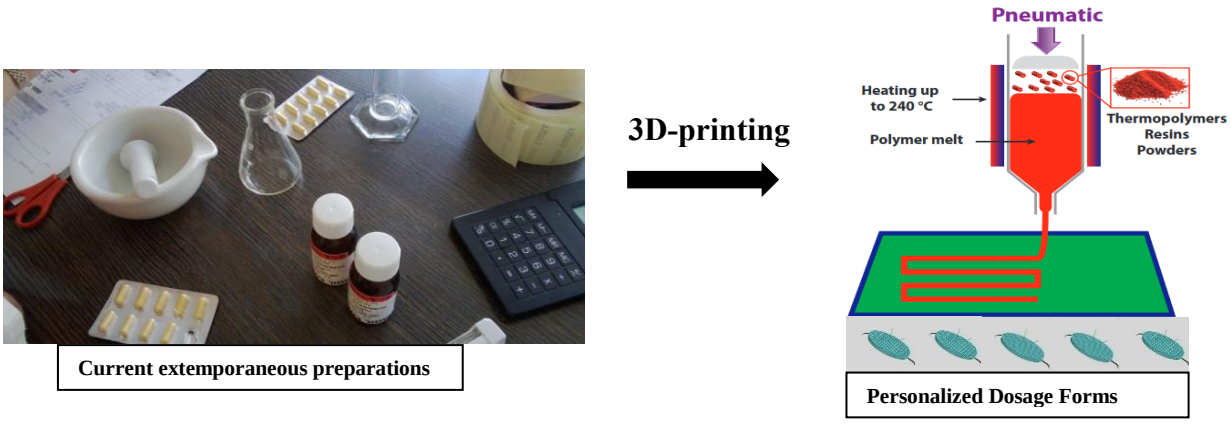

Fig.1.2. 3D-printing concept: digitalization and automatization of hospital extemporaneous preparations (adapted from [18])

Among several techniques available for 3D-printing, fused deposition modelling (FDM) has been a subject of extensive pharmaceutical research, being widely-used and low cost method [21]. In this method, filaments of thermoplastic polymers are extruded via narrow heated nozzle and subsequently deposited in a layer-by-layer manner to prepare models with desired geometry. FDM appears to be advantageous for decentralized production in hospitals and pharmacies as no solvents or loose powder is involved in the manufacturing process and post-processing can be avoided [22]. In addition, the opportunity to tailor dissolution rate within certain limits via tablet design modifications (i.e. changes in infill density and surface modifications) within the same formulation remains a unique attribute of FDM-printing. Fused deposition modelling a hot-melt process by design and could be used to create amorphous solid dispersions (ASDs) with enabling properties for poorly-soluble compounds.

Filaments for pharmaceutical application of FDM are manufactured by hot-melt extrusion (HME) technique [23]. Polymers widely used in HME and tested for FDM filaments manufacturing include various types of poly(vinyl alcohol), polyvinylpyrrolidone, and derivatives of methacrylates or cellulose [24]. Filaments with optimum mechanical properties, melt viscosity, thermal stability, uniformity content and diameter are required for successful FDM-printing. Plasticizers such as triethyl citrate, triacetin, polyethylene glycols and glycerol are added in order to improve melt flow properties of the polymers via the glass transition temperature reduction and potentially increasing the strain bearing ability of the filaments[25]. Miscibility and compatibility of the drug and polymers should be established in order to estimate the risk of possible physicochemical changes on storage.

The real-world growing requirement for personalized medicines including individualized dosing underlines the need in development automated dispensing techniques such as 3D-printing. FDM 3D-printing appears to be a promising technology for personalized medicines production at point-of-care, and was explored during this PhD work. There are several challenges that need to be overcome to make the selected technology a success. In particular, besides dependence on mechanical properties of the filaments, major limitation of 3D-printing with FDM is slow and incomplete drug release from the printed tablets [24]. Slow dissolution rates are inherent to the use of thermoplastic polymers which are characterized by erosion-controlled dissolution mechanisms [22, 26]. Exploring approaches for IR FDM 3D-printed tablets with hydrophilic and poorly-soluble model compounds could add value for future pharmaceutical development/application of 3D-printing for personalized dosage forms. For the wide application of 3D-printing, selecting excipients and tablet design to result in desired release/solid state profile and compliance to the critical quality attributes (CQAs) are required.

As FDM technique is a multi-step process, simplification of FDM paradigm via skipping the filament step might be required to increase chances for the real-world viability of 3D-printing. Manufacturing 3D-printed tablets directly from powder blend could simplify formulation development and omit the dependence on the mechanical properties of the filaments[27] [28]. Direct Powder 3D-printing approaches holds a promise for the future. The challenges to be overcome for Direct Printing include possibly higher drug degradation due to the prolonged heating, powder segregation and limited 3D-printers on the market suitable for this type of manufacturing.

1.2 Objectives

The objective of this PhD work was to explore pharmaceutical application of 3D-printing with focus on near-patient production and Immediate Release formulation development, which is a main release profile required for Oral dosage forms and a significant challenge derived from intrinsic properties of FDM-printed tablets. The work aimed to investigate an option for decentralized production and flexible tablets structure to create unique value proposition derived from FDM-specific aspects fundamentally different from standard manufacturing processes. Critical quality attributes (CQAs) set as success criteria for 3D-printed tablets included uniformity of content to deliver precise dosing (relative standard deviation of uniformity of content data), weight uniformity, dissolution profiles (targeting rapid release) and physico-chemical stability. Moreover, acceptable appearance and sizes of the developed 3D-printed dosage forms were considered.

In the third chapter, combinations of selected excipients were explored to achieve rapid or very rapid dissolution from 3D-printed tablets with a hydrophilic model compound. A toolbox approach potentially suitable for different APIs was applied to develop scalable hot-melt extruded formulations with a range of drug loads. Effect of selected water-soluble polymers and hydrophilic dissolution/process aids was studied on FDM compatibility and quality attributes of the formulations.

In the fourth chapter, expansion of the toolbox approach was pursued via selection of a poorly soluble compound. In addition, the link between programmed computer-aid designs and the achieved printed structure were investigated via computed microtomography. A unique potential of decentralized on-demand tablet manufacturing by FDM-printing was explored to investigate feasibility of (re)creating fully amorphous drug solid state from crystalline filaments.

Fifth chapter was focused on development of Immediate Release FDM-printed tablets with a poorly soluble model compound belonging to BCS (Biopharmaceutical Classification System) class IV. The formulations' toolbox was expanded via investigating of different main matrix former for poorly soluble compounds in order to achieve desired release. Basic butylated methacrylate copolymer was explored as previously developed formulation approaches failed to meet IR criteria for the tested poorly soluble model drug. Morphological characteristics affecting dissolution behavior of dosage forms were precisely quantified, including surface area, open and closed pores volume, as well as specific surface area by weight and by volume. The aim was to create a quantitative understanding of the link between the programmed design and printed structure, and determine critical structural attributes parameters responsible for dissolution rate enhancement. In addition, as the solid state of the API is known to critically influence its *in-vivo* bioavalability, the solid state characteristics (crystalline vs amorphous content) throughout manufacturing process was thoroughly investigated with a highly sensitive technique.

The sixth chapter of this PhD work aimed of to simplify current FDM paradigm by removing the hot-melt extrusion step. This has the advantage to overcome a frequent FDM-processability issue linked to the mechanical properties of filaments comprising Pharmaceutical APIs and excipients, particularly as the drug load of API increases. Feasibility of Direct Powder 3D-printing, which omits the reliance on mechanical properties of filaments as intermediate products, was explored for the production of immediate release dosage forms.

The pediatric population represent one of the main populations which could benefit from personalized dosing enabled by 3D-printing. Hence, only widely accepted pharmaceutical materials including for pediatric use were explored for this work. Moreover, in fourth and fifth chapter tablet designs with dimensions considered acceptable for children were implemented.

2 Theoretical section

2.1 Clinical background

In the recent years, the concept of precision or personalized medicine as the 'right drug to a right patient at the right time' is widely brought to the healthcare stakeholder's discussion[29, 30].Tailored medicinal treatment, which takes into account difference in human genotypes and phenotypes, as well as environment and lifestyles are recognized as factors for better responding to the patient needs for the best response and highest safety margin.

Dose personalization could improve safety and efficacy for some medications [3-5]. Doses of medicines with a narrow therapeutic index (NTI) should be carefully adjusted, as serious therapeutic failures and/or life-threatening adverse drug reactions could appear due to small differences in the drug concentration in the blood [9]. Antiarrhythmics, anticoagulants, antiepileptics, antineoplastics, aminoglycoside antibiotics, and immunosuppressants are typical therapeutic classes containing NTI drugs [10]. Patients in so called 'special populations' (patients with renal or hepatic impairment, pediatrics, older adults and patients taking concomitant medications that cause pharmacokinetic or pharmacodynamic drug–drug interactions) are at increased risk of medication-related harm compared to other groups and would benefit from precision dosing.

In small children pharmacokinetics (PK) are altered relative to adult PK, and the dose is calculated based on a child's age, weight and/or body surface [31]. During a child's growth, the developmental changes in metabolic capacity, distribution sites, gastrointestinal function, acquisition of the renal function and integumentary development occur rapidly, and determine age-related dose personalization [32]. According to FDA, pediatric patients are subdivided into 4 groups: neonates (up to 27 days/old), infants (28 days – 23 months old), children (2-11 years old) and adolescents (12-16 years old) [33]. During the neonatal period, basal acid output and the total volume of gastric secretions are reduced, resulting in the elevated intragastric pH>4 [34] [35]. This might critically affect both the stability and the degree of ionization of a drug, affecting its absorption. Hence, acid-labile compounds (i.e. penicillin G) will demonstrate higher bioavalaibility in neonates than in older infants and children, whilst weak acids (i.e phenobarbital) may require larger doses in the very young to achieve the required plasma levels. Further, intestinal activity of cytochrome P-450 1A1 (CYP1A1) increases with age affecting bioavailability of drugs such as theophylline and a fluoroquinolone antibiotic difloxacin [36]. Apparent hepatic clearance, affected by enzymes maturation (i.e. CYP3A4, CYP2D6, CYP1A2, and UGT287) is the primary PK determinant of difference in age-related doses of many drugs including carbamazepine, phenytoin and captopril[32]. Glomerular filtration rate increases from ~20 ml/min/1.73m^2 for a newborn to ~120 ml/min/1.73m^2 for a 6-year-old child, which requires careful age-related dose adjustment of drugs eliminated mainly by renal clearance (i.e. ranitidine). In addition to PK

aspects, influence of ontogeny on a compounds efficacy/safety with respect to age-dependent differences should be considered on pharmacodynamics (PD). Examples include age-dependent interactions between warfarin and cyclosporine with their receptors [37, 38].

Pharmacokinetics in the elderly is strongly influenced by co-morbidity, multiple-drug use or reduced organ functions. For an older adult the dose is calculated mainly based on the individual state of health (kidney/liver function, multimorbidity/polypharmacy, dementia, etc) [31]. Increased proportion of body fat in the older adults would result in the prolonged half-life of lipid-soluble drugs, including macrolides, benzodiazepines and amiodarone, resulting in prolonged effect and potential for further drug-drug interactions after discontinuation[39]. The opposite tendency could be observed for water-soluble drugs (i.e. β-lactams, lithium), for which the standard dose may be inadequate due to decreased lean body mass and total body volume in the elderly. The liver mass and hepatic blood flow decline with the age[40], which likely explains lower total clearance. Hepatic drug metabolism often shows decline in elimination of CYP450 metabolized drugs and wide interindividual variation. Moreover, the impact of first-pass metabolism decreases in the elderly, resulting in significant increase in bioavailability of high-clearance drugs such as opioids, verapamil, propranolol and metoclopramide[41, 42]. CYP450 enzymes might be often downregulated due to the nonspecific inflammation typical at the very old age, leading to the increased risk of overdose as a function of immune system status of the individual [43].Ageing-related histopathologic changes in kidney include decrease of renal weight, stroma chronic inflammation and fibrosis, a thickening of the intrarenal vascular intima, as well as sclerotic changes of the glomeruli [44]. The obtained decrease in creatinine clearance matches decline in the renal drug elimination. Polypharmacy and malnutrition/proteinuria play an important role in variable drug activity and/or toxicity in the elderly. Moreover, multiple medications lead to difficult prescribing regimens and low compliance in this group of patients. Chronological age is not an optimal criterion for dose personalization, and additional parameters reflecting biological age, such as frailty, physiological stress, and illness should be taken into account to tailor the drug dose for the older individual [39] [44].

In addition, regulators require to find a safe and effective dose for the study population as a whole, not the best dose for an individual[10]. The number of doses studied during clinical trials are limited mainly due to the cost/time reasons, as studying too many different doses/types of patients would be impractical. Inclusion and exclusion criteria lead to the homogenization of the populations studied. For instance, oncology trials will very often exclude older patients (>65 years old), patients with significant organ dysfunction or comorbidities and those taking potentially interacting medications [45], which might lead later to a gap in the professional data and challenges in therapeutic regiment adjustment for these patients. More evidence is emerging demonstrating the for further dose adaptation for females, possibly due to females of child bearing age often being excluded for clinical studies. Often the clinical necessity in dose tailoring is identified during phase IV, when the drug is already on the market [46].

In the last decade importance of pharmacogenomics has been recognized, as remarkable effects on the drug absorption, drug metabolism and drug interactions with receptors could be due to the genetic variability between the patients[7]. Polymorphisms modulate activity in drug membrane transport and drug metabolism. As a result, a patient could exhibit slow/rapid drug absorption, poor/rapid/ultrarapid drug metabolism and poor/efficient receptor

interaction for a specific drug. Currently US Food and Drug Administration (FDA) guide the prescribers to take into account the genetic polymorphisms data for about 200 drugs, including large portion of drugs where genotype should be considered for the drug dosing[8]. Examples of polymorphism in enzymes which should be taken into account for the dose tailoring include CYP2C9 (i.e. for celecoxib, fluvastatin, glipizide); CYP2C19(i.e. for lansoprazole, omeprazole, amitriptyline, citalopram); CYP3A4 (i.e. for cyclosporin); CYP2D6 (i.e. for eliglustat, aripiprazole, dolasetron, doxepin, fluoxetine, respiridone, tramadol) and 2B6 (i.e. for efavirenz). Examples of transporters, which display genetic variability critical for the dose adjustment, include TPMT (i.e. for azathioprine), OATP1B1(i.e. for atorvastatin, pravastatin), DPD (i.e. for fluorouracil),NAT2 (i.e. for hydralazine, isoniazid) and OCT1 (i.e. for ondasetron, sumatriptan).

However, pharmacogenetic knowledge comes mainly from studies in young and middle-aged individuals [47]. It is important to determine the most relevant factor for the dose personalization. For CYP2D6 substrates such as venlafaxine, paroxetine, fluvoxamine and codeine the plays the age plays more important role than pharmacogenetics for the dose prediction [47].

Traditional solid oral dosage form manufacturing limits possibilities for dosage forms individualization. Current large-scale production of dosage forms with a limited number of fixed strengths is deficient for dose individualization, not to mention tailoring release profile or drug combinations in one unit for the benefit of the specific patient. Selected examples of oral dosage forms for which the appropriate dose increments are not available on the market despite a clinically recognized need for dose tailoring/personalization are presented in Table 2-1.

Table 2-1 Selected medications for which appropriate strength increments are not available

Drug	Available dose strengths	Group/condition	Dosing recommendation	Dose personalization factors	Real world
Methylphenidate Hydrochloride	10 mg IR 10,20,30,40 mg LA 20 mg SR	ADHD (5% of population)	2.5 – 60 mg/d Start: dose adjustment once per week Different between IR/SR	Treatment and dosage must be tailored effectively to the individual needs of the child/adolescent Gradual dosage increase[46]	Based predominantly on the clinical response. Different guidelines in each country, very complex dispensing flexibility due to narcotic status. None of the trials included in their analysis directly compared fixed- versus flexible-dose regimens[46]
L-Dopa	100 mg, 250 mg, 500 mg	Parkinson	Usually 300 – 1000 mg/day [48]	Markers for dose adjustment: Val158Met (rs4680): low activity COMT (Val/Val):high activity DRD2 (CAn-STR)	Often reactive dose adaptation: waiting for off symptoms or dyskinesia [48]

				Gender [48]	
Ciprofloxacin	250 mg, 500 mg	Bacterial infections /obese patients (30% of US populatio n in 2007 [49])	Mg/kg, based based on an ABW (including ~45% of excess weight) with an interval appropriate for estimated renal function [49]	Therapeutic drug monitoring [49]	Usually the same dose for all adults (for instance, after/before dental intervention)
Eliglustat	84 mg	Gaucher disease	84 mg/d -84 mg/bid[50]	CYP2D6 genotyping CYP2D6: 3 grades of metabolizers, exclusion/adaptation criteria incl. DDI, hepatic function, cardiac conditions	Physician should choose between 2 regimens- only 2 actual treatment populations
Fluoxetine	10, 20 and 40 mg	Major Depressi on, other mood disorders	5-80 mg/day has shown to be effective [51] [5]		Reactive: based on patient response, sometimes not fast enough (black box warning: suicidal behavior in children and young adults)
Flecainide	50,100,150 mg	Arrhythm ias, paroxysm al heart fibrillatio n, other cardiac condition s	Children: 2 mg/kg/day Adults: titration From 50 mg/bid	NTI Drug. Steep concentration– response relationships for efficacy, toxicity or both in the usual dosing interval Dosing generally needs to be titrated according to clinical response. Monitoring of plasma levels is required in patients with severe Renal/hepatic impairment [52]	Approved in 1985, in 2015 still did not have NTI drug status by EMA and FDA Drug overdose with flecainide is frequently fatal [52]

2.2 Flexible dosing approaches for oral administration

Oral delivery is the most common drug administration route as it is safe and convenient for the patient, as well as affordable in terms of goods and manufacturing [2]. In a case of clinical necessity for dosage tailoring, several approaches exist for commercial or extemporaneous formulations with flexible dosage strength ("flexible formulations" such as liquids or multiparticulates). For the moment, only a single drug per product is incorporated, combinations of multiple APIs or near-patient formulation tailoring to the individual PK profile is not yet a reality.

For pediatric patients and adults/older adults with dysphagia, small sized particulates or liquid dosage forms are superior to classic tablets or capsules not only because of the need in dose personalization, but due to difficulties in swallowing oral solid dosage forms [31]. Predictable and safe drug release in the patient together with an acceptable dosage form to ensure safety and adherence are required, which in general makes development of appropriate drug formulations for these populations complex [6]. In addition, the drug handling and the readability of the product information are key issues in both subpopulations and often depends on the care-givers.

Administration of liquid dosage forms present a well-established widely used approach for a flexible dosing in oral drug delivery [31]. They are marketed as single- or multiuse ready-to-use liquids or powders/granules for reconstitution (incl. suspensions, solutions and emulsions). Ready-for-use examples of aqueous solutions include Epaned® (enalapril maleate), Desitrend® (levetiracetam), Buccolam® (midazolam) and Prexxartan™ (valsartan). Onfi® (clobazam), Felbatol® (felbamate), Purixan™ (mercaptopurine), Noxafil® (posaconazole) and Banzel® (rufinamide). For aqueous formulations, preservatives or antimicrobial devices are required to ensure the microbiological stability, however a strong recommendation for preservative-free pediatric formulations has lead to fewer multiuse solutions or suspensions in the recent years [53]. Overall, increased toxicity in pediatric patients with 'inactive' excipients used frequently for liquid formulations including benzalkonium chloride, benzyl alcohol, propylene glycol and sulfites was reported [54]. For instance, Epidiolex® (cannabidiol) oral solution to treat certain seizures in children contains ethanol as a main excipient. Powders to for oral solutions include Epaned® (enalapril maleate), Firvanq™ (vancomycin HCl) and Sabril® (vigabatrin). Oral suspensions could be prepared from powders (Promacta® (eltrombopag), Isentress® (raltegravir)) or granules (Zmax® (azithromycin), Prograf® granules (tacrolimus), Protonix® (pantoprazole sodium)). The palatability of the liquid dosage for is a major issue, especially when taste sensation difference between individuals is considered [6]. In addition, taste perception is altered by the cultural environment and it is hard to find globally acceptable flavors. Dosage precision is another issue with liquid dosage forms (i.e. reconstitution errors carried out by inexperienced caregivers), with several studies indicating suboptimal dosing accuracy with spoons and cups[11]. For instance, under-dosing of antibiotics might lead to the risk of microbial resistance, and over-dosing might result in toxicity [55].

Multi-particulates present another widely-accepted formulation approach, allowing to adjust the API dose by an administration of a required quantity of pellets, micropellets, granules or mini-tablets[56]. Xuriden™/Vistogard® (uridine triacetate) is an example of oral granules, while Lamisil® (terbinafine HCl) and Kalydeco® (ivacaftor) are formulated as mini-tablets. Depakote® (divalproex sodium), Tasigna® (nilotinib HCl), Tamiflu® (oseltamivir phosphate) and Creon® (pancrelipase) represent examples of commercially available multi-particulates' capsules, which can be swallowed whole or opened and the contents mixed with soft food. However, the type of soft food may affect PK of the active compound as a function of content and pH, ranging from pH ~3.6 for apple puree/orange juice to pH ~5.8 for an infant formula and pH ~6.8 for peanut butter [57]. Multi-particulate formulations could potentially combine particles with different drugs (including ones with chemical incompatibilities) and/or with various release profiles, allowing greater flexibility of the drug product design[12]. For instance, multi-particulates could be designed for API pulsatile release controlled by swelling and rupturing, dissolution or erosion, and changed permeability of the coating membrane [58]. Moreover, multi-particulates could

demonstrate shorter and more reproducible gastric emptying due to their reduced size in comparison to a tablet/capsule, which is particularly advantageous for controlled release products[6]. However, precise dose accuracy is not in-built and dependent on the caregiver, and use of specialized counting and dosing devices might be required.

With regards to pediatric oral formulations in general, flexible solid dosage forms are currently trending [53] in line with the recommendations of World Health Organization reports starting from 2008 [59].

Another option to prepare a flexible formulation is dissolving (oro)dispersible and soluble oral DFs, and administer to the patient an appropriate volume. Examples of the marketed orodispersible tablets include Prevacid solutab® (lansoprazole), Allegra® (fexofenadine hydrochloride), Orapred® ODT (prednisolone) and Parcopa® (levodopa/carbidopa). Another option would be to dissolve orodispersible lyophilisates (Zofran Zydis® (ondansetron), Zyprexa Velotab® (olanzapine), Clarinex Reditabs® (loratadine), Imodium akut lingual® (loperamide) or orodispersible films (Setofilm®/Zuplenz® (ondansetron) and Risperidone Hexal SF® (risperidone).The advantage is preparation of a liquid formulation without the need for crushing/milling of the dosage form, and the limitations include unknown stability of such preparations and risk of fast precipitation. Several soluble/dispersible tablets widely-used for cardiovascular disorders listed in the British National Formulary (BNF) contained increased sodium levels (more than 2.4 g or 104 mmol) [60, 61]. This is particularly critical for the older adults, as high intake of sodium disturbs electrolyte balance, increasing the risk of such cardiovascular conditions as stroke, hypertension and heart failure[62].

Crushing or extemporaneous modifications of marketed medications to adapt the dose the specific patients is often unlicensed and lacking dose accuracy, and might change bioavailability, toxicity and stability of the drug product [13]. For instance, mixing crushed tablets with liquid vehicles or food might alter the active moiety pharmacokinetics, e.g. thickening agents could hinder drug release[63]. In 2007, the European Union regulation on medicinal products for pediatric use was introduced in order improve rational and evidence-based prescribing, however many products still lack age-appropriate formulations for children, especially of pediatric modified release preparations [64, 65]. An automated manufacturing technology such as 3D-printing could address this need of individualized dosage forms.

2.3 Introduction to 3D-printing

According to the United States Government Accountability Office, 3D-printing is production of objects from digital models using a layer-by-layer process [66]. The term 3D-printing can be used synonymously with ‘rapid prototyping’, ‘solid free form fabrication’, and ‘additive manufacturing’ [67]. The concept of 3D-printing was introduced in 1970s’, however the first actual attempts were performed in the beginning of 1980s’ by Dr Hineo Kodama [68]. Almost 10 years later the Fused Deposition Modeling patent was issued by Scott Crump, a co-founder of Stratasys.

3D-printing technologies can be classified by the physicochemical mechanisms used to consolidate materials into layers. The main approaches include photochemical and thermal transformation, as well as binding/adhesion. Various 3D-printing types with different input materials and processing principles are recognized, including binder

jetting, directed energy deposition, material extrusion, powder bed fusion, sheet lamination or vat photo-polymerization [69] [70]. Here common denominators for most of 3D-printing processes are summarized [15]:

1. Digital design. 3D printing starts by designing an object using CAD (computer-aided design) software.

2. Conversion of the design to the compatible format with the 3D-printer. Conversion includes slicing of external surface of CAD object into printable layers and transfer the instructions to the printer. Multiple 3D-printing settings (e.g. speed, temperature, infill pattern) are defined at this step and might have critical influence on the product.

3. Starting material insertion. To facilitate the printing process, raw materials may be processed into pastes, gels, granules, filaments, or binder solutions.

4. 3D-Printing. Materials are added and solidified in an automatic, layer-by-layer fashion to produce the final object.

5. Post-processing. 3D-printed products may require drying, polishing or excess powder removal. In some cases, the excess material may be collected and recycled for the next printing process.

With regards to pharmaceutical drug products, 3D-printing has the potential to deliver individualized and on-demand medications[24]. Several approaches have been evaluated for pharmaceutical applications (Fig.2.1): stereolithography (SLA), selective laser/heat sintering, inkjet-powder bed, fused deposition modeling (FDM), liquid inkjet and semi-solids extrusion [16, 17].

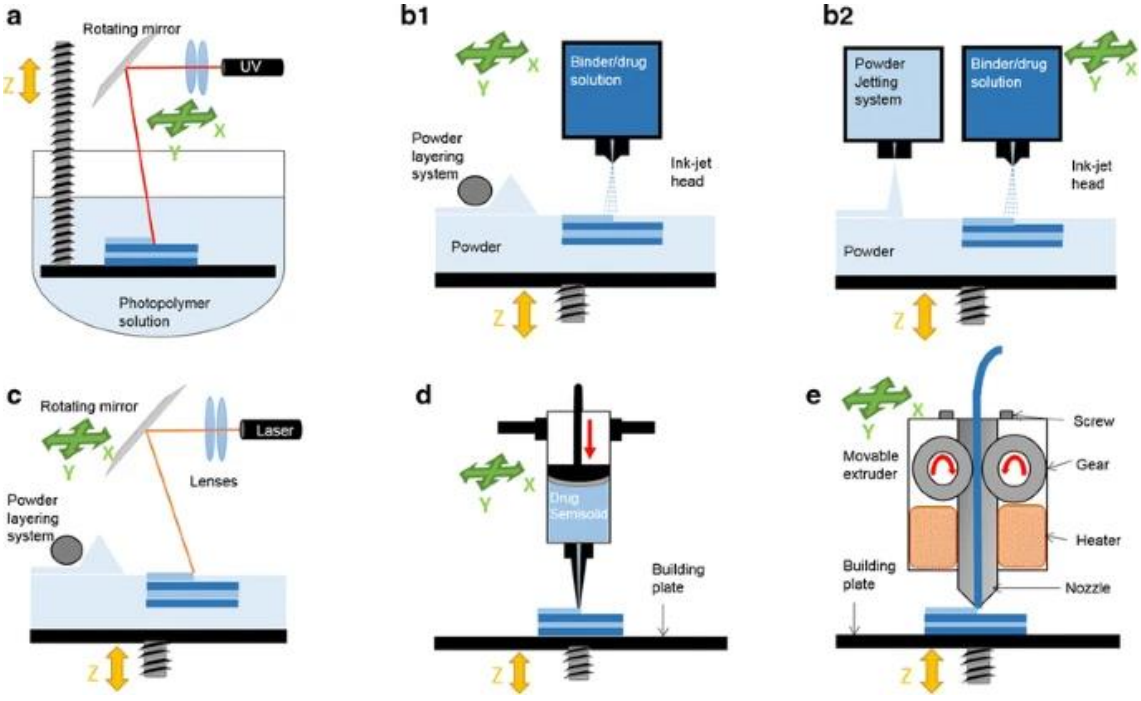

Fig.2.1. Mechanism of various 3D printing technologies: (a) Stereolithographic (SLA), (b1-2) Powder bed and powder jetting, (c) Selective laser sintering (SLS), (d) Semi-solid extrusion (EXT) and (e) Fused deposition

modelling (FDM) (Copyright © 2016, Springer Science Business Media New York, reprinted with permission from Springer Nature[16])

Stereolithographic 3D-Printing (SLA). SLA involves curing of photosensitive materials by UV light or digital light projection technique (DLP) [71]. Raw materials for SLA are usually low-molecular weight polyacrylates and epoxy macromers/monomers. The technology demonstrates high level of accuracy and resolution. The disadvantages of SLA include potential health hazards from the resins and long-term instability of photosensitive materials. In addition, the object created by stereolithographic 3D-printing requires post-processing.

Selective laser/heat sintering (SLS/SHS). SLS uses a high power laser beam (SHS – heat), which sinters the powder material and binds it in layer-by-layer fashion [17]. During the printing process, the laser creates a pattern onto the powder layer. Once the first layer is completed, a new layer of powder is spread on top of the previous one. The object recovered from underneath the powder bed following printing. SLS technology is a one-step solvent-free process with high resolution [72]. However, SLS involves exposure of the materials to high temperatures and high-energy lasers which may degrade APIs.

Powder bed. The product is formed in a layer-by-layer fashion, when binders/API solution is sprinkled over a powder bed [73]. Liquid binder aids the bond formation without involving step of melting/UV photopolymerization. Various pharmaceutical-grade materials could be used. Relatively fragile tablets produced by inkjet-powder bed often exhibit ultra-rapid disintegration[16]. The first FDA approved 3D printed tablet ZipDose® is a pioneering example of the commercialization of the powder bed technology. Disadvantages of inkjet-powder bed technology are moderate resolution, lengthy post-printing drying and impossibility to print hollow objects. In addition, this technology appears to challenging in terms of acceptable tablets appearance and applicability for decentralized manufacturing.

Fused deposition modeling (FDM). This is currently the most commonly explored technology for drug delivery systems [17]. FDM involves melting of a thermoplastic filament, which is deposited in ultrafine threads along the extrusion path through the printhead nozzle. The bond among the layers is formed through fusion with a previously extruded layer. After the object is formed, no post-processing is required in most cases. Additional advantages of FDM 3D-printing include its low cost and good mechanical properties of the printed forms [74]. Limitations of FDM include use of high printing temperatures (>120 °C), which may induce drug degradation and a relatively low resolution of the printed objects.

Semi-solids extrusion (EXT). The product is created by extruding semi-solids through a syringe-based tool-head onto a stage in layer-by-layer fashion [75]. Semi-solids (gels or pastes) are formulated by mixing optimal ratios of polymers and appropriate solvent(s). EXT printing requires lower processing temperatures and pharmaceutical-grade materials can be easily applied. Objects produced by EXT technology have relatively low resolution and may deform during post-printing drying.

Liquid inkjet. The technique involves jetting of a liquid on the surface[76], and is usually used as 2D-printing technique. For pharmaceutical applications, first use of a heated beeswax-based formulation was reported in 2017

[77]. The formulation was heated until the liquid state was achieved, and dispensed in a layer-by-layer manner following solidification. The obtained tablets demonstrated high level of accuracy and resolution [77] and slow dissolution rates.

Pharmaceutical 3D-printing of solid oral dosage forms has a potential to deliver individualized dosage forms [24]. In particular, it could bring unique opportunities to create a personalized dosage strengths, and affect release profile via shape and inner structure design [19] [20]. Installation of 3D-printers in pharmacies and hospitals could create an opportunity for decentralized near-patient manufacturing[78], serving approaches of patient centricity and precise medicine. On-demand preparation of multiple active pharmaceutical ingredients in one oral dosage form might enable pharmaceutical 3D-printing to fulfil as yet unmet clinical need in personalized dosing and release profile arising from concomitant use of interacting pharmacokinetically or pharmacodynamically APIs [79] [16] [80]. Complex designs and geometries, multiple APIs and tailored release profiles might enable pharmaceutical 3D-printing to fulfil as yet unmet clinical needs [16]. More specifically, 3D-printed tablets could be potentially used for the following applications:

- dose escalation during early phase clinical trials
- manufacturing on-demand for drugs with a short shelf-life
- personalized dosage (e.g. special populations, NTI drugs, pharmacogenomics)
- complex multi-drug tablet with different release profiles for personalized regimens [81]

To develop a personalized dosage form properly, a careful match of the starting materials to a suitable 3D-printing technology should be performed.

2.4 Fused deposition modeling

Among several techniques available for 3D-printing, widely-used and low cost method of fused deposition modelling (FDM) is widely explored for the development of oral dosage forms [82]. In this method, filaments of thermoplastic polymers are extruded via tiny heated nozzle and deposited in a layer-by-layer fashion to prepare solid objects with desired design. Pharmaceutical application of FDM will require FDM-processable filaments manufactured by hot-melt extrusion (HME).

Polymers evaluated for pharmaceutical FDM-printing include polyurethanes, polyvinyl alcohols, polyethylenpolyvinylpyrrolidone, polymethacrylate-based copolymers, polyethylene oxide (PEO), and cellulosic derivatives such as hydroxypropyl methylcellulose (HPMC), HPMC acetate succinate (HPMCAS), hydroxypropylcellulose (HPC) and ethyl cellulose[16, 20, 24]. Filaments for successful FDM-printing should have suitable mechanical properties, melt viscosity, thermal and long-term physical stability [18]. In addition, miscibility of the drug and polymers should be established in order to estimate possible crystallization during the shelf-life if amorphous solid solution/dispersion is created. Investigation of FDM-processability using mechanical tests is the subject of ongoing research. For instance, additions of plasticizers such as triethyl citrate, triacetin, polyethylene glycols and glycerol, could improve melt flow properties of the polymers via the glass transition temperature

reduction and could increase the strain bearing ability of the filaments[25]. However, no direct correlation between Tg of the filaments and their FDM-processability was demonstrated. Flexibility of the filaments are determined in force/distance plots measured by a texture analyzer attempt to define clusters of 'printable' and 'non-printable' filaments. Very recently Elbadawi et al. applied Machine Learning as an approach for predicting FDM-printability of medicines [83].

Often FDM-printed tablets exhibit a tendency for a slow dissolution due to APIs entrapment into the polymeric matrices, which are characterized by erosion-controlled dissolution mechanisms [26] [22]. Moreover, incomplete drug release from the 3D-printed tablets might be observed. A wide variety of extended release FDM-printed formulations were developed [79, 84-86], however the biopharmaceutical needs of most products require development of immediate release dosage forms[87, 88]. To overcome slow disintegration and dissolution, inherent to the use of thermoplastic polymers, several formulation and tablet design parameters approaches were investigated. Formulation approaches include high concentration of a non-melting inorganic filler in the formulation [22, 82]. For the thermostable drugs, polyvinyl alcohol could be used as primary matrix former to achieve faster dissolution[21]. In addition, rapidly dissolving polymers such as Kollidon VA64 and Kollidon 12PF could result in relatively fast dissolution [16, 89]. Design modifications of tablets include infill density decrease and incorporation of channels through the body and/or surface of the tablet [90, 91]. Incorporation of the hollow structures though often results in the increased size of the tablet for the given dosage strength [90], which might lead to the difficulties in swallowing. On other hand, the opportunity to tailor dissolution rate within certain limits via tablet design modifications, while keeping the given formulation remains a unique property of FDM-printing.

FDM printing presents a unique opportunity for decentralized manufacturing of drug products at points-of-care; no loose powders or solvents are involved and post-processing is generally does not required [92, 93]. Being a hot-melt process by design, FDM could be used to generate amorphous dispersions with enabling properties.

The current FDM paradigm is a multi-step process, with powder blending as a first step, prior to filament manufacturing by hot-melt extrusion, followed 3D-printing of the filament to give a tablet. In this manner, the drug product shelf life starts significantly earlier than manufacturing of the final dosage form. Further, mechanical properties of the obtained filaments to allow FDM processability is a critical for the formulation development. Dependence on the mechanical properties of the filament leads to a limitation in the excipients which can be used, significant amount of formulation development only improve FDM-processability, which might compromise drug load and release profile. Circumnavigating the need for intermediate filaments by manufacturing 3D-printed tablets directly from powder could simplify formulation development and allow a greater variety of excipients in the compositions toolbox, while staying maintaining the desired product profile. Recently, the first feasibility studies of direct powder extrusion [27] [28] and direct powder printing (DPP) [18] were reported. In order to 3D-print the molten polymer matrix, direct powder extrusion involved an in-built single screw extruder at the printing head, while DPP used applied pressure. In both processes, raw material homogeneity is a critical factor for the acceptable content uniformity of the obtained 3D-printed tablets.

2.5 Amorphous solid dispersions and hot-melt extrusion

Amorphous solid dispersion (ASD) is an established approach to create an enabling formulation for drugs with poor solubility and as such limited bioavailability, via an increase in the apparent solubility [94] [95] [96]. Aqueous solubility lower than 100 µg/mL are considered to exhibit dissolution-limited absorption *in vivo*[97], hence ASDs are usually formulated for compounds belonging to BCS classes II and IV. A concept of amorphous solid dispersions was introduced for the first time by Chiou and Riegelmann in 1969 due to the increasing number of the discovered poorly water-soluble compounds [98]. If API is dispersed molecularly in the amorphous carrier, the obtained drug product is defined as amorphous solid solution [99]. However, different types of amorphous solid solutions and amorphous formulations are still included under the umbrella of ASDs.

The main pharmaceutical technologies for manufacturing ASDs are spray-drying and hot-melt extrusion (HME); solvent evaporation, microprecipitation, hot-melt coating/granulation, cryogenic processing, electrospinning and rotating jet spinning are assessed as well [100]. In 2015 a review paper of 23 marketed products prepared by solid dispersion techniques were reported [101], while current PharmaCircle Database search shows ~140 drug products marketed in at least at one country[1] [102]. Examples of commercially available ASDs include Micardis® (telmisartan), Sporanox® (itraconazole), Reyataz® (atazanavir sulfate) and Prograf® (tacrolimus hydrate). HME is primarily used to enhance bioavailability via amorphous dispersion creation[103] [104] not only due to the higher saturation solubility, but also because of increased specific surface area [105] [106]. For example, bioavalability of an anti-malarial compound lumefantrine, belonging to BCS class IV, is increased up to 48-fold via hot-melt extruded ASD relative to that of the conventional formulation [107] [108]. The drawback of the increased free energy state of the amorphous material might lead to relaxation, nucleation and crystal growth phenomena during the storage[94] [109] [110]. Hence, any amorphous solid dispersion is at risk of recrystallization, as the crystalline form of the drug is thermodynamically more favorable resulting in phase separation and crystalization. The Avrami equation (1) is most frequently used to define and predict the solid-state recrystallization processes:

$$\alpha(t) = 1 - \exp(-kt^n) \quad (1)$$

In the above equation (1), α(t) represents relative crystallinity, k is the recrystallization rate constant and n is the Avrami exponent. Even partial recrystallization of the obtained ASD (as a function of miscibility, drug-polymer ratio and hygroscopicity) would often lead to the partial loss in increased apparent solubility [111], which was intended to be achieved via amorphization.

In the recent years HME technique was implemented for pharmaceutical filaments manufacturing intended for FDM printing [112] [23] [24]. Similarly to hot-melt extrusion, FDM may result in ASD if the drug dissolves in the molten formulation matrix and has sufficient miscibility with it, or if 3D-printing is performed at higher temperature than the compound's Tm [113] [85] [89] [24]. Near patient fabrication could address ASD physical instabilities risk by significantly reducing the time between manufacturing of the final dosage form and its administration to the patient.

[1] Status 25th September 2020, API repetition is included in search if marketed with different composition and/or by different company

For traditional solid dosage forms manufactured via HME, the extruded filaments are milled or pelletized in order to obtain a suitable particle size for pharmaceutical processing (i.e. compression, capsule filling) [114]. Brittle filaments are more suitable for tableting and require less time and effort to be milled/granulated as opposed to flexible materials, leading higher suitability of relatively brittle materials for this application [115]. Unsurprisingly, most pharmaceutical grade polymers developed for HME often yield readily fracturing extrudates, which limits those materials application for FDM. Following an increased interest around pharmaceutical and medical FDM-printing, several companies launched commercial production of biodegradable FDM filaments [116] [117].

3 Chapter 3

Development of Immediate Release (IR) 3D-printed oral dosage forms with focus on industrial relevance[2]

Summary

Pharmaceutical 3D-printing represents a potentially new dosing and manufacturing approach for the pharmaceutical industry, with unique opportunities for personalization of dosage strengths. Fused deposition modelling (FDM) is a 3D-printing technique, which presents advantages for decentralized on-site manufacturing in hospitals and pharmacies. This study presents industrially relevant development of formulations for filaments with the required mechanical properties to be 3D-printable and providing immediate release (IR) dosage forms using safe materials approved also for pediatric use. Hydroxypropyl-cellulose (HPC) SSL was chosen as hydrophilic polymer and caffeine with a load of 5-20% as thermally stable model drug. Poly-(vinyl pyrrolidone-vinyl acetate) copolymer (Kollidon VA64) and poly-(vinyl alcohol-polyethylene glycol) graft copolymer (Kollicoat IR) were additional water-soluble polymers tested in combination with HPC and xylitol and polyethylene glycol (PEG) 4000 were evaluated as hydrophilic plasticizers and PEG4000 and maltodextrin as pore formers. Formulations were hot-melt extruded using a scalable twin-screw extruder and 3D-printed into honeycomb geometry solid dosage forms with high (100%) and low (80%) infill density. Rapid or very rapid release was achieved via formulation selection and tablet design parameters. PEG4000 in combination with Kollidon VA64 demonstrated superior processability and significantly accelerated release properties of the matrix independently of infill density. Lowering caffeine content improved hot-melt extrusion processability for each formulation but prolonged dissolution. The use of Kollicoat IR resulted in superior mechanical properties of the manufactured filaments, with easy handling and successful 3D-printing for drug load of 5 to 20%. For most formulations, lowering infill density of 3D-printed tablets yielded faster drug dissolution in agreement with the literature. However, the extent of the infill density effect varied depending on formulation. Caffeine was present in stable crystalline state in 3D-printed tablets. Printing temperature appeared to be critical for drug dissolution *in vitro*. This wide-ranging excipient investigation epitomizes the beginning of a toolbox approach targeting FDM processability in combination with immediate release characteristics of personalized dosage forms.

[2] Fanous, M, Gold, S, Hirsch, S, Ogorka, Imanidis, G, *Development of Immediate Release (IR) 3D-printed oral dosage forms with focus on industrial relevance*. Eur J Pharm Sci, 2020. **155**: p.105558

3.1 Introduction

3D printing of dosage forms presents an opportunity to personalize dose to individuals, considering interpatient variabilities and potentially improving safety and efficacy for some medications [5]. Traditional dosage form manufacturing limits possibilities for a dosage form individualization. Pharmaceutical 3D-printing of solid oral dosage forms could bring unique opportunities for tailoring dosage forms strength, shape and inner structure affecting release profile [19] [20]. Installation of several types of small desktop 3D-printers could create an opportunity for point-of-care fabrication in pharmacies and hospitals, paving the path towards more patient-centered medications [78]. Decentralized preparation of dosage forms with complex designs and geometries, multiple active pharmaceutical ingredients and tailored release profiles might enable pharmaceutical 3D printing to fulfil as yet unmet clinical needs [79] [16] [80].

3D-printing technologies can fabricate objects of various shapes and size on demand based on digital models by depositing material layer by layer. Several technologies are evaluated for pharmaceutical 3D-printing such as stereolithography, powder based, selective laser sintering, fused deposition modelling (FDM) and semi-solid extrusion. For point-of-care fabrication in pharmacies and hospitals, manufacturing of dosage forms via customized FDM 3D-printers are considered to be advantageous over other 3D printing technologies as no powder or solvents [86] are involved in the printing process and post-processing can be avoided.

Object creation via FDM requires a thermoplastic filament, which is melted and deposited in ultrafine threads along the extrusion path through the printhead nozzle. The main challenges/limitations of pharmaceutical FDM 3D-printing are mechanical requirements of the filament [79], possible thermal degradation of pharmaceutical ingredients [118] and tendency for slow dissolution due to the high proportion of thermoplastic material in the formulation required in the FDM process, ensuing low drug load and generally small surface area [78]. These issues need to be resolved in order to enable commercial viability of this technology.

Pharmaceutically acceptable polymers explored for FDM included cellulosic derivatives, polymethacrylates, polyurethanes and polyvinyl alcohols [85]. Successful development of various FDM 3D-printed extended release formulations are widely presented in the literature [84] [85] [79] [86], whereas development of immediate release tablets appears to be more challenging. Formulation development using polymers such as hydroxypropylmethyl-cellulose (HMPC) and hydroxypropyl-cellulose (HPC) often results in slow dissolution rates consistent with extended release due to relatively slow erosion mechanism of release from polymeric matrices [78] [119]. However, availability of immediate release (IR) formulations is a major need towards the future of personalized dosage forms production meeting the biopharmaceutical needs of most active pharmaceutical ingredients (APIs) [87] [88]. Techniques to overcome some of the solubility and disintegration challenges inherent to 3D-printed solid dosage forms produced by FDM have been explored. For instance, channels in the form of tubular passages or grooves, through the body of the tablet or the surface thereof [90] and geometric shapes of tablets consisting of blocks with gaps and bridges [91] were proposed. These, although they do achieve the aspired IR goal might limit the dose or lead to increased tablet size linked to difficulties in swallowing, especially for older adults. Another approach involved the addition of fairly large amounts of non-melting inorganic fillers to the formulation [82]. Recently, Wei

et al. reported relatively rapid dissolution rate with PVA as primary matrix former [21], however high processing temperature (210°C) was required for 3D-printing. In another study, IR tablets were produced by FDM at low processing temperature, the used filaments however were liable to fracture during 3D printing requiring the assistance of a commercial filament to be pushed through the printer head [91]. Development of another IR formulation of 3D-printed tablets with rapidly dissolving polymers Kollidon VA64 and Kollidon 12PF [89] was limited to 3% drug load and required 20% of prone to oxidation plasticizer [120] [121]. Finally, polymer blends were investigated that provided filaments with adequate mechanical properties to be 3D-printed, the obtained rapid drug release, however, even at low infill density did not reach the IR criteria put forth by current pharmacopoeias [16].

Formulations yielding both immediate release (IR) dosage forms and printable filaments with the required mechanical properties remain challenging to develop. The objectives of this study therefore were:

- Develop scalable hot-melt extruded IR formulations, processable by FDM 3D-printing
- Use worldwide acceptable polymers, including for pediatric use
- Explore wide formulation design space to study effect of selected rapidly dissolving polymers, hydrophilic plasticizers and dissolution enhancers on processability including FDM suitability and quality attributes of tablets, particularly dissolution rate
- Take a toolbox approach in exploring several formulations for industrial tablet manufacture by FDM printing accommodating for a wide range of drug loads, and being potentially suitable for different APIs
- Study impact of process parameters on dissolution rate

3.2 Materials and methods

3.2.1 Materials

Anhydrous caffeine (Sigma–Aldrich, UK) was used as a model drug. Mixtures of hydroxypropyl-cellulose (HPC SSL, Nisso Chemical, Tokyo, Japan) as primary matrix former, with or without rapidly dissolving polymers poly-(vinyl pyrrolidone-vinyl acetate) copolymer (Kollidon® VA64, BASF, Ludwigshafen, Germany) or poly-(vinyl alcohol-polyethylene glycol) graft copolymer (Kollicoat® IR, BASF, Ludwigshafen, Germany) were used. Polyethylene glycol 4000 (PEG4000, powder grade P), Clariant, Sulzbach, Germany) or xylitol (Xylisorb300, Roquette, Lestrem, France) were employed as solid hydrophilic plasticizers. PEG4000, maltodextrin (Maldex 120,Tereos, Freiburg, Germany) and dibasic calcium phosphate (DCP, Budenheim, Germany) were added as pore formers / dissolution aids. Percoffedrinol N 50 (Aristo Pharma GmbH, Germany) tablets were commercially sourced and used for comparison of dissolution profiles of caffeine.

3.2.2 Methods

3.2.2.1 Hot-melt extrusion

Powders with batch size at least 100 g were weighed into 0.5 L bottles and the compositions were mixed via diffusion blending at 32 upm for 10 min using T2 Turbula™ mixer.

A twin-screw hot melt extruder (Thermo Scientific™ Pharma 11™, Karlsruhe, Germany) was used to produce filaments. Screw design is shown at Fig. 3.1.

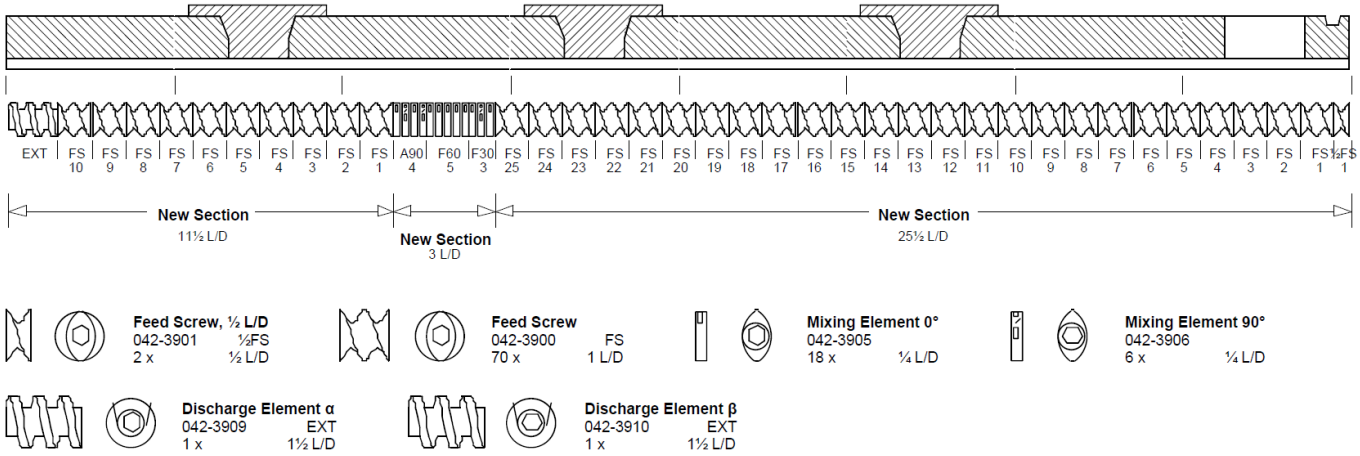

Fig.3.1. Screw configuration of Pharma 11™ twin-screw hot melt extruder used for filament production

The actual temperatures for zones 2, 3, 4,5-8 was 35-58°C, 50-100°C, 100-140°C, 120°C-140°C respectively; die temperature was 120°C - 145°C depending on the formulation (see Table 3-1). Extrusion was carried out through a 1.75 mm die nozzle with a pressure control (maximum 90 bar). Feeding rate was up to 5 g/min, screw speed 10-25 rpm depending on the formulation.

Table 3-1 Formulations compositions and process parameters with caffeine resulting in successful filament manufacturing

	Formulation code[a]											
Formulation component (% w/w)	**10% HPC0**	**10% HPC4**	**5% HPC7**	**10% HPC7**	**5% XYL5**	**10% XYL5**	**20% XYL5**	**5% XYL7**	**10% XYL7**	**20% XYL7**	**5% DCP1**	**10% DCP1**
Caffeine	10.03	10.06	4.99	10.00	5.02	9.97	20.00	5.00	9.99	19.90	4.98	10.08
HPC SSL	89.97	58.51	47.70	45.19	23.94	22.69	21.07	47.53	45.04	40.08	39.46	37.34
Kollidon VA64		31.42	33.08	31.34				28.48	26.98	24.01		
Kollicoat IR					47.34	44.87	42.07					

PEG4000			14.22	13.47							16.10	15.24
Malto-dextrin					9.48	8.99	4.23	4.75	4.50	4.00		
Xylitol					14.22	13.48	12.63	14.24	13.49	12.01		
DCP											39.46	37.34
	Process parameters											
T zone2 (°C)	43	40	40	35	44	45	50	50	58	42	40	40
T zone3 (°C)	80	100	50	53	80	80	100	100	84	70	100	100
T zone4 (°C)	120	130	100	100	120	130	135	120	130	130	135	140
T zone5 (°C)	120	130	120	125	120	130	135	120	130	135	135	150
T zone6 (°C)	130	130	120	125	120	135	135	130	130	135	135	150
T zone7 (°C)	130	140	125	125	130	135	140	130	130	135	135	140
T zone8 (°C)	135	140	125	125	135	140	145	130	130	130	130	130
T die (°C)	135	140	125	120-125	135	140	145	130	130	130	130	130-135
Screw speed (rpm)	25	10 - 25	20	25	15	20	25	20	25	20	15	15
Torque (%)	53	74	up to 18	20	up to 45	38	24	up to 26	27	47	7	6
Pressure (bar)	4	7	0	0	up to 18	11	15	0	up to 90	10	4	up to 17
FDM 3D-printable	yes	yes	yes	yes	yes	yes	yes	yes	no	no	yes	no

[a]Three letters in formulation code denote hydroxypropyl-cellulose (HPC), xylitol (XYL), dicalcium phosphate (DCP). The numeral preceding the three letters declares the drug load in percent and the numeral at the end is historically derived from the testing sequence

3.2.2.2 Fused deposition modeling (FDM) 3D-printing

BoltPro 1.75 mm 3D-printer was used for FDM (LeapFrog, Netherlands). 3D-printing was performed through nozzle with d=0.35 mm at 900-1200 mm/min speed with primary layer speed of 50% of the default and height of 0.15 mm. The lowest possible printing temperature was used that still allowed an appropriate formulation processability (155-180°C).

The dosage form was designed with FreeCAD 0.13 Software. The selected geometry was an oval tablet (see Fig.3.2). The tablet size was set to 8x16x4 mm (width x length x height) with one continuous outer layer (altitude shell) and no bottom/top layers. Printing was performed on a surface heated to 40°C using honeycomb infill pattern

as determined by LeapFrog software. Tablets with two infill densities a low (80%) and a high (100%) one were 3D-printed. At least 12 tablets were manufactured per formulation.

3.2.2.3 Drug load and uniformity of percent drug content

The drug content was determined using a spectrophotometric method. A tablet (minimum triplicate per each formulation) was dissolved in 1000 mL 0.01 HCl. The drug concentration was determined after reading the sample at 273 nm in Perkin Elmer Lambda 25 UV spectrophotometer (Perkin Elmer Inc., USA) using ARGUS software. The values were normalized by weight to calculate drug load. Excipient amounts equal to those present in a tablet were separately dissolved in the same medium. No absorption of the mix of excipients at 273 nm was found by the same method.

3.2.2.4 Solid state analysis

3.2.2.4.1 X-ray powder diffraction (XRPD)

Powders were analyzed on a quartz sample holder. 3D-printed tablets were manually ground with mortar and pestle, and powder blends were directly dispensed on the holder surface. XRPD analyses were performed on a diffractometer using a K430 X-ray generator with a copper anode
(voltage: 40 kV, current: 40 mA). XRD patterns were recorded in transmission mode using quartz capillaries (1.5 mm diameter, GLASS W. Müller, Berlin, Germany). The X-ray generator was a long line focus sealed tube (Siemens; Germany, Cu anode with a Kα line at 1.54 Å, operating
at voltage of 40 kV and current of 20 mA). One 2D VÅNTEC-500 Area detector (4 channels, filled with argon-ethane mixture) was used to collect the data. With the settings used, 2θ angles were calculated, ranging from 1 to 18° and from 18 to 36°. Diffractograms were generated with the software Diffrac.EVA V4.0 from Bruker.

3.2.2.4.2 Differential scanning calorimetry (DSC)

DSC measurements were performed using a Q2000 DSC (TA instrument, New Castle, PA) under nitrogen flow 50 mL/min. Samples between 1 and 2.5 mg were analyzed using punctured aluminum cells, an empty cell was used as reference. A heating rate of 10°C/min was set between -20°C and 300°C. Software used for analysis was Trios v4.4.1 (TA Instruments, Inc., Waters Corporation, MA, USA).

3.2.2.4.3 Confocal Raman microscopy

Pure caffeine as reference and formulation XYL5 with 20% drug load (20% caffeine: 42.07% Kollicoat IR: 21.1% HPC: 4.23% Maltodextrin: 12.63% Xylitol) were chosen for Raman microscopy.
The molecular fingerprint (vibrational spectra), form and special distribution characteristics of caffeine were established by performing tablet surface scanning and compared to those of the precursor (starting) substance.

Three surface hyperspectral scans were performed for the 3D-printed tablet. Additionally, a suitable amount of the reference (precursor) substance was placed on a microscopy glass slide and four single spectra, and one surface hyperspectral scan were performed.

Software used for data processing was Project FIVE 5.1 (WITec, Germany). Anhydrous caffeine spectra was established by the use of sum spectral filter centered at 975 rel. cm^{-1} and corresponding intensity maps were

calculated by the application of 200-1000 threshold. This was followed by establishing corresponding average spectra. Spectral spatial localizations together with a level of component analysis (to establish polymer matrix average spectra) were subsequently performed and spectral micrographs were produced and merged when applicable.

3.2.2.5 Dissolution studies

A semi-automatic tablet dissolution system Sotax AT7 (Sotax AG, Aesch, Switzerland) fulfilling requirements for USP2 dissolution method was used to perform the studies. In vitro release profiles of the tablets (n=3 for each formulation) were studied in 0.01 N HCl (pH=2, the most representative of the gastric environment in the fasted state [122]. The medium was degassed with helium for 30 min on the day of experiment. Each tablet was placed in the dissolution vessel containing 1000 mL 0.01 N HCl. Dissolution was carried out with a paddle speed of 50 rpm at 37 °C for 2 hours. The paddle speed was then increased to 150 for a further 0.5h to ensure full dissolution, and obtain an "infinity" value. Samples (10 mL each) were collected at time points 0, 5, 10, 15, 20, 30, 45, 60, 120 and 150 min. The dissolution medium was replenished after each sampling with an equivalent amount of 0.01 N HCl solution. The drug concentration of the samples was analyzed for concentration as above using Perkin Elmer Lambda 25 UV spectrophotometer at 273 nm. The values of separately analyzed samples (n=3) were normalized by weight to estimate drug load, and taken as 100% dissolution value. Expected 100% dissolution value was calculated based on the average drug content of the formulation. Dissolution profiles were visualized by plotting percentage of drug dissolved against time. At least 85% of drug relative dissolved amount (average n=3) after 30 min was set as immediate release criteria according to more stringent FDA guidance [123].

3.2.2.6 Data analysis

The data are presented as mean ± SD, and the differences between various groups were analyzed by two-way ANOVA followed by Tukey's post hoc test (GraphPad Prism, version 7.0, GraphPad Software, San Diego, CA). The effect printing temperature on relative dissolved amount at 15 min time point was analyzed by unpaired two-tailed t-test with Welch's correction which takes into account unequal variances of the two populations and inequality of sample size. The statistical significance was considered at $p < 0.05$.

3.4 Results and discussion

Formulation strategy was as follows: hydroxypropyl-cellulose was chosen as hydrophilic primary matrix former [124] with potential to achieve rapid release [78] .The addition of two rapidly dissolving polymers, poly-(vinyl pyrrolidone-vinyl acetate) copolymer (Kollidon® VA64) and poly-(vinyl alcohol-polyethylene glycol) graft copolymer (Kollicoat® IR) in the development of FDM-printable formulations was assessed for the potential to achieve rapid drug dissolution rate. Of these, Kollidon® VA64 was reported to be non FDM-printable as single matrix former, however increasing dissolution rate when combined with hydroxypropylmethyl-cellulose (HPMC) [24]. Further, polyethylene glycol (PEG4000) and maltodextrin were evaluated as pore formers, PEG4000 acting also as hydrophilic plasticizer. Xylitol was used as solid hydrophilic plasticizer as alternative to prone to oxidation PEG [121] [120], in combination with maltodextrin as this combination was reported in the past as IR formulation for injection molding [125]. Finally, dibasic calcium phosphate (DCP), a non-melting filler was investigated for its

action as dissolution/disintegration facilitator in a cellulosic matrix instead of rapidly dissolving polymers, based on a similar approach reported previously with poly-methacrylate matrices for FDM 3D-printing [126]. A hydrophilic model active pharmaceutical ingredient, caffeine, was employed. Different compositions of the above excipients and different drug loads were used for hot-melt extrusion and 3D-printing of the filaments with variable process parameters and evaluated in order to develop suitable formulations with respect to processability and rapid drug release and determine the quality relevant factors. Acceleration of dissolution rate, if possible, by modifying formulation without compromising the dose, if possible, was prioritized. Thus only 20% decrease in infill density was explored, as for certain tablet size lower infill would lead to lower weight and consequently lower dose.

3.4.1 Processability

Following development of formulations, filaments that could be loaded and were robust enough to withstand the pressure exerted by the drive gear during 3D-printing, moreover, that could be advanced by gear wheels and did not jam or break and had a melt viscosity allowing them to pass through the nozzle were selected. This assessment of printability was performed empirically. Overall, addition of caffeine to corresponding placebo formulations resulted in worsening of FDM processability. This was because filaments appeared more brittle leading to breakage. Poly-(vinyl pyrrolidone-vinyl acetate) copolymer, Kollidon VA64, in combination polyethylene glycol PEG4000 demonstrated superior HME processability compared to a combination of xylitol-maltodextrin as referenced by torque and die pressure (Table 3-1, HPC7 vs XYL7). For the combination of xylitol-maltodextrin as plasticizer for HME, formulating with Kollicoat IR was superior to Kollidon VA64 when drug load was more than 5%. As a general trend, good processability for hot-melt extrusion reflected good printability for this set of formulations. High torque and/or high die pressure during hot-melt extrusion indicated poor 3D-printability of the obtained filaments. For example, challenging HME processability of 10%HPC4, 10%XYL7 and 10%DCP1 was reflected in impaired FDM printability for these formulations. Lowering caffeine load demonstrated better 3D-printability for each formulation.

For processable filaments, manufacture of tablets by FDM printing with honeycomb geometry was achieved with appropriate resolution and size (Fig.3.2). For randomly measured samples within and among all formulations, deviation from the programmed size was up to 2% for x and y axis and up to 5% for the z axis. It has to be mentioned, that diameter of in-house manufactured pharmaceutical filaments was less uniform than a benchmark for commercial plastic filaments (up to ±0.18 mm vs ±0.05 mm variability, respectively). This diameter variability may cause deviations in internal micro-structure, potentially affecting drug product quality and uniformity in dissolution profiles. In the future, even more accurate and repetitive structure of tablet should be achieved via equipment and processes development for pharmaceutical 3D-printing.

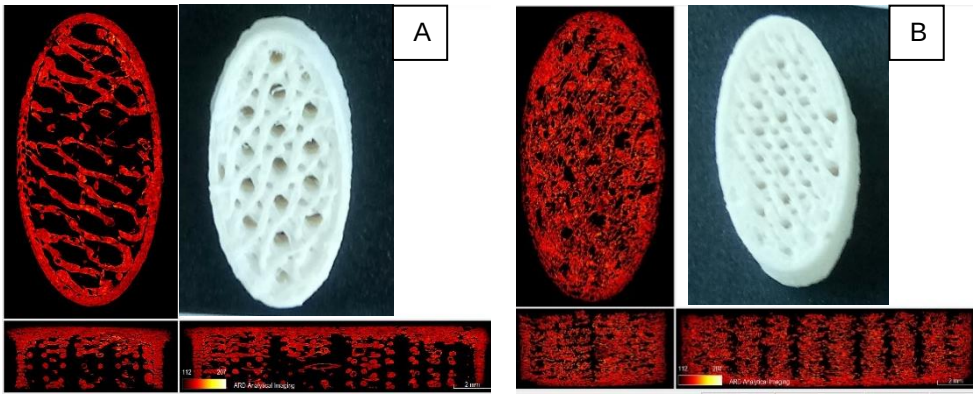

Fig.3.2. Representative photograph (white) and mid-section microCT scan (red) parallel to the plane (elliptical shape) and perpendicular to the plane in the direction of the long and the short axis of honeycomb FDM 3D-printed 10% XYL5 tablet with infill density set to 80% (A) or 100% (B) in FDM 3D-printer

The filaments were 3D-printed with low (80%) and high (100%) infill density with similar temperature for both geometries. Combination of small nozzle diameter of 0.35 mm and speed adjustment to 900-1200 mm/min allowed achieving accurate 3D-printing of honeycomb infill as judged by CT images of the obtained tablets. Manufacture of one tablet took about 7 minutes, including preheating and extruder/printing bed equilibration time. As format of manufacturing is of major importance for future industrial development, current speed might be sufficient for decentralized production in hospitals and pharmacies but too slow for centralized manufacturing where parallelization could be a solution. Absence of a plasticizer, higher drug load and incorporation of thermostable filler required increase in HME and 3D-printing temperature.

3.4.2 Uniformity of weight and drug load

Majority of 3D-printed formulations demonstrated weight variability less than 10%, however about a third of the formulations demonstrated higher weight variability (Table 3-2).Tablets with low and high infill density demonstrated similar weight uniformity. Interestingly, high drug load XYL5 formulation (20% Caffeine, 21.1% HPC, 42% Kollicoat IR, 12.6% Xylitol, 4.2% Maltodextrin) demonstrated superiority in terms of weight uniformity with less than 2% weight variability for low infill density. This might be due to superior hot-melt processability of XYL5 possibly leading to more uniform filament diameter. Overall, a reason for obtained weight variability of 3D-printed tablets might be variable diameter of the filaments as no diameter control was performed during hot-melt extrusion, and an incomplete control over melt flow and viscosity during printing. Notably, considerable differences in average tablet weight between formulations were observed for the same infill density although the outer dimensions of the tablets were the same. This may be related to differences in filament diameter but also in melt viscosity and density between formulations resulting in different deposition behavior upon 3D-printing.

Table 3-2 3D-printed caffeine tablets: Uniformity of weight and drug load

Nominal drug load (%)	Formulation code	Programmed infill density (%)	Average weight (mg) ± std (%)	Assay (%) ± std (%)
10	HPC0	80	201±15.9	87.4±0.4
10	HPC0	100	222.7±11.1	
10	HPC4	80	201.6±15.4	96.5±4.9
10	HPC4	100	254.7±18.6	
10	HPC7	80	190±15.9	98.4±1.0
10	HPC7	100	203.25±6.4	
5	XYL5	80	273.4±8.6	104.7±1.7
5	XYL5	100	307.1±4.0	
10	XYL5	80	269.8±5.9	96.0±0.9
10	XYL5	100	254.7±18.6	
20	XYL5	80	237.1±1.7	96.8±2.3
20	XYL5	100	291.8±6.0	
5	XYL7	80	266.5±9.8	100±0.8
5	DCP1	80	312.5±6.3	98.3±0.8
5	DCP1	100	306.9±7.7	

The obtained 3D-printed tablets demonstrated very good uniformity of drug load with less than 5% variability for all tested formulations (Fig.3.3). In fact, majority of the formulations demonstrated less than 1% variability, with the exception of HPC4 formulation showing 4.9% variability. Probably, this resulted due to the addition of Kollidon VA64 in the absence of PEG4000 possibly negatively impacting FDM processability [24].

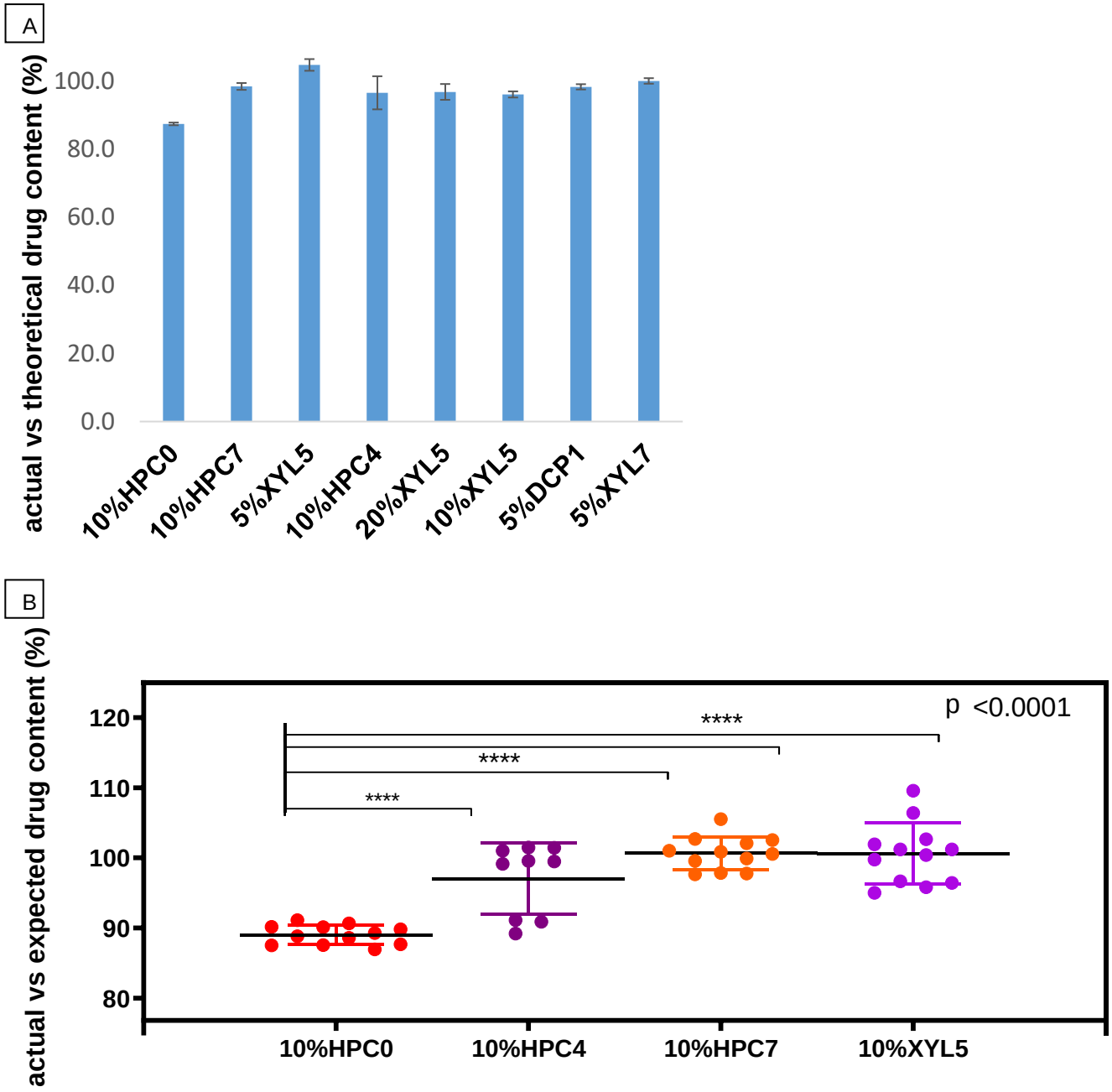

Fig.3.3. Actual drug content of FDM-printed tablets in percent of theoretical values calculated based on tablet weight given as mean (columns) and SD (bars) for different formulations (panel A). Individual values of selected formulations including mean and standard deviation (panel B). (****p<0.0001 HPC0 vs HPC7, HPC4 and XYL5). Composition of formulations given in Table 2-1

Average drug load measured on individual 3D-printed tablets was 8.76±0.04% (expected 10%, measured filament drug load 8.6%) for 10%HPC0, 9.84±0.10% (expected 10%, measured filament drug load 9.1%) for 10%HPC7 and 9.58±0.09% (expected 10%, measured filament drug load 9.9%) for 10%XYL5. Actual drug content of FDM-

printed tablets versus theoretical values calculated from tablet weight is visualized in Fig.3.3. For the majority of formulations, caffeine load in 3D-tablets was similar to target, showing accuracy of nearly 100% versus expected ,however use of HPC as single excipient (HPC0 formulation with 10% caffeine and 90% HPC), resulted in lower than expected (87%) assay (see Table 3-2). This might be attributed to the adherence of powder drug to the walls of feeding hopper or inner surfaces of the extruder [86] [82]. Flowability and caking issues occurred only with the HPC0 formulation which had the highest HPC content and may be the cause of the adherence of powder drug to the walls. The difference of assay between HPC0 and other 10% formulations was statistically significant. HPC0 though showed good uniformity of content despite the low assay (Fig.3.3). This suggests a homogenous distribution of caffeine within the polymer matrix following hot-melt extrusion at industrial setup. Incorporation of Kollidon VA64 into HPC-based matrix improved assay value, however combination of Kollidon VA64 with plasticizer PEG4000 was required to achieve both uniformity of drug load and desired load accuracy (Fig.3.3B). Similar drug load values in filaments and in 3D-printed tablets indicated that no notable degradation occurred during 3D-printing. Moreover, previous studies proved caffeine to be thermostable, with no degradation after hot-melt extrusion at 180°C followed by very high temperature (200°C) FDM 3D-printing [82] or by longer heating at 180°C during Direct Printing [18]. In general, however, active pharmaceutical ingredient degradation during filaments and 3D-tablets production remains one of main concerns, as for any drug product manufacturing at elevated temperatures.

Taken together, homogenous API distribution within the filament was achieved by HME so that tablet weight correlated closely with the determined drug load as the measured drug content was nearly 100% of the expected with one notable exception attributed to an artifact. Tablet weight and weight uniformity was variable possibly due to variable filament diameter and incomplete control over 3D-printing process. Clear benefit was gained from inclusion of plasticizers to the formulation in terms of uniformity of weight and drug load probably related to the processability of the formulations. In general, formulations with plasticizer exhibited less variability than those without plasticizer. Yet among formulations with plasticizers 10%HPC7 with 80% infill density and 10%XYL5 with 100% infill density exhibited higher weight variability presumably due to deviations in melt viscosity and lack of control of flow rate during printing.

3.4.3 Solid state analysis

DSC thermograms of caffeine showed a melting temperature of about 238°C for pure API, this peak, however, was absent in powder blends, filaments and 3D-tablets of both formulations shown in Fig.3.4. The absence of this peak in the powder blends suggested that caffeine dissolves in the molten polymeric mass at a temperature below 238°C. It is assumed that dissolution of caffeine took place also in the filaments and the tablets, hence no conclusion regarding caffeine crystallinity in the products could be reached based on DSC data.

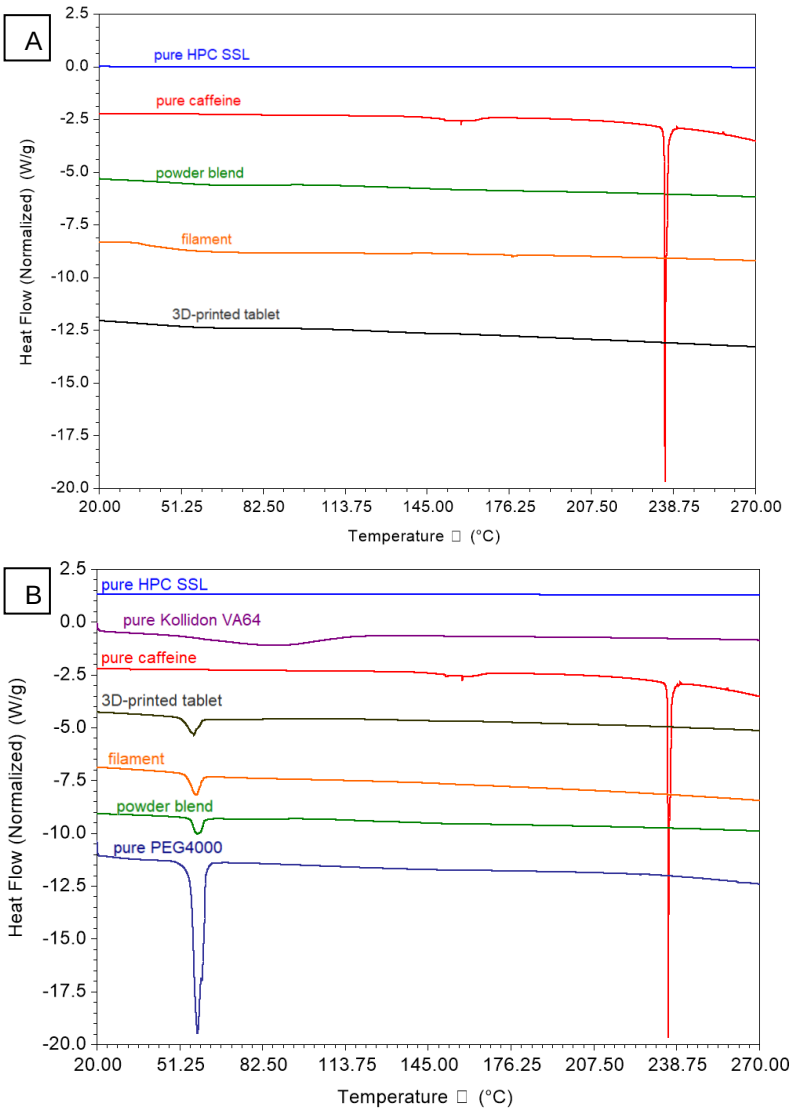

Fig.3.4. DSC thermograms of pure substances, powder blends and 3D-printed tablets for two formulations: (A) HPC0 (10% Caffeine, 90% HPC); (B) HPC7 (10% Caffeine, 45% HPC, 31.5% Kollidon VA64, 13.5% PEG4000)

Comparable results were obtained for the rest of the formulations (not shown). XRPD analysis of filaments and 3D-printed tablets provided evidence of crystalline caffeine with characteristic diffraction peaks at 12° and 27° 2θ (Fig.3.5). However, the double-peak which is characteristic of the stable polymorph II and was observed for pure caffeine and the powder blend at 27° 2θ was replaced in the filaments and the 3D-printed tablets by a single peak which is characteristic of the metastable polymorph I. This XRPD result raises concern about polymorphic transformation of caffeine in the products which would be indicative of instability and was observed for all formulations (not shown). On the other hand, there have been reports of polymorphic transition of form II to form I of caffeine due to mechanical stress [127]. Since the filaments and the 3D-printed tablets were manually ground prior to XRPD measurement, this method was not conclusive as to the crystal modification of caffeine in the

products. For deeper solid-state investigation, Raman spectral analysis was performed, which does not require mechanical manipulation or other stress for sample preparation. Spectral fingerprints of 3D-printed tablet corresponded fully to the ones of pure anhydrous caffeine used as reference (Fig.3.6). This confirmed the presence of the stable polymorphic state of caffeine in 3D-printed tablets. Needle-like particles characteristic of stable polymorph II material without aggregates as in starting caffeine powder could be seen in optical micrographs on the surface of 3D-printed tablets. These results confirm the presence of the stable polymorph II of caffeine in needle-like crystal form in 3D-printed tablets. This confirmation is essential for monitoring and control of the full cycle of manufacture by a process involving two consecutive melting steps i.e., hot melt extrusion and 3D-printing, and likely dissolution of the API in the melt and recrystallization. It is especially crucial for understanding of novel, non-established pharmaceutical production techniques such as 3D-printing and is required by regulatory bodies. Finally, knowledge of crystal modification of the API is critical for the interpretation of dissolution results of the dosage form.

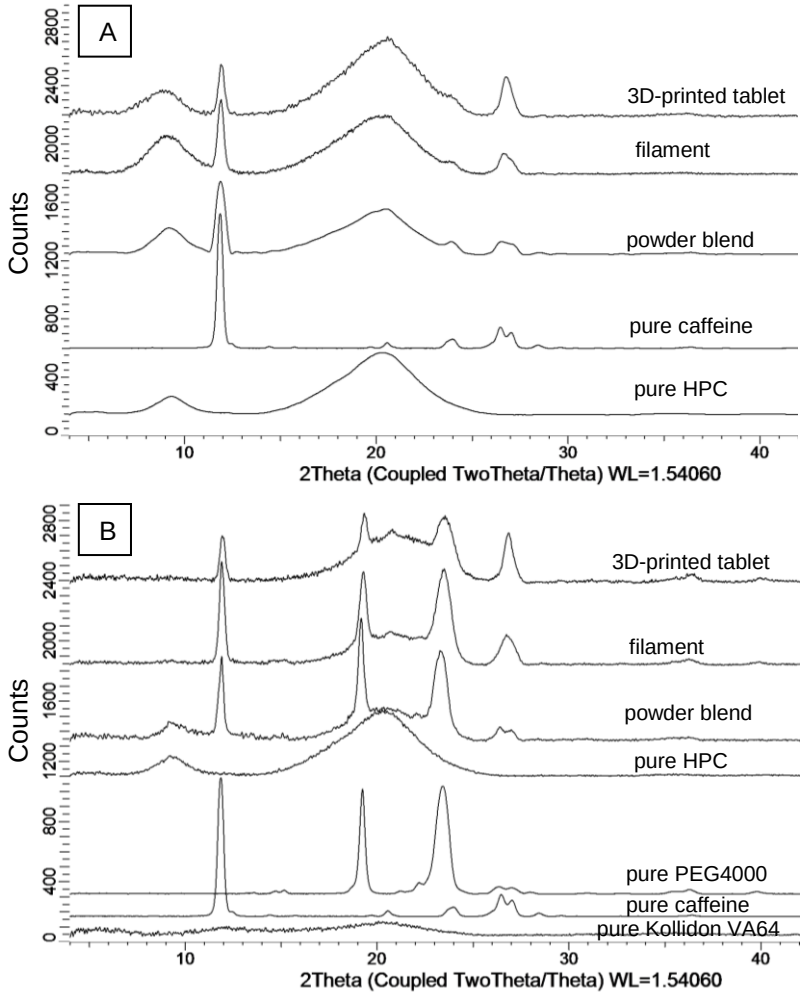

Fig.3.5. X-ray powder diffractograms of pure substances, powder blends, filaments and 3D-printed tablets for two formulations: (A) HPC0 (10% Caffeine, 90% HPC); (B) HPC7 (10% Caffeine, 45% HPC, 31.5% Kollidon VA64, 13.5% PEG4000)

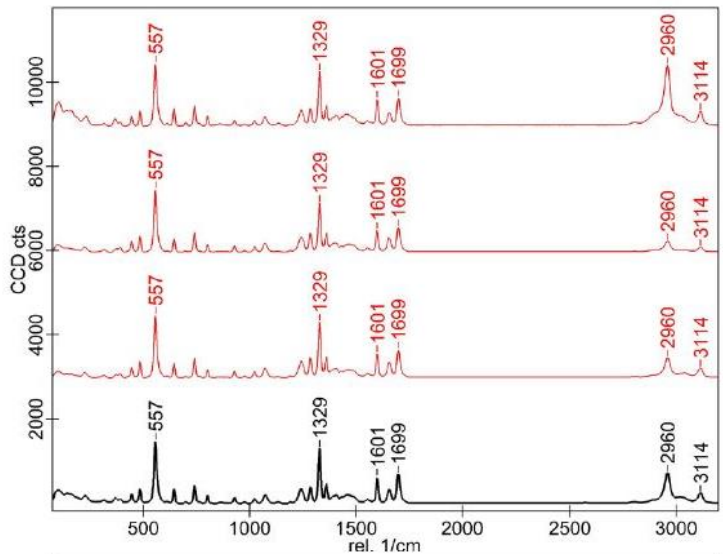

Fig.3.6. Raman cascaded spectral comparison of caffeine: Three averaged spectra for 3D-printed tablet individual Raman maps of the 20% XYL5 formulation (red spectra) compared to that of anhydrous caffeine used as reference (black spectrum)

3.4.4 Dissolution studies

Caffeine has a pKa = 14.0 at 25°C and is freely soluble in the used dissolution media [128]. Dissolution tests on different formulations are shown in Fig.3.7. Tablets of all compositions qualified for rapid release (> 85% dissolution after 30 minutes) or very rapid release (> 85% dissolution after 15 minutes). Release profiles were enabled via formulation selection and tablet inner and outer geometry design parameters. Infill density, drug load and printing temperature were found to influence significantly dissolution rate depending on the formulation (see below). It should be pointed out that rather high infill densities were generally chosen in order to maximize weight and dose of the tablets.

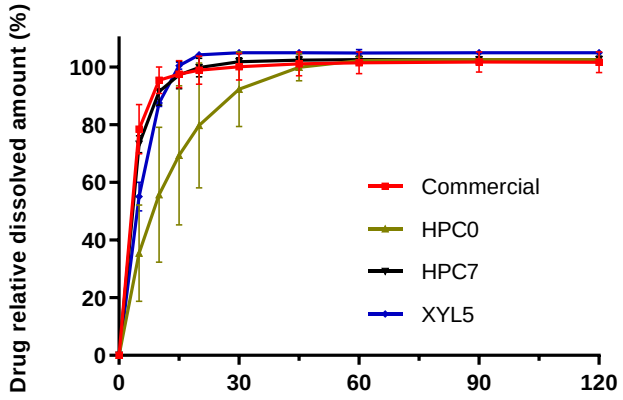

Fig.3.7. Drug dissolution profiles of FDM 3D-printed caffeine tablets. Three formulations with 10% drug load at low (80%) infill density are shown in comparison to commercial tablets

Formulations HPC7 (main component HPC SSL) and XYL5 (main component Kollicoat IR) with 10% drug load and 80% infill density met very rapid release criteria and demonstrated similar drug release profile to the commercial tablets (Fig.3.7). Using HPC SSL as a single matrix former resulted in slower dissolution rate than commercial film coated tablet and variable drug release at early time points (Fig.3.7). Possible synergism of rapidly dissolving polymer Kollidon VA64 with pore-former PEG4000, or hydrophilic plasticizer xylitol with pore-former maltodextrin when incorporated in polymeric matrix is thought to explain the faster dissolution rate.

Further, the infill density was increased to 100% to investigate feasibility of producing higher drug load while keeping the same tablet dimensions. For the majority of the formulations, tablets with denser network demonstrated slower dissolution rate (Fig.3.8 and Fig.3.9) consistent with previous reports [24] [129]. The faster dissolution rate from lower density tablets is likely attributed to its higher surface area to volume ratio as compared to high density tablets [24]. Interestingly, extent of the infill density effect varied depending on formulation from a critical effect (XYL5; 10% Caffeine, 23% HPC, 45% Kollicoat IR, 13% Xylitol, 9% Maltodextrin), through trending (HPC0; 10% Caffeine, 90% HPC or HPC4: 10% Caffeine, 58.5% HPC, 31.5% Kollidon VA64), to negligible (HPC7, 10% Caffeine, 45.2% HPC, 31.3% Kollidon VA64, 13.5% PEG4000) (Fig.2.8). This difference of infill density effect between the formulations may be related, on one hand, to the difference in tablet weight between the two infill densities. The measured weight difference for HPC7, for instance, is much smaller than for HPC4 (Table 3-2). This would conceivably correspond to a smaller difference in internal surface area between the infill densities for HPC7 than for HPC0 since the outer dimensions of the tablets were identical, which is reflected in the dissolution rate [130]. On the other hand, the difference of infill density effect on dissolution rate between HPC7 and XYL5 (Fig.3.8) might be explained by their composition. XYL5 formulation containing a high amount of Kollicoat IR was visually observed to dissolve rather slowly as also described before [24] resulting in matrix erosion controlled system for which infill density played a statistically significant role (Fig.3.8) not meeting rapid release criteria at high infill density, while HPC7 was observed to dissolve much faster allowing no detectable infill density effect. The inclusion of PEG4000 as well as Kollidon VA64 in HPC7 notably resulted in this fast dissolution rate, with both low and high infill densities meeting very rapid release criteria (Fig.3.8) while incorporation of solely Kollidon VA64 in HPC4 led to a statistically significant lower dissolution rate at high infill density (Fig.3.8) which, however, may be related to the large tablet weight of this formulation (see above). Clearly, measurement of tablet porosity and specific surface area will be required in the future to better delineate these effects.

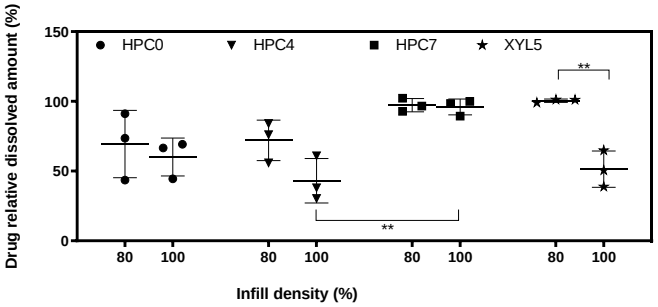

Fig.3.8. Panel A: Drug dissolution profiles of FDM 3D-printed caffeine tablets. Comparison between low (80%) and high (100&) infill density of three formulations with 10% drug load. Panel B: Relative dissolved drug amount at 15 min time point of FDM 3D-printed caffeine tablets of four formulations with 10% drug load at low (80%) and high

(100%) infill density. **P<0.01 80% vs 100% infill density of XYL5 formulation. **P<0.01 100% infill density of HPC4 formulation vs 100% infill density of HPC7 formulation

Further, formulation XYL5 enabled to study effect of drug load (5-20%) on drug release due to its most favorable mechanical properties leading to 3D-printability within the desired drug load range. Dissolution rate was found to be dependent on drug load (Fig.3.9). For low-density tablets, 10% and 20% drug load showed superiority over 5% in terms of dissolution rate, meeting very rapid release criteria (more than 85% drug dissolved in 15 min). Surprisingly though, the formulation with 10% drug load exhibited faster dissolution than the one with 20% drug load. For 100% infill density, increasing drug load to 20% seemed to slow down dissolution rate in comparison to 10%, but both formulations did not meet rapid release criteria. Hence, also among high density FDM-tablets, those with 10% drug load showed the fastest release nearly meeting rapid release criteria, even though dissolution rate was highly variable between the samples (87±12.4% after 30 min). This result was unforeseen as high drug load was expected to have the fastest release rate and might be related to differences in tablet weight, the 10% tablets having a smaller weight that the 20% tablets at the high infill density (Table 3-2), or the difference in process parameters (see also below). Tablets with 5% drug load demonstrated slowest dissolution such that rapid release criteria were not met either for low or high infill density (Fig.3.9). This is probably due to higher polymer-to-drug ratio impeding dissolution, as the API particles become more engulfed by the polymer and are less accessible to solvent [131].

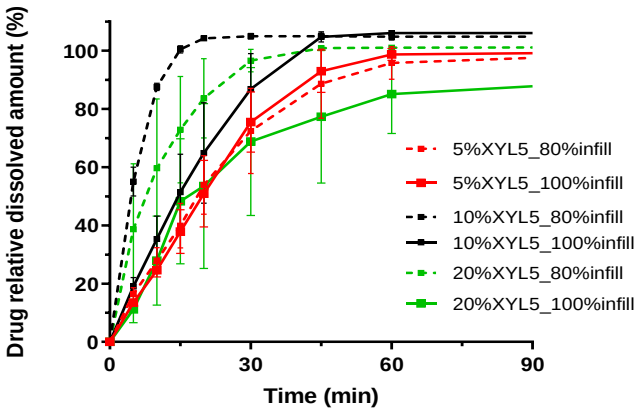

Fig.3.9. Drug dissolution profiles for FDM 3D-printed caffeine tablets. Comparison of three drug loads, 5%, 10% and 20% at low (80%) and high (100%) infill density of XYL5 formulation

The slower drug release tentatively shown by low drug loads , needs to be addressed due to the increased need for low-dosage forms required for pediatric patients and the rapidly growing segment of highly potent APIs in pharmaceutical industry [132]. In this study, incorporation of dibasic calcium phosphate (DCP) in combination with PEG4000 to the formulation resulted in achievement of rapid release requirements (Fig.3.10, DCP1) for 3D-printed tablets with 5% drug load and both low and high infill density. This was a considerable improvement upon the XYL5 formulation and is in line with previously reported [126] potential of high-melting fillers to accelerate dissolution rate of FDM 3D-printed tablets. Increase of drug load to 10% in DCP1 formulation resulted in non-printable/brittle filaments and further increase in drug load was not evaluated for this formulation. Interestingly, denser network exhibited minor effect on caffeine release profile for dosage forms with 5% drug load within both

tested formulations (Fig.3.10) contrary to the observations made at higher drug loads. Incorporation of xylitol-maltodextrin as a pore-forming combination into HPC plus Kollidon VA64 matrix (instead of Kollicoat IR plus HPC, i.e., XYL7 versus XYL5) resulted in rapidly dissolving tablets at low infill density (Fig.3.10). However, the mechanical properties were poor and FDM printing with higher infill density or drug load was not feasible.

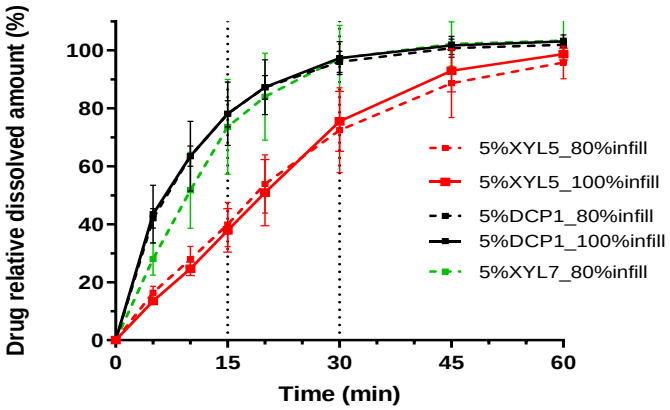

Fig.3.10. Drug dissolution profiles of FDM 3D-printed caffeine tablets. Comparison of three formulations with low-drug load (5%) at low (80%) and high (100%) infill density

Interestingly, a posteriori analysis of the results showed that small difference of 10°C in 3D-printing temperature may have an impact on drug dissolution rate independently of formulation and infill density. After 15 min, mean relative drug amount dissolved was 52.6±5.6% for the formulations 3D-printed at 170°C vs 81.7±7.7% for formulations 3D-printed at 160°C. 8 formulations with 3 replicates each (total n=24) for $T_{printing}$=160°C and 5 formulations with 3 replicates each (total n=15) for $T_{printing}$=170°C were included in this evaluation. Among possible reasons, stronger cohesion between the printed layers and polymer chemical crosslinking [133] [134] might be suggested and needs to be further investigated . This evokes a risk for robustness, as temperature tolerances could be wide for various 3D-printers. Hence, well-controlled 3D-printing parameters during the process as part of quality assurance strategy should be considered.

3.5 Conclusions

Successful development of rapid release 3D-printable formulations was demonstrated via formulation selection and process parameters adjustment. Industrial relevance of the work consisted in the use of scalable hot-melt extrusion equipment and process, choice of wide drug load, use of broadly accepted excipients approved also for pediatric use, scalable batch size of several hundred grams, use of lowest possible temperature and quality control pertinent for batch release. Necessary process temperature depended on plasticizer, drug load and thermostable filler, while plasticizer, drug load, infill density depending on the formulation, and, interestingly, printing temperature influenced immediate release product characteristics *in vitro* with a hydrophilic model compound. Formulation and process development for IR dosage forms containing poorly water-soluble / lipophilic drugs presents a greater challenge to be addressed in subsequent studies.

In the future, the list of developed formulations should be expanded and tested with additional model compounds with varying physicochemical properties with respect to printability, quality and release profile in order to move

towards establishing a formulation toolbox for FDM tablet printing. Studies encompassing measurement of filament brittleness and viscosity of formulation melt should be part of a systematic formulation toolbox development. Moreover, process analytical technologies such as online measurement of filament thickness during hot-melt extrusion and online measurement of the amount of deposited mass during 3D-printing should be introduced to guarantee process robustness and reproducibility. Finally, as internal tablet microstructure may affect uniformity in dissolution profile and other drug product quality attributes, material and process development should be targeted towards accuracy and low variability of structural characteristics of pharmaceutical 3D-printed tablets.

4 Chapter 4

(Re)Creating amorphous solid dispersions on-demand for BCS class IV model drug via 3D-printing[3]

Summary

Interest in Fused Deposition Modeling (FDM) 3D-printing has been emerging due to its potential for personalized dosage strengths and flexible near patient manufacturing. To formulate biopharmaceutically challenging poorly water-soluble compounds, the approach of formation of amorphous solid dispersions (ASDs) for dissolution enhancement, potentially improving bioavailability is generally established. Hot-melt extrusion (HME) is widely used to achieve ASD but the risk of recrystallization during storage due to thermodynamic instability is a common issue. This study investigates the manufacture of ASD of a poorly water-soluble API by FDM 3D-printing in view of the potential advantage of shorter stability requirement in case of on-site production. Lumefantrine, a BCS class IV compound, and hydrophilic polymers hydroxypropyl-cellulose (HPC) SSL with or without Kollicoat® IR were used as matrix formers containing additionally hydrophilic plasticizers and pore formers. Small grid-designed tablets with a size acceptable for children from 6 years of age with 10% drug load were successfully 3D-printed, exhibiting good uniformity of weight and percent drug content for both 80% and 100% infill densities. FDM printability declined with the use of Kollidon® VA64 because of filament brittleness. Moderate (≈5%) chemical degradation of thermolabile lumefantrine resulted during filament production by HME with no additional degradation during 3D-printing for HPC-based formulation, but additional degradation of about 10% for Kollicoat® IR-based formulation. Crystalline lumefantrine was found in filaments already two months after manufacturing and lumefantrine was present in filaments in a mixture of crystalline and amorphous state at the time of tablet manufacture, as determined by highly sensitive and specific confocal Raman micro-spectroscopy. Raman mapping confirmed that the API was in the fully amorphous state in tablets at least one month after manufacturing. Hence, following 3D-printing of the filaments it was possible to (re)create ASD in the final tablets. Solid and total volume, closed and open pore volume, as well as surface area of 3D-printed tablets were measured by µCT. Dissolution studies in-vitro did not show significant impact of infill density modifications on the drug release profile, which correlated with morphological measurements for HPC-based formulation but not for Kollicoat® IR-based formulation. To conclude, it was feasible to (re)create fully amorphous solid dispersions by 3D-printing on-demand, even when drug was present partly in crystalline form in the filaments. FDM 3D-printing featuring two hot-melt process steps could be an interesting possibility to produce ASD at the point-of-care for improving bioavailability. This is particularly promising for manufacturing of personalized dosage forms with poorly water-soluble drugs in a near patient setting where no long-

[3] Fanous, M, Sobczuk, A, Gold, S, Malak, B, Hirsch, S, Ogorka, J, Imanidis, G, *(Re)Creating amorphous solid dispersions on-demand for BCS class IV model drug via 3D-printing*, Eur J Ph Bioph, 2021, *submitted*

term stability is required. Formulation-dependent differences in processability, morphological tablet characteristics and dissolution behavior require further investigation to reach mechanistic understanding and manufacturing process control.

4.1 Introduction

Over the past years, scientific interest in 3D-printing of pharmaceutical dosage forms has been increasing [135] [67] [16]. Via 3D-printing, solid dosage forms with tailored dosage strengths, release profiles and designs could be fabricated through layer-by-layer addition of materials based on a digital model [16, 19]. Moreover, 3D-printing could create a unique opportunity for decentralized manufacturing of drug products at points-of-care such as hospitals and pharmacies [80]. For on-site production, Fused Deposition Modeling (FDM) 3D-printing could be beneficial as the process involves melting and deposition of a thermoplastic filament without loose powders or solvents [92]. Moreover, FDM generally does not require post-processing and creates mechanically strong tablets [93]. Challenges of FDM include risk of heat-induced drug degradation and slow dissolution, as well as dependence on mechanical properties of the filament [92] [26] [84].

The need to develop 3D-printed dosage forms with specific drug release profile to meet bioavailability and therapeutic requirements has been addressed and possibilities utilizing formulation and dosage form design for immediate and controlled release were discussed [21] [136]. Active pharmaceutical ingredients (APIs) with poor water solubility, i.e., biopharmaceutics classification scheme (BCS) class II and IV compounds potentially exhibiting limited bioavailability may be particularly challenging in this respect. Amorphization in general is a well-known approach to create an enabling formulation providing increase in apparent API solubility [94] [95] [96]. Hot-melt extrusion (HME) technology is used to create amorphous solid dispersions (ASD) to serve this purpose [103] [104]. Moreover, HME often leads to bioavailability enhancement not only due higher saturation solubility, but also because of increased specific surface area [105] [106]. For example, bioavailability of poorly-soluble anti-malarial drug lumefantrine could be increased via hot-melt extruded ASD up to 48-fold relative to that of the conventional formulation [107] [108]. However, any amorphous solid dispersion is at risk of recrystallization during storage, given that the crystalline form of the drug is thermodynamically more favorable due to lower Gibbs energy [94] [109] [110]. Depending on drug-polymer ratio and miscibility and material hygroscopicity, partial or full recrystallization may occur [137] [21]. Recrystallization would often lead to partial loss in increased apparent solubility [111], which was intended to be achieved via amorphization.

Being a hot-melt process by design, FDM may lead to drug amorphization e.g. if the printing process is performed at higher temperature than the melting point of the compound, or following its dissolution in molten formulation and the compound has sufficient miscibility with the formulation matrix [136] [113] [85] [89] [24]. Hydroxypropyl-cellulose (HPC)- and Kollicoat® IR-based formulations were previously demonstrated to be FDM-processable [22] yet the explored model API (caffeine) is a compound with bad glass forming ability and was non-miscible in solid state with these polymers, hence ended up in crystalline form in the produced 3D-printed tablets. It was, therefore,

interesting to investigate whether another API, such as lumefantrine, which as noted above produced ASD in conventional formulations, would also result in ASD with the mentioned polymeric matrix formers by FDM 3D-printing. Given that FDM 3D-printing entails two consecutive hot-melt processes, i.e., preparation of filament by HME and 3D-printing of the tablets, the question arises as to whether amorphous or crystalline state of API in the filament would influence the solid state of API and thus ASD production in the final tablets. This question is particularly relevant as it impacts flexibility of formulation development. It should be further considered that plasticizers which are often added to improve HME and FDM processability of the polymer matrix via reduction of glass transition temperature (Tg) may lead to phase separation and drug recrystallization. Importantly however, since 3D-printing is intended for near patient manufacturing, the risk of recrystallization could potentially be circumnavigated because of the significant reduction of the time between formation of ASD and drug administration to the patient.

Since such critical product parameters as dissolution rate, apparent drug solubility and bioavailability may be influenced by solid state conversions, it was important in the present work to determine with maximal analytical precision (such as using Raman microscopy) evidence of drug recrystallization in drug products and intermediates. A narrow range of infill density of 80% and 100% was used, as the work was focused on achieving ASD and not studying acceleration of release rate by morphological variation.

The aim of this work was to investigate FDM 3D-printing technology as a tool to achieve ASD at the point-of-care to guarantee bioavailability independently of the solid state of the intermediate product. This comprised to:

- Explore feasibility of (re)creating fully amorphous solid dispersions from filaments in which a BCS class IV drug substance was at least partially crystalline
- Develop tablets with good uniformity of weight and content based on pharmacopoeia requirements
- Develop appropriately sized tablets for pediatric populations
- Translate between programmed CAD design and 3D-printed structure

4.2 Materials and methods

4.2.1 Materials

Lumefantrine (Novartis Pharma AG, Switzerland), molecular weight 528.9 g/mol, was used as a model compound. Formulation strategy described previously was followed (Fanous, 2020). Hydroxypropyl-cellulose (HPC SSL, Nisso Chemical, Japan) and polyvinyl alcohol/polyethylene glycol graft copolymer (Kollicoat® IR, BASF, Germany) were admixed with lumefantrine as primary matrix formers. Polyethylene glycol (PEG4000P, Clariant, Germany) or xylitol (Xylisorb® 300, Roquette, France) were employed as hydrophilic plasticizers and pore formers. Maltodextrin (Maldex® 120,Tereos, Germany) was was added as disintegration aid to Kollicoat® IR-based formulation.

4.2.2 Methods

4.2.2.1 Hot-melt extrusion (HME)

Powders were accurately weighed into 0.5 L bottles to give a batch weight of 100 g and were mixed via diffusion blending for 20 min at 32 upm by T2 Turbula™ mixer. A twin-screw hot melt extruder (Thermo Scientific™

Pharma 11™, Karlsruhe, Germany) was used to manufacture filaments. The screw design used was described previously [22].

The measured temperatures for zones 2, 3, 4,5-8 were 38-43°C, 60-80°C, 100-140°C, 120°C-141°C; die temperature was 120 °C-142°C depending on the formulation (see Table 4-1). Feed rate was about 4 g/min, screw speed 17±7 rpm. Extrusion was carried out through a 1.75 mm die nozzle with a pressure control (maximum 90 bar).

Table 4-1 Formulations compositions and process parameters

Formulation component (% w/w)	H0	H7	X5	X8
LUM566	10.0	10.0	10.0	10.0
HPC SSL	90.0	44.8	22.6	44.6
Kollidon VA64		31.6		22.3
Kollicoat® IR			44.8	
PEG4000		13.5		
Maltodextrin			9.0	9.5
Xylitol			13.7	13.7
Process parameters				
T zone2 (°C)	40	25	25	25
T zone3 (°C)	80	60	60	60
T zone4 (°C)	100	100	100	100
T zone5 (°C)	140	120	140	140
T zone6(°C)	140	130	140	140
T zone7 (°C)	142	135	140	140
T zone8 (°C)	142	140	145	135
Tdie (°C)	142	135	145	135

Feeding speed (rpm)	12	10	8	10
extrusion speed (rpm)	20	15-20	15	15
Torque (%)	21	8	22	10
Pressure (bar)	1-2	0	up to 8	0
3D-printability	yes	no	yes	no

4.2.2.2 Fused deposition modeling (FDM) 3D-printing

The template used to print the dosage form was designed with FreeCAD 0.13 software. The selected geometry was an oval tablet with grid infill pattern (Fig.5.1). The tablet was designed with a size of 9 x 5 x 4 mm (width x length x height) with one continuous outer layer (altitude shell) and no continuous bottom/top layers. A BoltPro™ 3D-Printer (LeapFrog™, Netherlands) was used for FDM. 3D-printing was performed through a nozzle with d=0.5 mm, using a printing speed of 1000 mm/min, with a primary layer speed of 50% of the default 1000 mm/min and height of 0.15 mm. Tablets with both 80% and 100% infill densities were printed at 165°C for FDM processable formulations. The manufactured tablets were weighed and their dimensions were measured with a caliper.

4.2.2.3 Drug load, degradation products and uniformity of percent drug content

A tablet was dissolved in 100 mL of sample solvent (consisting of hexanesulfonic acid, water, acetonitrile, TFA) and the drug concentration was determined by HPLC (HP-1100, Agilent Technologies, UK) with YMC Pack-Pro C-18 5 µm, 150 x 3 mm column (YMC Co., Japan), maintained at 30°C. The injected volume was 10µl. The gradient consisted of two components: mobile phase A (20 mM hexanesulfonic acid: acetonitrile: TFA; 490:510:1, v/v/v) and mobile phase B (acetonitrile: TFA, ; 1000:1 v/v) starting with the former at 100% and decreasing gradually to 48% after 16 min, and increasing back to 100% after 20.1 min. The flow rate was 1 ml/min and the UV detection was carried out at a wavelength of 265 nm. All measurements were performed in triplicate. A value of each by/degaradation product (BDP) was measured as area percentage and 3 main BDPs were reported. Values of randomly selected (n=3) and separately analyzed samples were normalized by weight to calculate the average percent drug content.

4.2.2.4 Dissolution test conditions

A USP2 semi-automatic tablet dissolution system Sotax AT7 (Sotax AG, Aesch, Switzerland was used to perform the studies. In vitro release profiles of the tablets (n=3 for each infill density) were studied at 0.1N HCl with 0.5% cetyl trimethylammonium bromide (CTAB). Each tablet was pre-weighed and placed in the vessel containing 900 mL of dissolution medium. Dissolution was carried out with a paddle speed of 100 rpm at 37 °C for 90 minutes. The paddle speed was then increased to 250 rpm for further 30 minutes to ensure full dissolution. Samples (10 ml each) were collected at time points 0, 5, 10, 15, 20, 30, 60, 90 and 120 min. The dissolution medium was replenished after each sampling with an equivalent amount of 0.5%CTAB 0.1N HCl solution. The drug concentration of the

samples was measured by a spectrophotometer (Perkin Elmer Lambda 25 UV) at 342 nm. Expected 100% dissolution value was calculated based on the expected amount calculated from the tablet weight. Dissolution profiles were visualized by plotting percentage of drug dissolved against time. At least 80% of drug relative dissolved amount (average n=3) after 30 min was defined as rapid release criteria in agreement with Food Drug Administration (FDA) guidelines[123].

4.2.2.5 X-ray powder diffraction (XRPD)

Powder blends were directly dispensed onto the surface of a quartz sample holder. 3D-printed tablets were gently/manually ground with mortar and pestle prior dispensing onto the sample holder. Filaments were analyzed about 2.5 months after manufacturing, 3D-printed tablets – during the 1st month after manufacturing. XRPD analyses were performed on a diffractometer using a K430 X-ray generator with a copper anode (voltage: 40 kV, current: 40 mA. The X-ray generator was a long line focus sealed tube (Siemens; Germany, Cu anode with a Kα line at 1.54 Å, operating at voltage of 40 kV and current of 20 mA). One 2D VÅNTEC-500 Area detector (4 channels, filled with argon-ethane mixture) was used to collect the data. 2θ angles were calculated, ranging from 1 to 18° and from 18 to 36°. Diffractograms were generated with the software Diffrac.EVA V4.0 from Bruker, USA.

4.2.2.6 Differential scanning calorimetry (DSC)

DSC measurements were performed using a Q2000 DSC (TA instrument, New Castle, PA) under nitrogen flow of 50 ml/min. Samples between 1 and 2.5 mg were analyzed using punctured aluminum pans, an empty pan was used as reference. A heating rate of 10°C/min was set between -20°C and 300°C. Software Trios v4.4.1 (TA Instruments, Inc., Waters Corporation, MA, USA) was used.

4.2.2.7 Raman mapping

Raman spectra were obtained with a Confocal Raman microscope (WiTec alpha 300 R, Germany) as described previously [138]. In brief, filaments and their corresponding printed tablets were embedded in epoxy resin and processed using an ultra-microtome to obtain level block cross-sections. For printed tablets, surface scans were also performed on the ready-made tablet prior to sample cross-sectioning. Filaments were analyzed 3-4.5 months after manufacturing, tablets – at least 5 weeks after manufacturing. Reference material spectra, including that of lumefantrine in both crystalline and amorphous states, were obtained by single spectral measurements whereby characteristic peaks for each species were defined for hyperspectral processing.

Area scans and their corresponding hyper-spectra generation were performed firstly on a large-scale, low resolution modes to gain an overview. These were 1100x1100 µm at 10 µm spatial resolution and 4000x3500 µm at 20 µm spatial resolution for the filament and printed tablets respectively. This was followed by 400x300 µm at 1 µm spatial resolution scans performed at two different spots for each sample. Average spectra extraction took place based on reference spectra peak evaluation performed automatically by the software. These were 1635 rel. cm–1 for crystalline lumefantrine and 1631 for cm–1 for amorphous lumefantrine. Hyperspectral data offset and baseline polynomial correction, cosmic ray removal, spectral filter application, average spectral extraction and spectral map deconvolution were performed using Witec Project FIVE 5.1 software.

4.2.2.8 Xray microcomputed tomography (microCT)

The internal structure of 3D-printed dosage forms was visualized using X-ray microcomputed tomography (Skyscan 1172, Skyscan, Kontich, Belgium). Samples were scanned using 2000 projections at a resolution of 5.93 μm/voxel at 59 kV Acceleration voltage and 167 μA current. Image reconstruction was conducted with NRecon software (Bruker, USA). For visualization of the created mesh, DataViewer software (Bruker, USA) was used. Threshold and post processing settings were as following: 1. For Renyi's entropy on pilot sample: 101 gray value; 2. Denoise: Outlier removal at 3 pixel (10 iterations); 3. Closed volume generation: 3x reslice and binary fill holes respectively. For solid, open and closed pores volume voxel count was performed, for surface area pixel count was executed following marching cubes algorithm.

4.2.2.9 Data analysis

The data are presented as mean ± SD, and the differences between two infills for each formulation were analyzed by Holm-Sidak t-tests method (GraphPad Prism, version 7.0, GraphPad Software, San Diego, CA). The statistical significance was considered at $p < 0.05$.

4.3 Results and discussion

4.3.1 Processability of hot-melt extrusion and 3D-printing

Table 4-1 shows details regarding compositions and process parameters. HPC- and Kollicoat® IR-based filaments with 10% drug load were successfully extruded, while the settings were adjusted in a continuously monitored process. Extrusion was carried out at higher temperature than melting temperature of lumefantrine. Both formulations H0 (10%lumefantrine - 90%HPC SSL) and X5 (10%lumefantrine - 23%HPC SSL - 45%Kollicoat IR - 9%Maltodextrin - 14%Xylitol) were easy to handle and 3D-printable at 165°C. Incorporation of Kollidon® VA64 (formulations H7 and X8) caused increased brittleness of filaments as reported previously [24], which resulted in nonprintable formulations despite addition of plasticizers. This observation about the X8 formulation containing 10% lumefantrine is in agreement with the result obtained previously with XYL7 formulation containing 10% caffeine [22] which had very similar composition as X8 and was also non-FDM-printable. On the contrary, a 10% caffeine - Kollidon® VA64 - PEG4000- formulation, which had a comparable composition as formulation H7 (Table 1) was processable by 3D-printing [22]. This difference is probably due to the effect of the different API on the filament's mechanical properties which becomes apparent for Kollidon® VA64 - PEG4000 but not Kollidon® VA64 – Maltodextrin – Xylitol formulation. One should be mindful, therefore, that adequacy of excipient compositions for FDM 3D-printing can be dependent on the API in question. The mechanism of API – excipient interaction and its influence on filament mechanical properties and printability clearly requires further investigation.

When HPC SSL and Kollicoat® IR were used as main components, the formulations were printable both with 10% lumefantrine and previously investigated 10% caffeine [22]. Notably, Kollicoat® IR-based formulation was printable with up to 20% caffeine load, which in combination with the above Kollidon® VA64 - PEG4000 results may suggest that caffeine favors FDM printability with the present formulations.

The formulation with Kollicoat® IR, however, requires elevated extrusion temperature and pressure, as Kollicoat® IR has high melt viscosity (above 10 kPa*s at processable temperatures). Further, Kollicoat® IR has a high Tm (208 °C) and exhibits a smaller difference between T_g/T_m and $T_{degradation}$ in comparison to Kollidon VA64 (208 and 200 °C versus 101 and 230 °C, respectively) [139]. The processing temperature of Kollicoat® IR thus could not be further increased due to degradation onset, making Kollidon® VA64 easier to work with.

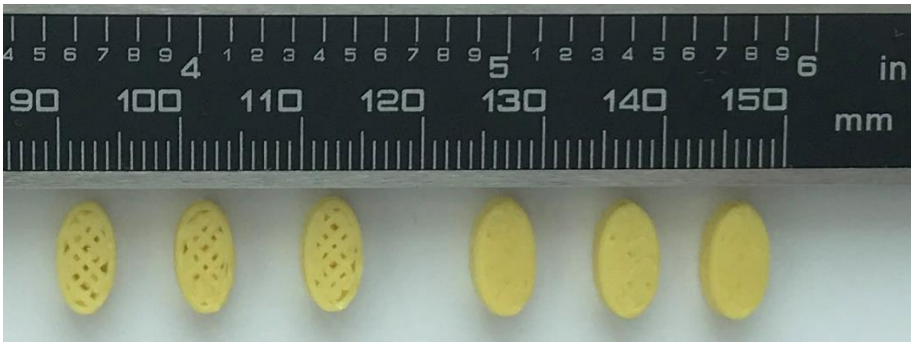

Fig.4.1. Photographs of 10% lumefantrine 3D-printed tablets (H0: 10% lumefantrine - 90% HPC SSL) with (left) 80% and (right) 100% infill density

4.3.2 Weight uniformity and morphological characteristics of 3D-printed tablets

Measured dimensions of 3D-printed tablets were in good agreement with the design, showing deviation less than 1.7%, 1.1% and 1.6% for x, y and z axis, respectively, for both FDM-printable formulations (Table 4-2). Tablets programmed with 100% infill density demonstrated excellent weight uniformity with relative standard deviation of approximately 1.5%. For 80% infill density, Kollicoat ® IR-based tablets showed up to 4.2% weight variability and HPC-based ones up to 7.2% weight variability. This variability was larger than the one obtained for 100% infill density, but still met regulatory standards for weight uniformity according to US Pharmacopoeial Convention, 2003 [140] . The increase in weight at 100% compared to 80% infill density (≈13% for H0 and ≈16% for X5) was for both formulations similar and statistically significant.

Accessible porosity, relative and solid density, close pores volume, as well as specific surface area by weight and by volume were precisely quantified based on µCT measurements. For formulation X5, 3D-printed tablets with denser network (100% infill density) showed significant increase in relative density ($p<0.000001$) and decrease in accessible porosity ($p< 0.001$) compared to 80% infill density tablets (Table 2), while differences in specific surface area did not reach statistical significance. For the formulation H0, on the other hand, 3D-printed tablets with programmed 80% and 100% infill density showed similar morphological characteristics that did not differ statistically. Actual densities (Vsolid/Vtotal) of the X5 formulation were closer to the programmed infill values, than for H0 which exhibited lower measured than programmed density values. In addition, 3D-printing of formulation H0 resulted in tablets with more variable structural characteristics within the same infill design. One explanation for this might be the air entrapment which resulted in less consistent FDM 3D-printing for the formulation H0. This assumption is supported by higher percentage of closed pores per weight in H0 tablets (see Tab.4-2). Higher average weight recorded for 3D-printed Kollicoat® IR-based tablets compared to HPC-based tablets was in line with

differences in solid densities calculated by µCT (about 1.23 g/cm3 versus 1.15 g/cm3, respectively). Different morphological response of the formulations to the same infill modification might be related to different melt viscosity of the formulations during 3D-printing process and post-process shrinkage. These results indicate a need for process verification for each individual formulation in order to achieve precise drug dosing by FDM 3D-printing.

Table 4-2 Uniformity of weight and morphological characteristics for lumefantrine tablets

Formulation code	Programmed infill density (%)	Measured relative density* (%) (mean±std)	Finished printed tablet weight** (mg) (mean±std)	Accesible porosity* (%) (mean±std)	Closed pores volume* (mm3) (mean±std)	Specific surface area by volume* (mm-1) (mean±std)	Specific surface area by weight* (mm2/g) (mean±std)
H0	80	73.9±9.1	128±9.1	13.2±4.4	1.2±0.8	4.8±0.8	5.8±0.8
H0	100	83.9±12.4	152±2.3	7.9±6.4	1.9±1.1	4.2±2.2	4.6±3.0
X5	80	82.9±2.2	142±5.9	8.6±1.1	0.9±0.1	4.7±0.4	4.6±0.4
X5	100	95.6±1.0	163±2.3	2.1±0.7	1.1±0.2	2.7±0.2	2.3±0.2

* Average ± standard deviation of n=3 ** Average ± standard deviation of n=6

4.3.3 Drug load and degradation products

The drug load was ≈9.4% in filaments versus 10% nominal drug load in powder blends for both H0 and X5 formulations (see Table 4-3) after 8 months of storage at ambient laboratory conditions with minimal protecting packaging. This might be explained by lumefantrine degradation primarily during hot-melt extrusion supported by the presence of degradation products after filament production. Lumefantrine is known to degrade under thermal stress, however the degradation mechanism is complex and not fully understood [141] [142]. Degradation products were not detectable in representative powder blends of drug substance and excipients (not shown). Assay values of 3D-printed tablets demonstrated very good uniformity of content with less than 0.15% variability. For formulation H0, assay values for 3D-printed tablets and filaments were similar, suggesting no additional degradation during FDM printing process and storage for additional 3 months. Interestingly, a lower level of degradation products in H0 3D-printed tablets was observed, which might suggest further decomposition of by-products during/after FDM-printing. 3D-printing of X5 filaments resulted in lower drug load (≈8.6%) and higher levels of degradation products in the tablets, measured after 5 months storage at room temperature. Taking into account similar FDM processing temperatures, chemical interaction between formulation components and lumefantrine most likely caused its higher degradation following 3D-printed tablet production. In particular, polyethylene glycol (PEG) chains in Kollicoat® IR might be a cause of oxidative stress [120, 121], leading to degradation of lumefantrine.

Table 4-3 Assay and degradation products in selected lumefantrine formulations

Formulation	Product type	Theoretical drug load (%)	Actual drug load (%)	By/degradation product (BDP)1 (%product)	BDP2 (%product)	BDP3 (%product)	HME temperature (°C)	3D-printing temperature (°C)	Age (months)
H0	Filaments	10	9.37±0.027	0.40±0.002	1.42±0.006	1.84±0.003	142	n.a.	8
H0	3D-printed tablets	10	9.26±0.145	0.14±0.005	0.50±0.021	0.16±0.001	142	165	3.5*
X5	Filaments	10	9.38±0.014	0.16±0.004	0.67±0.020	0.63±0.005	145	n.a.	8
X5	3D-printed tablets	10	8.58±0.110	0.31±0.007	1.33±0.085	1.80±0.130	145	165	5**

*3D-printed from 4.5-months' old filaments

**3D-printed from 3-months' old filaments

4.3.4 Solid state analysis

4.3.4.1 Filaments

DSC analysis showed a melting temperature of about 130°C for pure drug, with corresponding thermal event in powder blends and absence of lumefantrine melting peak in filaments (Fig.4.2A-D). The lack of expected melting peak in powder blends might be attributed to lower concentration of LUM than needed for peak observation or to dissolution of drug in molten mass [143] [144] [145] [146]. The latter is more probable as other crystalline excipients PEG4000 and xylitol, which were contained in the formulations in similar concentration to lumefantrine, exhibited clear melting peaks in powder blends (Fig.4.2B and Fig.4.2C-D, respectively). Hence, absence of lumefantrine melting peak in drug product filaments could not serve as an evidence of drug amorphous state due to possible lack of detection or dissolution of the drug in formulation components during DSC experiment.

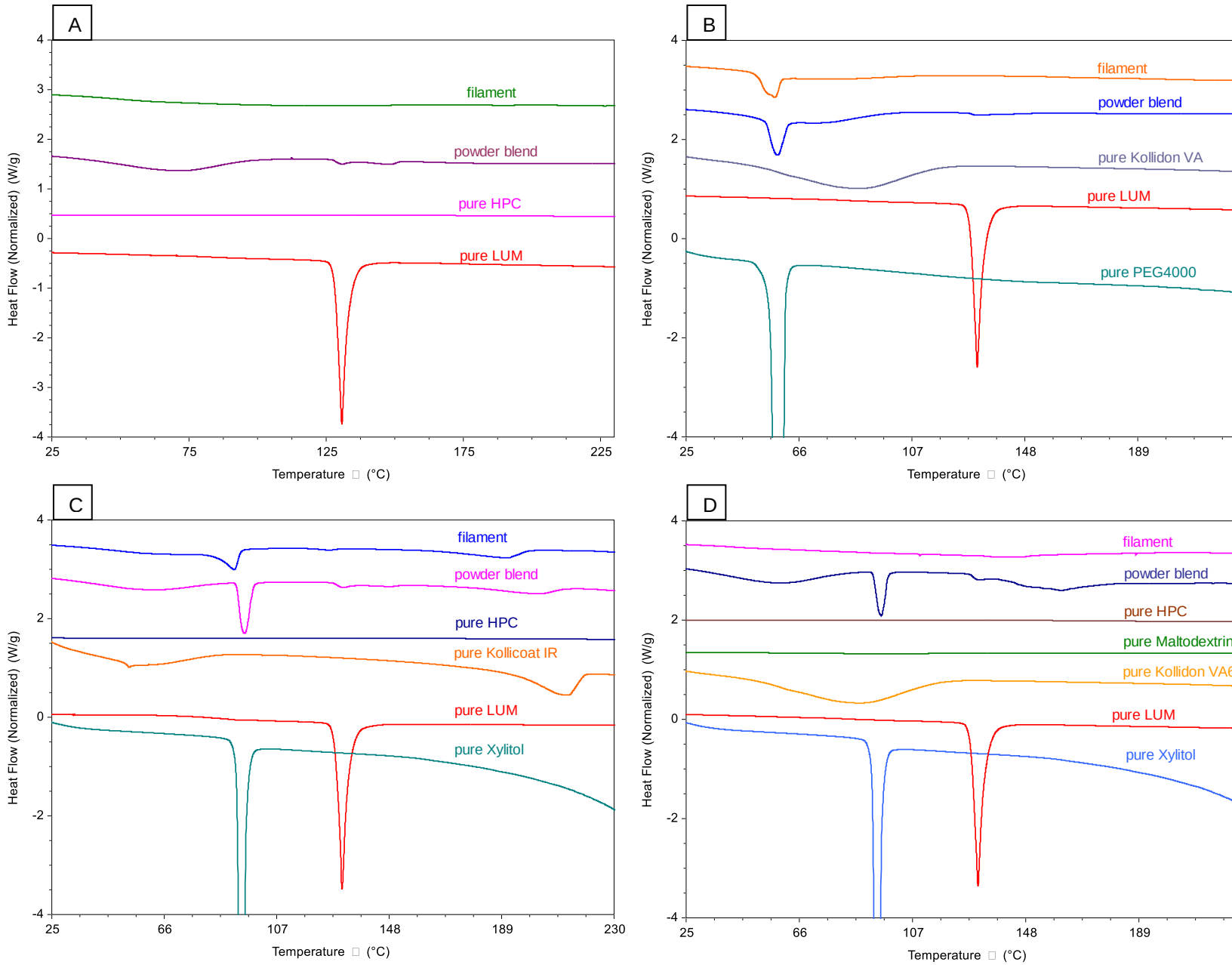

Fig.4.2. DSC curves of pure substances, powder blends and filaments for formulations (A) H0: 10% lumefantrine - 90% HPC SSL, (B) H7: 10% lumefantrine - 45% HPC SSL- 31.5% Kollidon VA64 - 13.5% PEG4000, (C) X5: 10% lumefantrine - 23% HPC SSL- 45% Kollicoat® IR -14% Xylitol - 9% Maltodextrin, (D) X8: 10% lumefantrine - 44.6% HPC SSL – 22.3% Kollidon VA64 -13.7% Xylitol -9.5% Maltodextrin.

XRPD analysis of pure drug substance and powder blends showed diffraction peaks at 11°,15°,18°,20°-27° 2θ characteristic to crystalline lumefantrine (Fig.4.2B), with the major peaks appearing at 20° and 23° 2θ. Kollicoat®-based filaments demonstrated presence of crystalline lumefantrine (Fig.4.3B), whereas crystallinity was not detected in HPC-based formulations (Fig.4.3A). Due to the limited ability of XRPD to detect crystalline traces at relatively

low drug substance concentration, a technique with high sensitivity and accuracy for solid state determination – Raman mapping – was further employed.

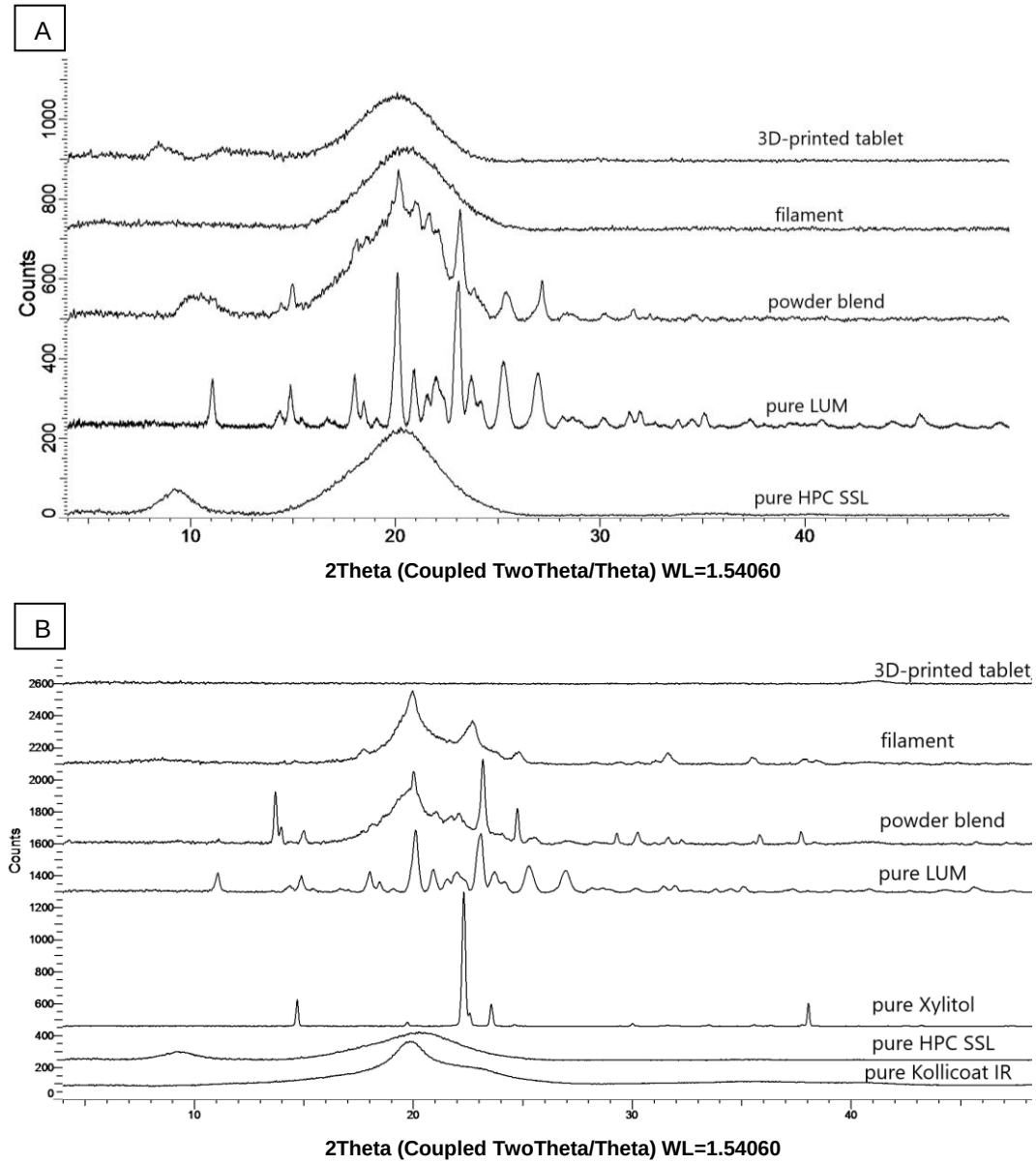

Fig.4.3. X-ray powder diffractograms of pure substances, powder blends and 3D-printed tablets for formulations (A) H0: 10% lumefantrine - 90% HPC SSL, (B) X5: 10% lumefantrine - 23% HPC SSL- 45% Kollicoat® IR -14% Xylitol - 9% Maltodextrin.

Raman analysis of the active substance references produced well-defined and characteristic spectral fingerprint. Lumefantrine solid state spectra showed distinct peak differences evident at 1630-1632 cm-1 for crystalline drug substance and at 1634-1635 cm-1 for amorphous lumefantrine (Fig.4.4A).

Raman molecular mapping of both H0 and X5 filaments revealed the presence of lumefantrine crystalline particles. The crystalline entities were randomly distributed with an elongated to quasi-spherical shape for formulations H0 (Fig.4.4B) and X5 (Fig.4.4D), and measuring between 1-20 µm and 10-50 µm, respectively, in length. Crystalline entities in filaments H7 (Fig.4.4C) and X8 (Fig.4.4E) had elongated plate-like columnar shape of lengths 5-150 µm and 5-100 µm respectively. Hence, crystalline entities in printable filament formulations exhibited quasi-spherical shape with upper size limit of 50 µm, as opposed to columnar shape with upper size limit of 150 µm in non-printable ones. The question arises if the increased brittleness might be due to the larger size of lumefantrine crystals in non-printable formulations. More studies are required, however, to elucidate potential link of FDM printability with shape and size of crystalline entities in filaments.

To conclude, filaments evaluated in this study contained both amorphous and crystalline lumefantrine. Raman mapping revealed presence of crystalline lumefantrine, which was undetectable with XRPD in the H0 formulation and confirmed that lumefantrine was mostly dispersed as crystalline particles in the X5 formulation. This data highlights the importance of more sensitive solid-state analysis techniques than XRPD for BCS class IV compounds, where amorphous solid state is critical for bioavailability. It is worth mentioning, however, that since Raman was performed later than XRPD, crystallization in the filaments of formulation H0 might in theory have happened in the elapsed time interval. Yet Raman also confirmed presence of amorphous material 3.5 months after manufacturing of filaments.

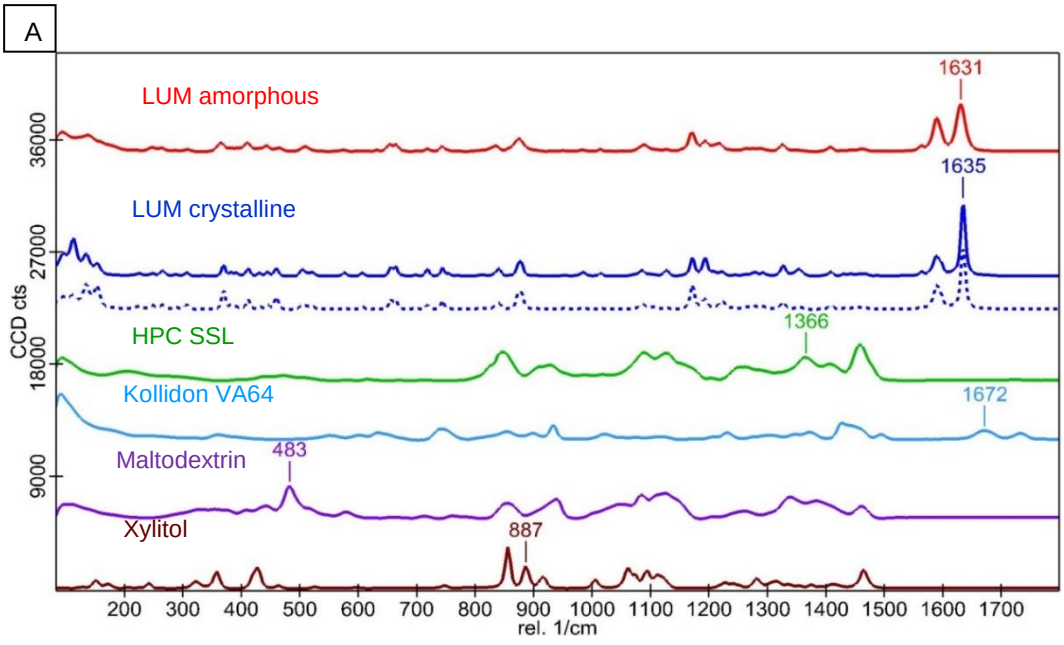

B

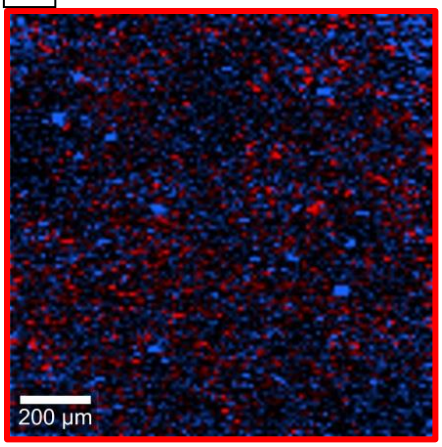
200 µm

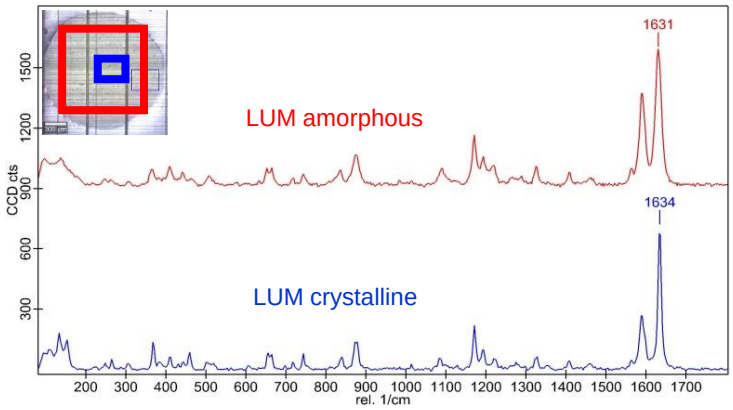
1631
LUM amorphous
1634
LUM crystalline
CCD cts
rel. 1/cm

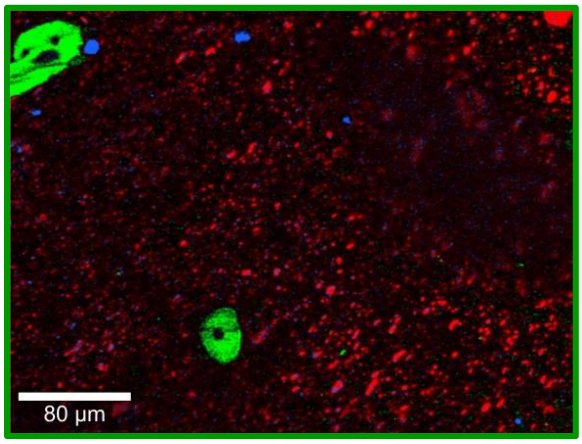
80 µm

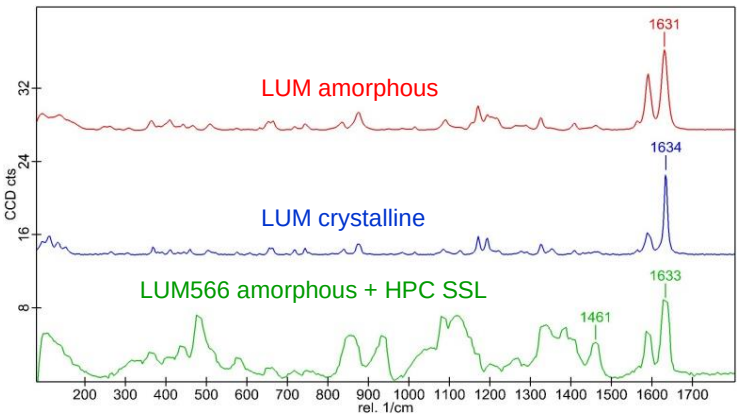
1631
LUM amorphous
1634
LUM crystalline
1633
LUM566 amorphous + HPC SSL
1461
CCD cts
rel. 1/cm

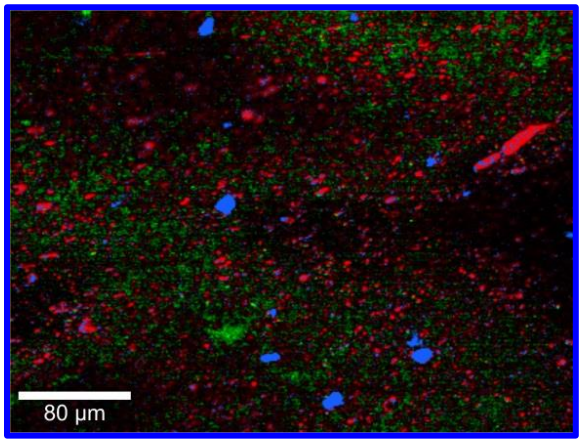
80 µm

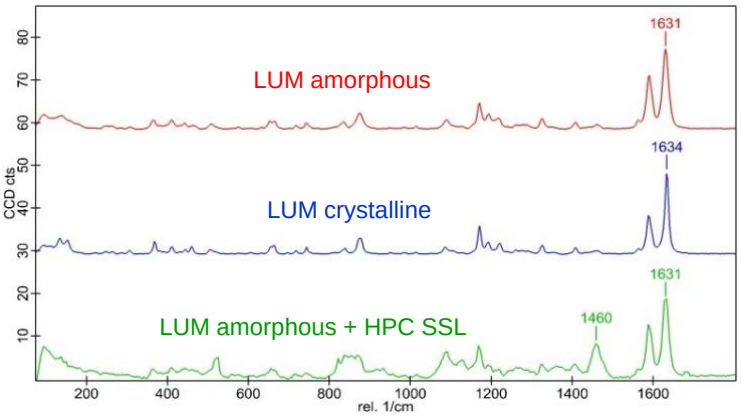
1631
LUM amorphous
1634
LUM crystalline
1631
LUM amorphous + HPC SSL
1460
CCD cts
rel. 1/cm

C

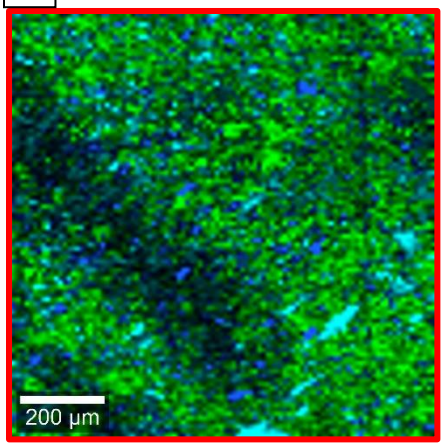
200 µm

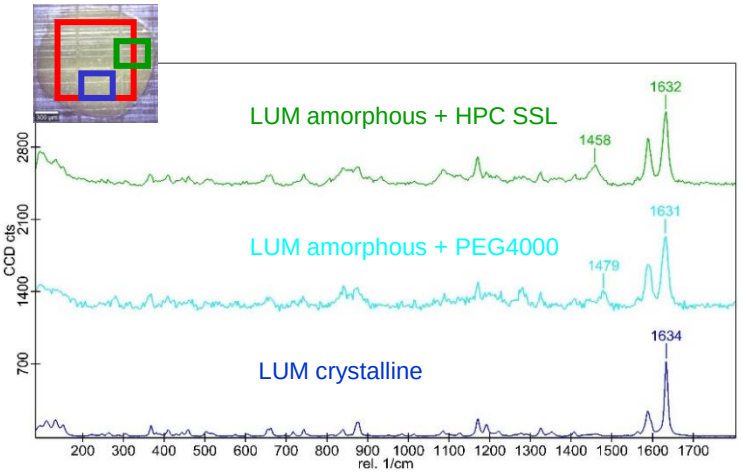
LUM amorphous + HPC SSL
1632
1458
LUM amorphous + PEG4000
1631
1479
LUM crystalline
1634
CCD cts
2800
2100
1400
700
200 300 400 500 600 700 800 900 1000 1100 1200 1300 1400 1500 1600 1700
rel. 1/cm

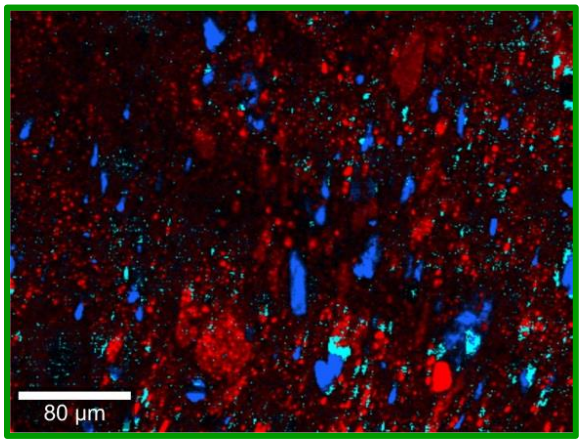
80 µm

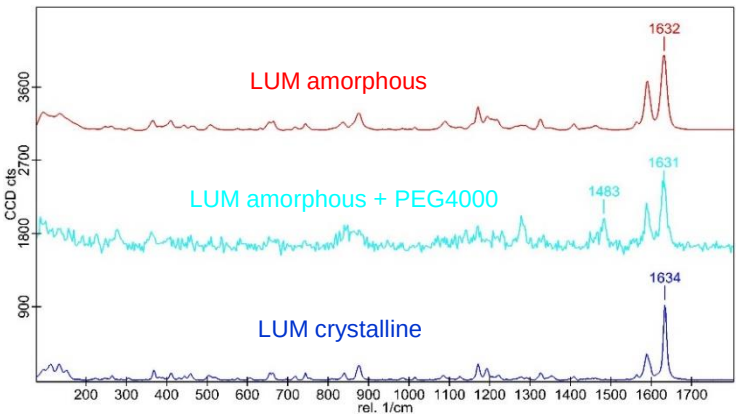
LUM amorphous
1632
LUM amorphous + PEG4000
1631
1483
LUM crystalline
1634
CCD cts
3600
2700
1800
900
200 300 400 500 600 700 800 900 1000 1100 1200 1300 1400 1500 1600 1700
rel. 1/cm

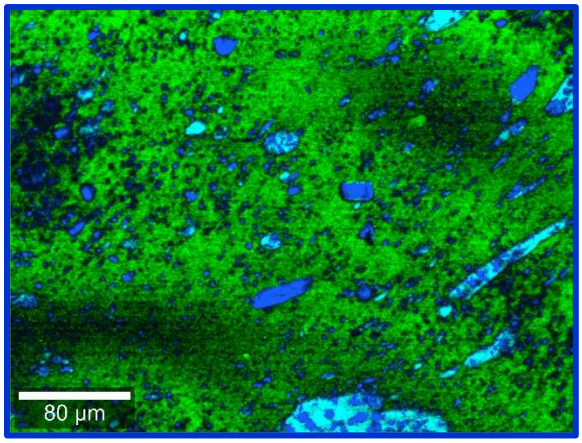
80 µm

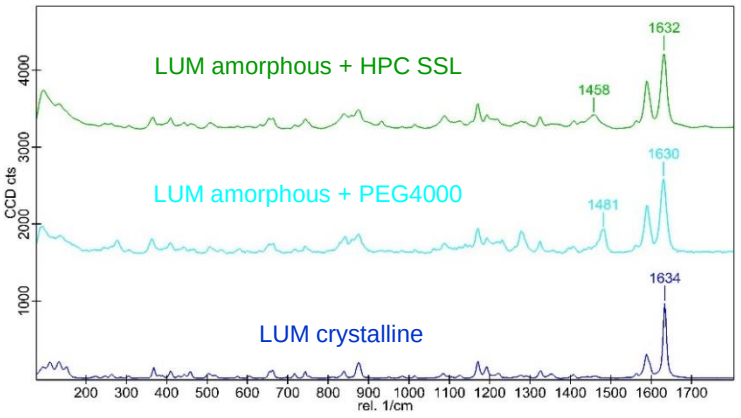
LUM amorphous + HPC SSL
1632
1458
LUM amorphous + PEG4000
1630
1481
LUM crystalline
1634
CCD cts
4000
3000
2000
1000
200 300 400 500 600 700 800 900 1000 1100 1200 1300 1400 1500 1600 1700
rel. 1/cm

D

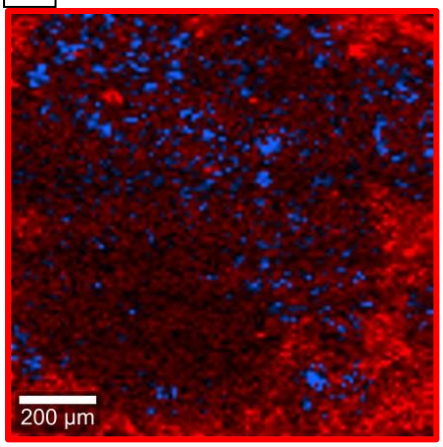
200 µm

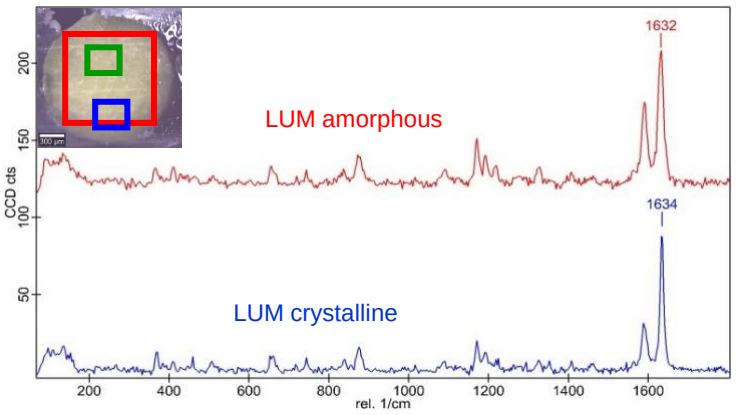
1632
LUM amorphous
1634
LUM crystalline
CCD cts
rel. 1/cm

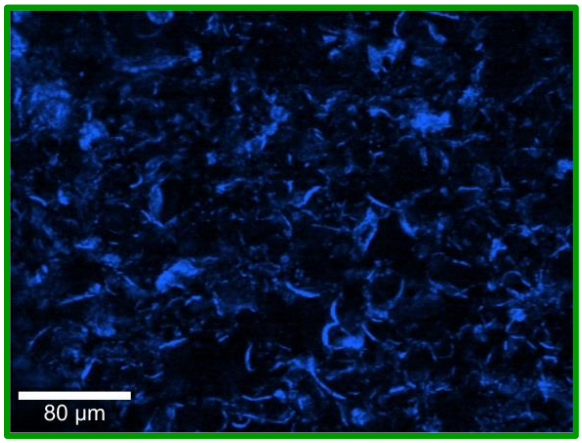
80 µm

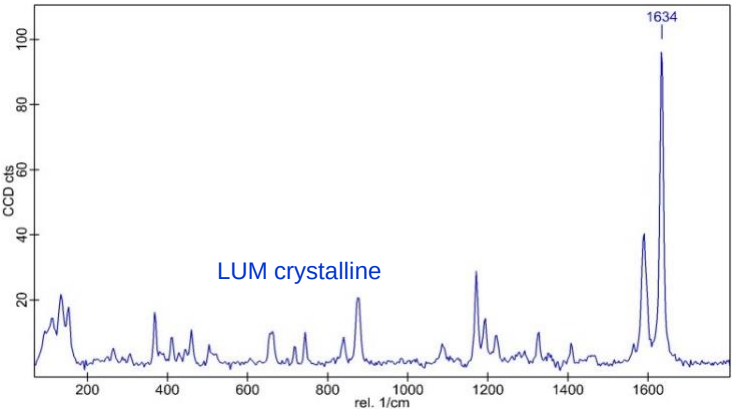
1634
LUM crystalline
CCD cts
rel. 1/cm

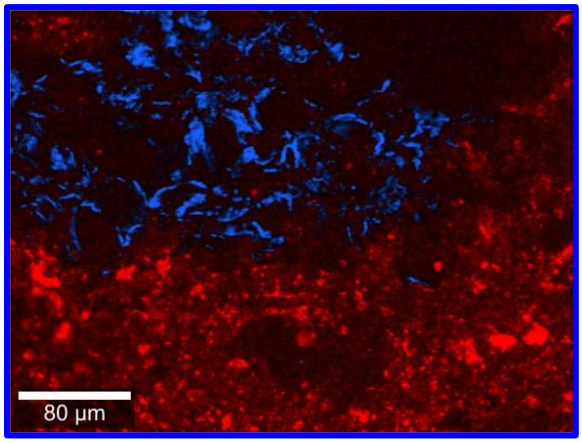
80 µm

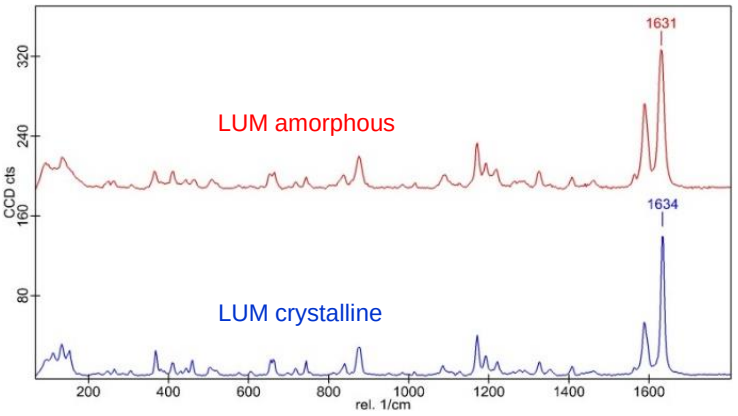
1631
LUM amorphous
1634
LUM crystalline
CCD cts
rel. 1/cm

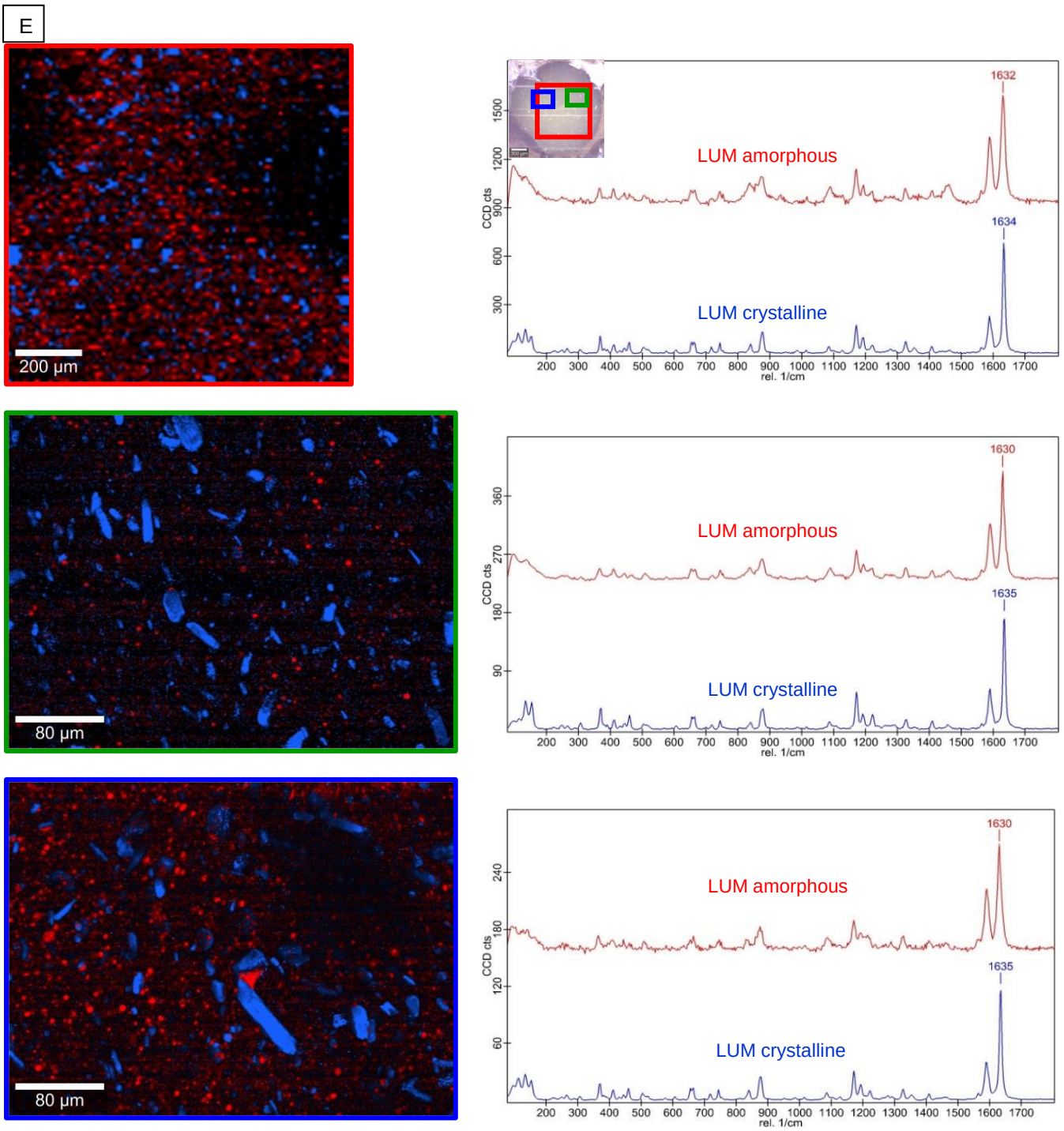

Fig.4.4. (A) Cascaded Raman spectra of crystalline and amorphous lumefantrine (LUM), as well as different excipients. (B), (C), (D), (E), reflection optical micrographs with Raman spectral maps at two different magnifications and corresponding extracted spectra of filament cross sections of formulations H0, H7, X5, X8, respectively. Red, green and blue squares in the insets of the spectra panels indicate the three sites of recording

4.3.4.2 3D-printed tablets

XRPD analysis of H0 (10% lumefantrine - 90% HPC SSL) 3D-printed tablets revealed no presence of crystallinity, as seen also for H0 filaments (Fig.4.3A). X5 (10% lumefantrine - 23% HPC SSL- 45% Kollicoat® IR -14% Xylitol

- 9% Maltodextrin) 3D-printed tablets appeared amorphous in XRPD, as opposed to filaments which showed major diffraction peaks at 20° and 23° 2θ characteristic to crystalline lumefantrine (Fig.4.3B). Notably, tablet analysis by XRPD took place after a shorter storage time compared to the filaments.

Raman mapping confirmed amorphous drug in 10% lumefantrine 3D-printed tablets for both H0 and X5 formulations at least 5 weeks after manufacturing, (Fig.4.5B,D and 4.6B,D). 3D-printed tablet matrices contained exclusively amorphous lumefantrine with no evidence of crystalline drug substance. Raman molecular mapping of both formulations therefore strongly suggests that the active substance became amorphous during the 3D-printing process. This amorphous state appears to be stable for at least five weeks which is relevant from a practical perspective as this period would likely be sufficient for personalized tablets produced via near patient manufacturing.

To conclude, lumefantrine was present in amorphous form in 3D-printed tablets creating enabling formulation [107] [108]. In filaments, on the other hand, crystallinity in parallel with amorphous material was detected. The hot melt extrusion process employed for filament manufacture is arguably responsible for the generation of amorphous API while some crystallization probably occurred in the time elapsed until Raman analysis. These findings provide evidence for the ability of FDM 3D-printing to (re)create the amorphous state of the API. Hence, FDM 3D-printing is demonstrated to act in the sense of HME process for producing amorphous solid dispersions. Compounds for which solid state is critical for in-vivo bioavailability (i.e. BCS class IV drugs), could therefore be formulated as

ASDs that are created directly on clinical site and administered to patients within specified timelines, even if the filaments contained partially crystalline drug substance.

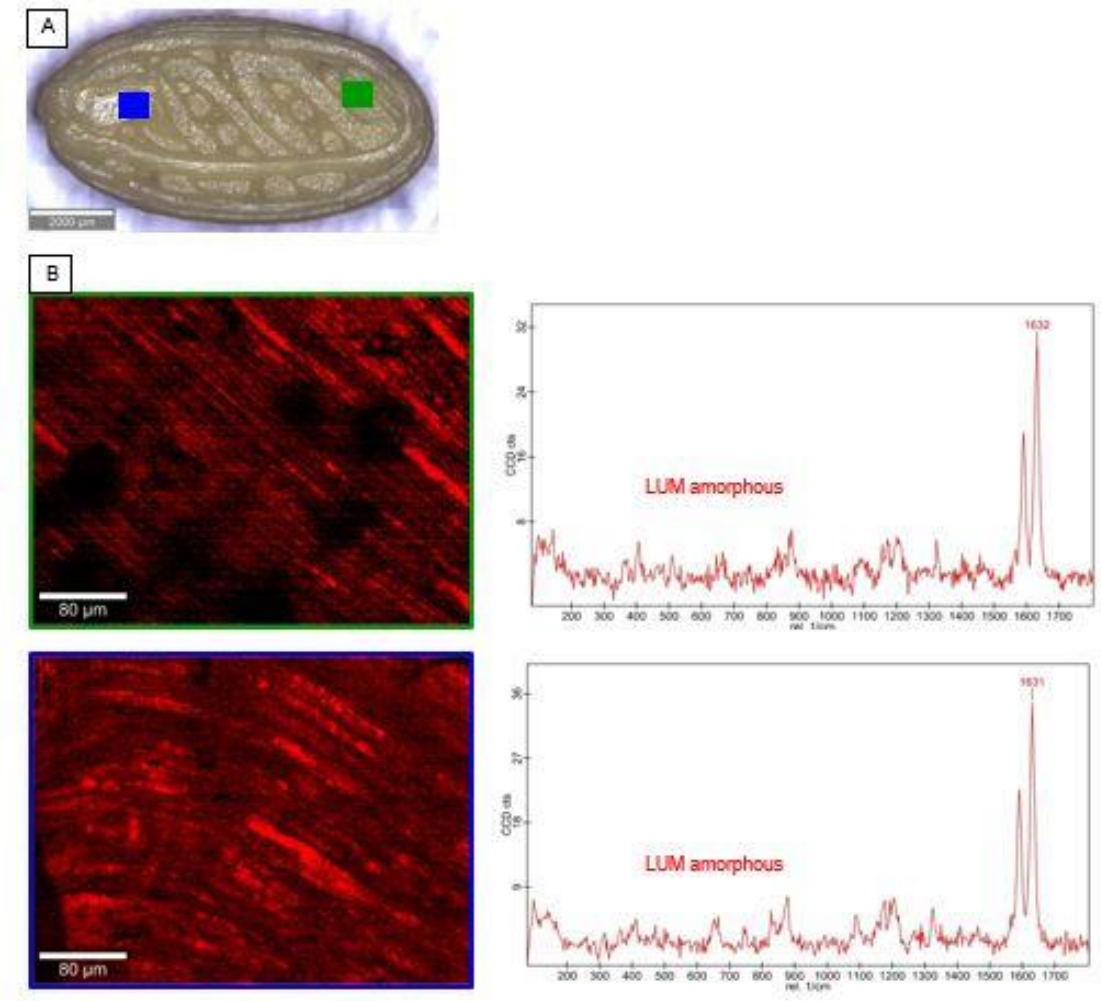

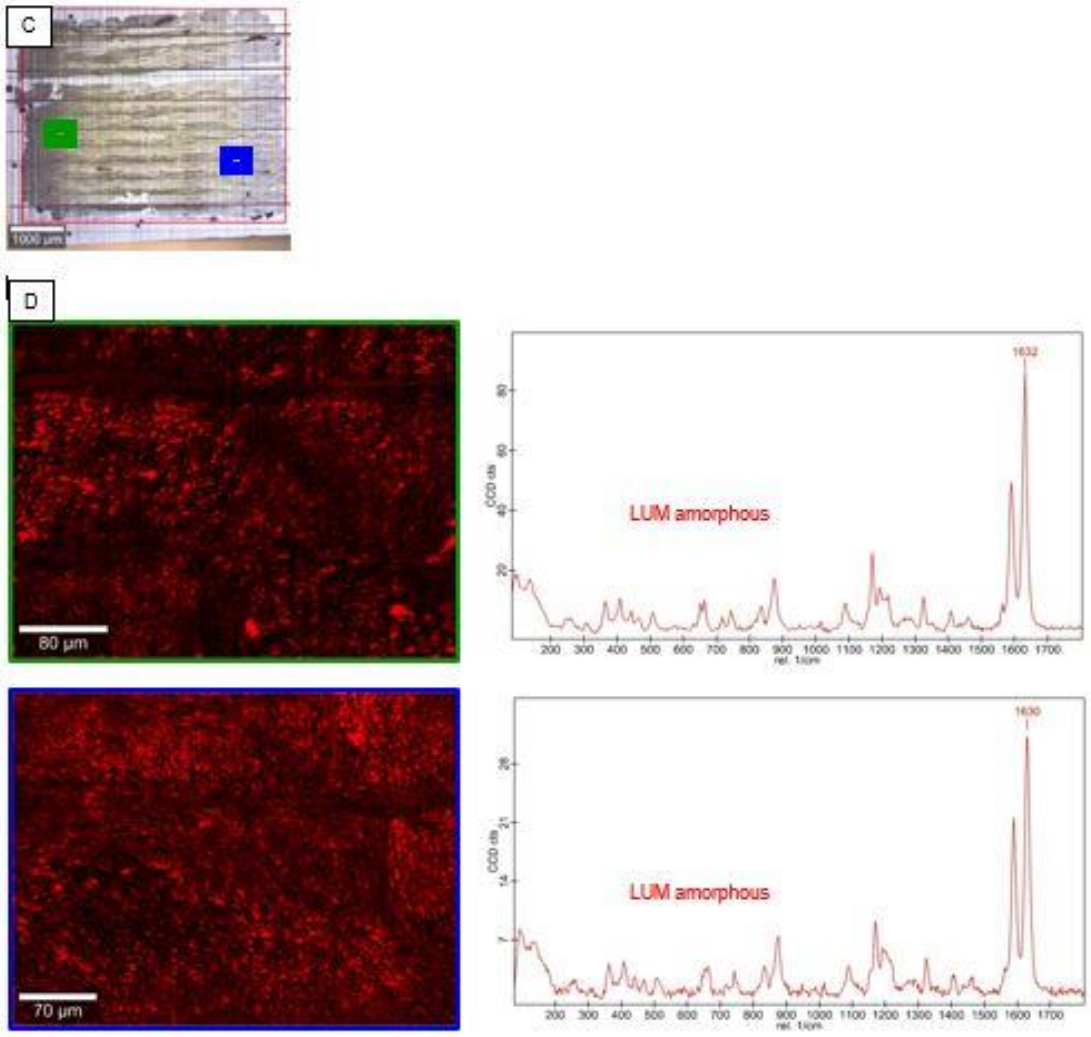

Fig.4.5. Reflection optical micrograph of 10% lumefantrine (LUM) H0 formulation 100% infill density 3D-printed tablet. (A) and (B) surface, (C) and (D) cross-section. Blue and green squares in (A) and (C) indicate the two sites of recording of Raman spectral maps with corresponding extracted spectra shown in (B) and (D), respectively

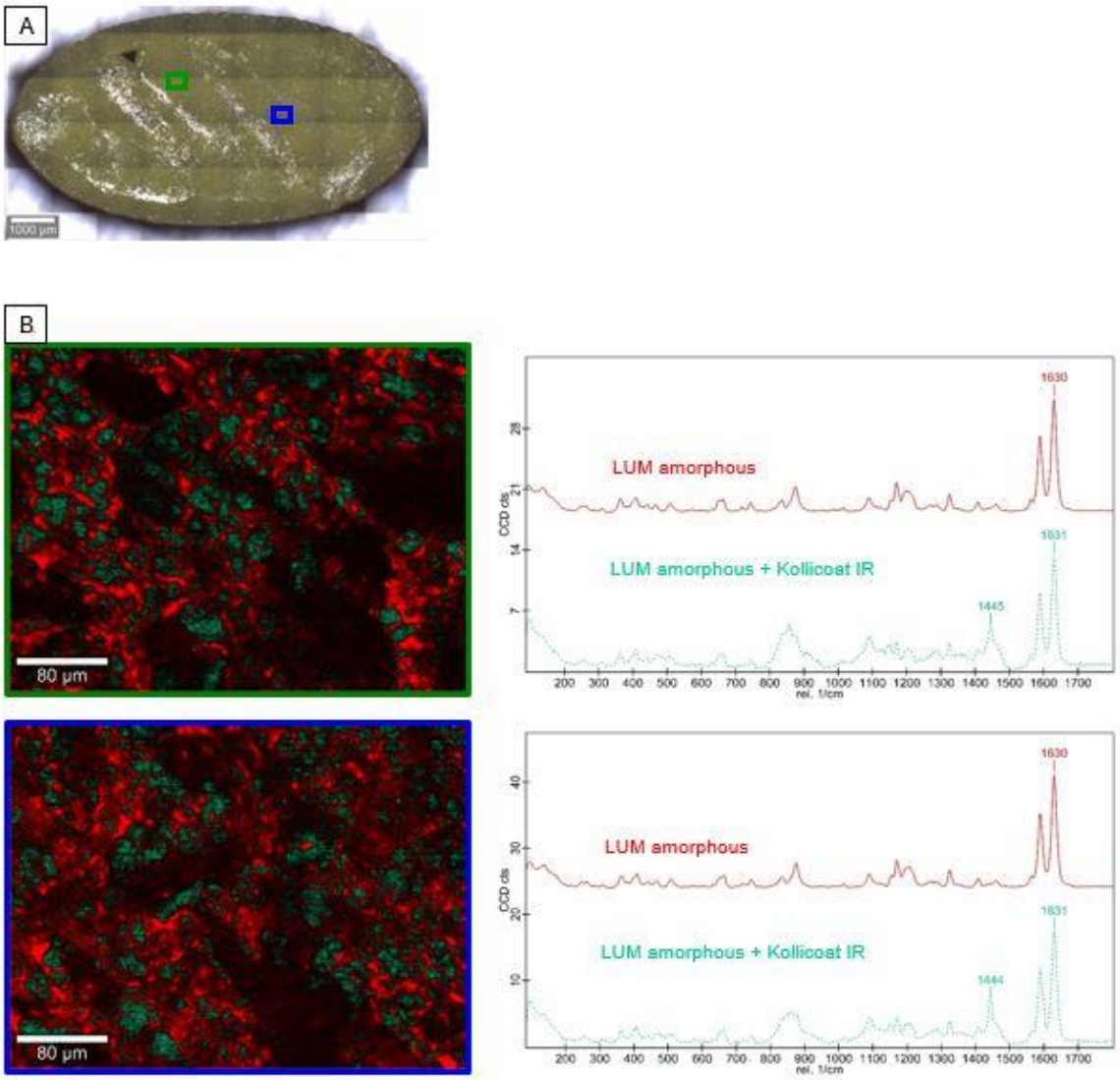
A
1000 µm
B
80 µm
LUM amorphous
LUM amorphous + Kollicoat IR
1630
1631
1445
CCD cts
rel. 1/cm
80 µm
LUM amorphous
LUM amorphous + Kollicoat IR
1630
1631
1444
CCD cts
rel. 1/cm

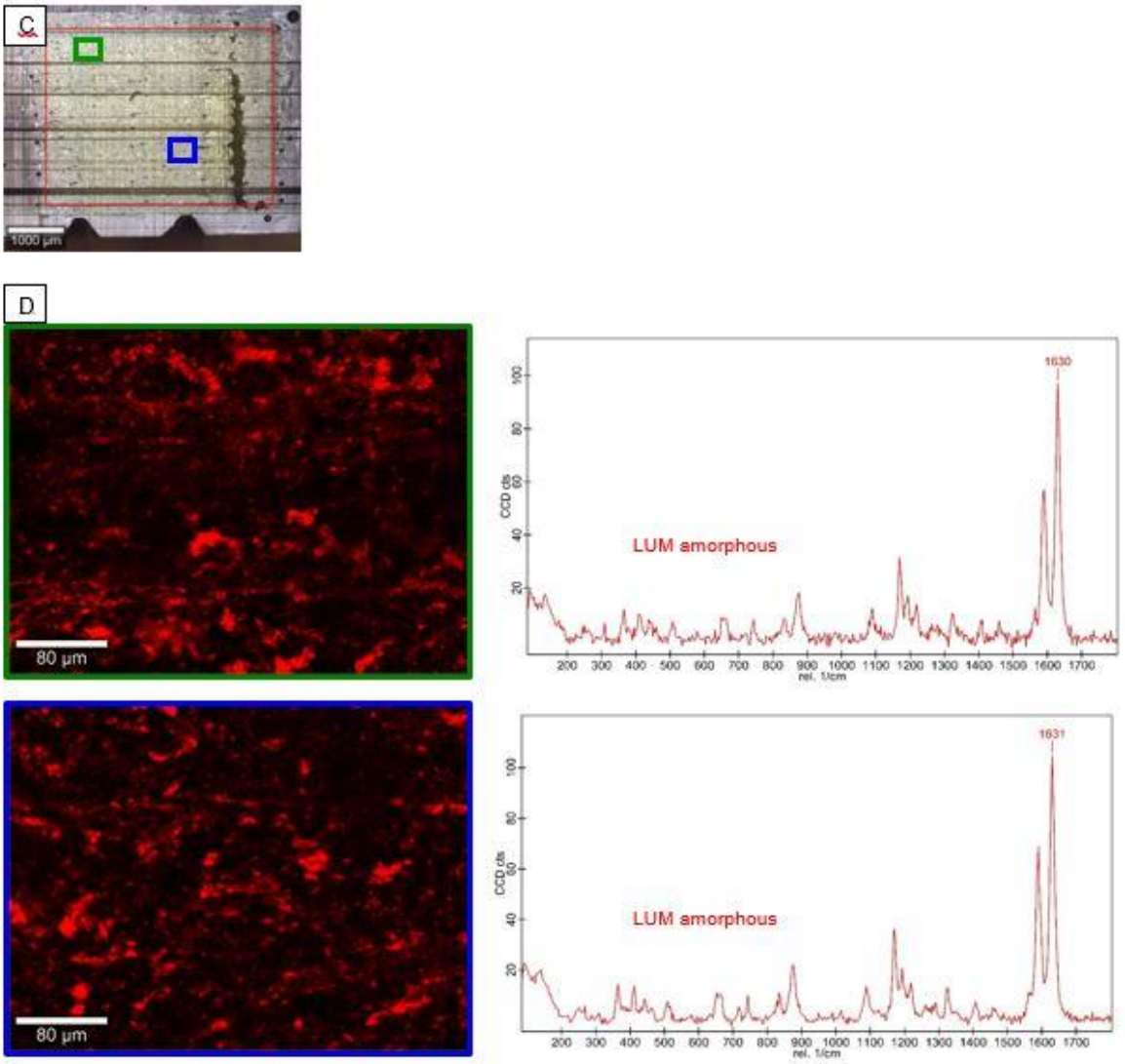

Fig.4.6. Reflection optical micrograph of 10% lumefantrine (LUM) X5 formulation, 100% infill density 3D-printed tablet. (A) and (B) surface, (C) and (D) cross-section. Blue and green squares in (A) and (C) indicate the two sites of recording of Raman spectral maps with corresponding extracted spectra shown in (B) and (D), respectively

4.3.5 Dissolution studies

Dissolution tests of 10% lumefantrine 3D-printed tablets with the different infill densities are shown in Fig.4.7. Relatively slow lumefantrine release from both formulations was observed in comparison to a previous report with the same formulations and BCS class I model drug [22]. In addition to the poor solubility of lumefantrine, the observed slow release could be due to an erosion-controlled dissolution of the tablet matrix (Solanki, 2018). Formulating lumefantrine with HPC SSL as single excipient without plasticizer(s), or with Kollicoat® IR as primary matrix former and Xylitol/Maltodextrin combination resulted in similar dissolution profiles in 0.5% CTAB/0.1 N HCl. Although after 30 min H0 tablets showed about 50% average relative drug dissolution versus 40% for X5, the difference was not statistically significant due to variability of release between the tested units. The present

formulations did not show a potential to meet IR criteria contrary to Eudragit EPO-based formulations of lumefantrine [138], underscoring the role of matrix excipients for dissolution of FDM 3D-printed tablets.

Increase in infill density to 100% did not affect dissolution profile in-vitro, which is in line with the similar morphological parameters measured for both infill densities with H0 formulation. For X5 formulation, 80% and 100% programmed infill densities showed significant difference in relative density and accessible porosity, this difference in morphology, however, did not translate into distinct release profiles. Interestingly, a hydrophilic model compound (caffeine) formulated with Kollicoat® IR was reported to have significantly faster release from 80% programed infill density tablets in comparison to 100% [22]. This might be due to the hydrophilic nature of caffeine (BCS class I) as opposed to lipophilic nature of lumefantrine (BCS class IV). Yet head-to-head comparison is not possible due to the different diameter of the used 3D-printer nozzle, being larger for lumefantrine than for caffeine. Furthermore, this difference in dissolution between 80% and 100% programmed infill density of caffeine formulations with Kollicoat® IR was not universally valid pointing out that besides morphological modifications, additional factors such as mechanism of release play an important role in Kollicoat® IR -based formulations.

.

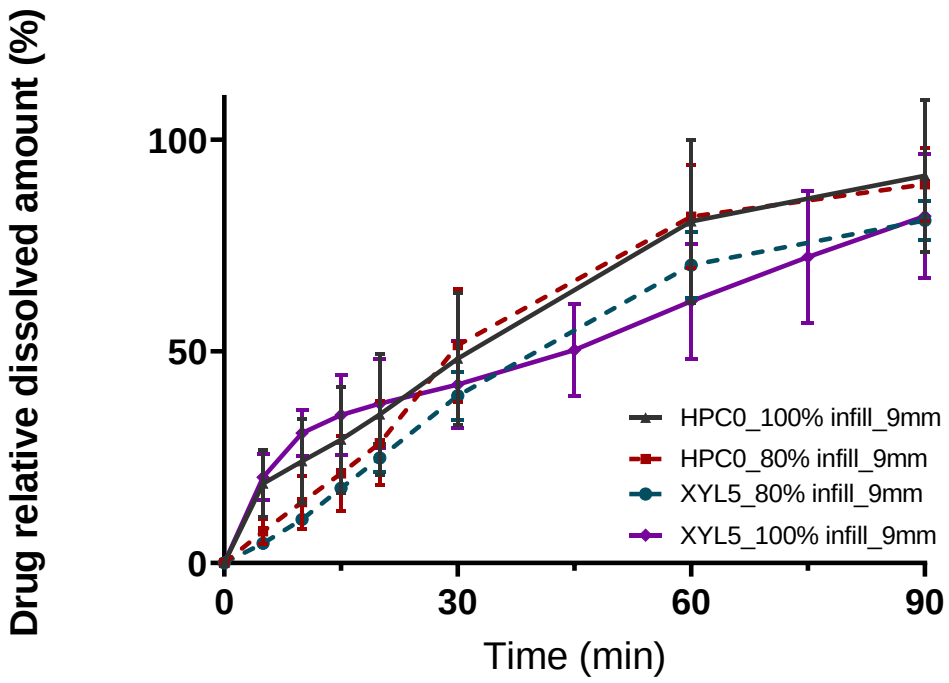

Fig.4.7. Dissolution profiles of X5 formulation (10% lumefantrine - 45% Kollicoat® IR - 22.5% HPC SSL - 13.5% Xylitol - 9% Maltodextrin) and H0 formulation (10% lumefantrine - 90% HPC SSL) 3D-printed tablets with 100% and 80% infill density in 0.5% CTAB/0.1 N HCl

4.3.6 Conclusions

Lumefantrine tablets with good uniformity of weight and percent drug content were successfully 3D-printed. The Kollicoat® IR-based formulation demonstrated advantages for weight and structural uniformity, while the HPC-based variant was beneficial for drug chemical stability. Increasing infill density from 80% to 100% resulted in diminished accessible porosity and elevated relative density for Kollicoat® IR-based tablets but did not affect drug release profiles for either formulation. Data suggest erosion-controlled dissolution.

Following FDM 3D-printing, it was feasible to (re)create amorphous BCS class IV model compound in manufactured tablets from filaments with crystalline drug substance present. Drug substance in the tablets was demonstrated to be fully amorphous for both formulations after at least five weeks from manufacturing date, which would be a sufficient in-use period for near patient manufacturing and dispensing. This fully amorphous drug substance in 3D-printed tablets represents a promising way to ensure optimized bioavailability, with reduced risks due to changes during storage. This represents both an advantage for the patient, and also reduces some of the development risks of enabled formulations, where recrystallization late in stability studies may lead to reduced shelf life or even necessitate reformulation.

Current limitations or risks to overcome include potential thermal drug degradation and filament printability, which should be investigated with other formulations and model compounds. Additionally, to further improve the 3D-printing process, customized 3D-printers for pharmaceutical use which are adapted to pharmaceutical polymers and materials would be beneficial.

5 Chapter 5

Development of Immediate Release 3D-Printed Dosage Forms for Poorly Water-Soluble Drugs by Fused Deposition Modeling: Study of Morphology, Solid State and Dissolution [4]

Summary

3D-printing technologies such as Fused Deposition Modeling (FDM) bring a unique opportunity for personalized and flexible near patient production of pharmaceuticals, potentially improving safety and efficacy for some medications. However, FDM-printed tablets often exhibit tendency for slow dissolution due to polymer erosion based dissolution mechanisms. Development of Immediate Release 3D-printed dosage with poorly water-soluble model compounds is even more challenging, but required to ensure wide applicability of the technology within pharmaceutical development portfolios. In this work, morphology and process for a selected formulation were considered, using BCS class IV compound lumefantrine as a model drug. Basic butylated methacrylate copolymer (Eudragit EPO) as matrix former, as well as hydrophilic plasticizer xylitol and pore former maltodextrin were selected as a promising formulation approach to achieve fast dissolution rates. Tablets of size 9 x 5 x 4 mm, i.e. acceptable for children from 6 years old, were successfully 3D-printed. Tablets with 5% lumefantrine and corresponding placebo were printed, higher drug load as required for clinically relevant dosage strength however lead to increased brittleness incompatible with FDM printing. Residual crystallinity in manufactured tablets and filaments was explored by highly sensitive Raman mapping technique. Lumefantrine was present in the fully amorphous state in the tablets as intended. Grid-designed 3D-printed tablets with 65% infill density met rapid release criteria, while 80% and 100% showed slower dissolution. For the first time, the critical structural characteristics of 3D-printed tablets with non-continuous surface such as accessible porosity, specific surface area by weight and by volume were quantified by an automated micro-CT based methodology, and were confirmed to be responsible for the dissolution rate acceleration. Increase in accessible porosity, total surface area, specific surface area by weight and by volume and decrease in relative density appeared to be critical factors for modification of lumefantrine dissolution rate, whereas increase in closed pores volume did not contribute to accelerating dissolution rate. To conclude, Immediate Release FDM-tablets with BCS class IV compound were developed and key dissolution parameters were detected with non-destructive accurate morphological analysis.

[4] Fanous, M, Malak, B, Gold, S, Sobczuk, A, Hirsch, S, Ogorka, J, Imanidis, G, *Development of Immediate Release 3D-Printed Dosage Forms for Poorly Water-Soluble Drugs by Fused Deposition Modeling: Study of Morphology, Solid State and Dissolution*. Int J Pharm, 2021, under revision

5.1 Introduction

3D-printing of pharmaceuticals could improve individualization of drug therapy through personalized dosage strengths [67], which has the potential to improve safety and efficacy for some medications [3, 4]. Solid dosage forms of various designs, fabricated through layer-by-layer addition of materials based on a digital model can be created via numerous 3D-printing technologies [147]. Manufacturing of drug products at hospitals and pharmacies with multiple APIs and tailored release profiles, possibly involving complex designs and geometries, might enable pharmaceutical 3D-printing to fulfil as yet unmet clinical needs [16]. Examples of 3D-technologies explored for pharmaceutical applications include selective laser sintering, powder bed/jetting, 3D-inkjet printing, fused deposition modelling (FDM) and semi-solid extrusion, which vary with respect to process parameters, spatial resolution of fabrication, processability of required raw materials, versatility, and viability for decentralized manufacturing[17, 71, 147].

In particular, Fused Deposition Modeling (FDM) 3D-printing brings a unique opportunity for flexible and personalized production of pharmaceuticals [67, 135]. For FDM, a thermoplastic filament obtained via hot-melt extrusion, is deposited in ultrafine threads through the print head nozzle [85].This technology could be advantageous for dosage forms manufacturing via low-cost FDM 3D-printers in clinical settings and decentralized locations as no powder or solvents [92] are involved in the printing process, post-processing maybe avoided and mechanically strong tablets are produced [93]. In addition, different dosage strengths with a variety of drug release profiles were delivered within certain limits from the same filament [78]. The challenges to overcome are risk of thermal degradation during processing [84] and FDM processability dependent on mechanical properties of the filament [16]. Moreover, FDM-tablets show tendency for slow dissolution often due to being trapped into the polymeric matrices characterized by erosion-controlled dissolution mechanisms [26]. Most of the developed formulations for FDM demonstrate slow release even for hydrophilic model drug substances embedded in water-soluble polymers [78, 82, 84, 85, 148, 149]. Development of immediate release (IR) dosage forms is more demanding [21, 24], yet necessary if the technology is to be applied commercially [87, 88].This limitation is particularly critical for poorly water-soluble drugs, belonging to Biopharmaceutics Classification System (BCS) classes II and IV. Orally administered compounds with aqueous solubility lower than 100 µg/mL, generally present dissolution-limited absorption potentially resulting in low bioavailability [97]. Sometimes even a small increase in dissolution rate of poorly water-soluble drugs results in a large increase in bioavailability [150]. Development of rapidly dissolving 3D-printed tablets for lipophilic compounds, therefore, is a clear need towards the future of personalized dosage form production, since majority of discovered drug candidates display poor aqueous solubility [151, 152].

To overcome slow dissolution of oral dosage forms, various approaches have been developed with a focus on enhancement of the solubility, dissolution rate, and oral bioavailability of poorly water-soluble drugs [97]. In particular, FDM 3D-printing could facilitate dissolution rate modification within certain limits via design modification i.e. lowering infill density without changing formulation composition [78] [129], opposed to standard dosage forms where failure to meet set dissolution criteria often necessitates changes in formulation composition, possibly resulting in stability and incompatibility. In addition, hot-melt extrusion is used as intermediate step for filaments manufacturing. Depending on miscibility and satisfactory stability of the extruded formulation, an

amorphous solid state could be obtained by HME [106, 153], often improving solubility and bioavailability of poorly soluble drugs by design.

Defining key parameters impacting dissolution rate of 3D printed-tablets and understanding the link between intended and realized morphology are of major importance for future FDM medicine development. It is known that decrease in programmed infill density often accelerates drug dissolution rate for both hydrophobic [24] and hydrophilic drugs [18], however very few studies have explored how programmed structure is translated into actual morphology. Goyanes et al [82], for example, determined the effect of micropore volume on dissolution rate of caffeine/paracetamol from polyvinyl alcohol (PVA)-based 3D-printed tablets with 100% programmed infill density, measured by mercury porosimetry. This technique nonetheless is destructive to the sample and limited by the lack of mercury penetration into enclosures in certain cases [82]. The authors concluded that porosity of the caplets did not help to predict the different drug release profiles possibly due the swelling layer of the PVA hindering water penetration through the pores, resulting in ultimately diffusion/erosion- controlled drug dissolution. Further, this group pioneered to study the effect of 3D-printed tablet geometry (cube, pyramid, cylinder, sphere and torus) on drug dissolution rate [154]. The authors found geometrical shape affected paracetamol release, which was not dependent on the surface area but instead on surface area to volume ratio. The morphology measurements used were non-destructive, however precision of the measurements was limited, as surface areas and volumes of the tablets were calculated based on manually measured dimensions of the tablets, as well as photographs of the tablets taken a camera. Moreover, this method appears to be not applicable to tablets' designs with infill density lower than 100% and/or without outer shells, as pores larger than 100 µm are often created by design.

Korte et al. [129] applied non-destructive micro X-Ray computer tomography (µCT) to explore effect of surface area on Eudragit RL-based tablets dissolution rate. The authors found that specific surface area of the network hardly varied with changing fill density. Dissolution studies showed a slower drug release for dosage forms with a denser network and higher surface area. In work of Arafat et al [78] surface area and spaces in 3D-printed tablets were measured with µCT, where the rate of *in-vitro* drug release was directly related to the distance between the structural blocks. Accelerating drug release was primarily connected to ability to break into mini-structures due to big gaps, the low density of the tablets resulted a large tablet size that could limit patient acceptability due to difficulty to swallow. Dissolution rate was independent on surface/mass ratio. Measured porosity, which might play a critical role in dissolution behavior of the structures, was not reported. These studies, nonetheless, did not provide an extended, potentially relevant, structural evaluation; were qualitative in case of the latter and for both; image post processing outcome was not correlated to provide an estimate of virtual 3D structural build accuracy.

Understanding how variety of structural factors such as relative density, volume of accessible and closed pores, surface area, polymer volume affect dissolution profile is crucial towards tailoring desired release profile of a given dosage form.

The objectives of this study were:

- develop Immediate Release FDM 3D-printed dosage forms (DFs) with BCS class IV model compound
- manufacture tablets suitable also for pediatric population above 6 years old with several designs

- develop automated non-destructive, imaging based, morphological analytical approach for precise quantification of 3D-printed DFs morphological characteristics
- bridge between programmed and actual structure (incl. detailed and extended structural evaluation covering specific surface area accessible for dissolution and pore volume by microCT, and identify key structural parameters responsible for dissolution rate acceleration in 3D-printed DFs
- investigate residual crystallinity after each manufacturing step using Raman as highly sensitive technique

This study involved consideration of formulation, process and structure design for 3D-printed dosage forms with BCS IV model compound lumefantrine. FDM-tablets were manufactured above melting temperature of API, with infill density of 65-100%. Basic butylated methacrylate copolymer (Eudragit EPO) was chosen as matrix former, since methacrylates have shown potential to achieve IR [126] and ability to form amorphous solid dispersion with lumefantrine [108, 155, 156]. Hydrophilic plasticizer xylitol and pore-former maltodextrin was selected as promising combination to achieve fast dissolution rate. Although lumefantrine might require stabilizer/anti-oxidant in the formulation [108], such additives were not used in this study in order to estimate lumefantrine stability following hot-melt extrusion and 3D-printing.

5.2 Materials and methods

5.2.1 Materials

Lumefantrine (Novartis Pharma AG, Switzerland), molecular weight 528.9 g/mol, was used as a model compound. Powder mixtures of basic butylated methacrylate copolymer (Eudragit EPO, Evonik, Germany) as primary matrix former, xylitol (Xylisorb300, Roquette, France) as hydrophilic plasticizer and maltodextrin (Maldex 120,Tereos, Germany) as pore former were prepared. Formulations containing increasing concentrations of model drug were hot-melt extruded to produce filaments, whose 3D-printability was assessed. Amorphous lumefantrine (Novartis Pharma AG, Switzerland) was used as a reference for Raman microscopy. Lumefantrine 120 mg tablets (Novartis Pharma AG, Switzerland) were used for the comparison in dissolution studies.

5.2.2 Methods

5.2.2.1 Hot-melt extrusion (HME)

Powders were accurately weighed into 0.5 L bottles to make a total batch weight of 100 g and were mixed via diffusion blending for 20 min at 32 upm by T2 Turbula™ mixer. A twin-screw hot melt extruder (Thermo Scientific™ Pharma 11™, Karlsruhe, Germany) was used for filaments manufacturing. The screw design was TIP / 10 x FE / 4 x 90° / 5 x 60° / 3 x 30° / 25 x FE / 1 x ½ FE / FEEDING.

The measured temperatures for zones 2, 3, 4,5-8 was 38-43°C, 60-80°C, 100-140°C, 120°C-141°C; die temperature was 120 °C-142°C depending on the formulation (see Table 5-1). Extrusion was carried out through a customized 1.75 mm die nozzle with a pressure control (maximum 90 bar). Feeding rate was about4 g/min, screw speed 10-25 rpm depending on the formulation.

5.2.2.2 Fused deposition modeling (FDM) 3D-printing

The template used to print the dosage form was designed with FreeCAD 0.13 software. The selected geometry was an oval tablet with grid infill pattern. The tablet dimensions of 9 x 5 x4 mm (width x length x height) were selected, with one continuous outer layer (altitude shell) and no continuous bottom/top layers. The continuous outer layer enclosed the perimeter of the structure which had no bottom or top layer. BoltPro 3D-Printer (LeapFrog, Netherlands) was used for FDM. 3D-Printing was performed through nozzle with d=0.5 mm at 1000 mm/min speed with primary layer speed of 50% of the default and height of 0.15 mm. The lowest possible printing temperature was used that still allowed an appropriate formulation processability (165°C for placebo and 160°C for active formulation). Sticking and removal of the printed object from the surface was with the bed heating to 35°C. Three infill densities were printed: 100%, 80% and 65%. After 3D-printing, the manufactured tablets were weighed and their dimensions were measured manually with a caliper.

Drug load, degradation products and uniformity of percent drug content

A tablet was dissolved in 100 mL of sample solvent (20 mM hexanesulfonic acid: water: acetonitrile: TFA) and the drug concentration was determined by HPLC (HP-1100, Agilent Technologies, UK) with YMC Pack-Pro C-185 µm, 150 x 3 mm column (YMC Co., Japan), maintained at 30°C. The injected volume was 10µl. The gradient consisted of two components: mobile phase A (20 mM hexanesulfonic acid: acetonitrile: TFA; 490:510:1, v/v/v) and mobile phase B (acetonitrile: TFA,; 1000:1 v/v) starting with the former at 100% and decreasing gradually to 48% after 16 min, and increasing back to 100% after 20.1 min. The flow rate was 1 ml/min and the UV detection was carried out at a wavelength of 265 nm. All measurements were performed in triplicate. To calculate the average percent drug content, values of randomly selected (n=3) and separately analyzed 3D-printed tablets were normalized by weight. Each sample was measured in triplicate.

5.2.2.3 Dissolution test conditions

A semi-automatic tablet dissolution system Sotax AT7 (Sotax AG, Aesch, Switzerland) fulfilling requirements for USP2 dissolution method was used to perform the studies. *In vitro* release profiles of the tablets (n=3 for each infill density) were studied at 0.1N HCl with 0.5% cetyl-trimethylammonium bromide (CTAB). Each tablet was pre-weighed and placed in the vessel containing 900 mL of dissolution medium. Dissolution was carried out with a paddle speed of 100 rpm at 37 °C for 90 minutes. The paddle speed was then increased to 250 rpm for further 30 minutes to ensure full dissolution. Samples (10 ml each) were collected at time points 0, 5, 10, 15, 20, 30, 60, 90 and 120 min. The dissolution medium was replenished after each sampling with an equivalent amount of 0.5% CTAB 0.1N HCl solution. The drug concentration of the samples was analyzed for concentration as above using Perkin Elmer Lambda 25 UV spectrophotometer at 342 nm. Expected 100% dissolution value was calculated based on the nominal value in the initial formulation blend. Dissolution profiles were visualized by plotting percentage of drug dissolved against time. At least 85% of relative dissolved drug amount (average n=3) after 30 min was set as rapid release criteria [123].

5.2.2.4 X-ray powder diffraction (XRPD)

Powders were analyzed on a quartz sample holder. Powder blends were directly dispensed on the holder surface, 3D-printed tablets were gently/manually ground with mortar and pestle. XRPD analyses were performed on a diffractometer using a K430 X-ray generator with a copper anode (voltage: 40 kV, current: 40 mA). XRD patterns in temperature were recorded in transmission mode using quartz capillaries 1.5 mm diameter (GLASS W. Müller, Berlin, Germany). The X-ray generator was a long line focus sealed tube (Siemens; Germany, Cu anode with a Kα line at 1.54 Å, operating at voltage of 40 kV and current of 20 mA). One 2D VÅNTEC-500 Area detector (4 channels, filled with argon-ethane mixture) were used to collect the data. With the settings used, 2θ angles were calculated, ranging from 1 to 18° and from 18 to 36°. Diffractograms were generated with the software Diffrac. EVA V4.0 from Bruker, USA.

5.2.2.5 Differential scanning calorimetry (DSC)

DSC measurements were performed using a Q2000 DSC (TA instrument, New Castle, PA) under nitrogen flow of 50 ml/min. Samples between 1 and 2.5 mg were analyzed using punctured aluminum pans, an empty pan was used as reference. A heating rate of 10°C/min was set between -20°C and 300°C. Software Trios v4.4.1 (TA Instruments, Inc., Waters Corporation, MA, USA) was used.

5.2.2.6 Confocal Raman microscopy

Raman spectra were obtained with a Confocal Raman microscopy (WiTec alpha 300 R, Germany). The excitation wavelength 633 nm were provided by a HeNe laser (Melles Griot, USA). Offset correction was performed for each study by calibration against silicate substrate.

Reference material spectra, including that of lumefantrine in both crystalline and amorphous states, were obtained by single spectral measurements whereby characteristic peaks for each species were defined for hyperspectral processing.

Extruded filaments and their corresponding printed tablets were embedded in epoxy resin and processed using an ultra-microtome to obtain level block cross-sections. Thereafter, cross-section surfaces were analyzed by large area scans. For printed tablets, surface scans were also performed on the ready-made tablet prior to sample cross-sectioning.

Area scans and their corresponding hyper spectra generation were performed firstly on a large-scale, low resolution modes to gain an overview. These were 1100x1100 µm at 10 µm spatial resolution and 4000x3500 µm at 20 µm spatial resolution for the filament and printed tablets respectively. This was followed by 400x300 µm at 1 µm spatial resolution scans performed at two different spots for each sample.

Average spectra extraction took place based on reference spectra peak evaluation performed automatically by the software. These were 1635 rel. cm^{-1} for crystalline lumefantrine, 1631 for cm^{-1} for amorphous lumefantrine, 1728 rel. cm^{-1} for Eudragit EPO, 483 cm^{-1} for Maltodextrin and 1062 cm^{-1} for Xylitol.

Hyperspectral data offset and baseline polynomial correction, cosmic ray removal, spectral filter application, average spectral extraction and spectral map deconvolution were performed using Witec Project FIVE 5.1 software.

5.2.2.7 X-ray microcomputed tomography (microCT)

3D printed tablets were evaluated in triplicate or each variant using Skyscan 1172 X-ray microtomograph (Bruker, Kontich, Belgium). Multi-projection acquisition took place at 5.93 μm resolution, 59 kV Source Voltage and 167 μA Source Current. Following the application of appropriate ring artifact and beam hardening filter, image reconstruction (tomography generation) took place using NRecon software (Bruker, USA) at -0.102355 to 0.186187 attenuation coefficient (dynamic) range output. For qualitative specimen visualization, DataViewer software (Bruker, USA) was used.

Image processing and morphometry evaluation took place using ImageJ 1.52p (NIH, USA). 3D-printed tablet homographs were binarised based on pilot Renyi's entropy output [157]. Thereafter, scatter removal was performed by the application of appropriate iterations of outlier removal from the binarised tomography stacks. Inner pore extraction took place by 3D fill-hole and subtraction and, on the other hand, enclosed perimeter extraction took place by 3 iterations of multidirectional fill-hole process [158]. Solid, enclosed perimeter and pore volumes were established by voxel count whilst surface area pixel evaluation was performed using marching cubes algorithm [159]. Following the development of processing and data mining sequences, all operations were carried out in an automated manner by the application of IJ1 based Macros.

5.2.2.8 He-pycnometry

Densities of 5% LUM filaments with and w/o drying overnight were measured by helium pycnometry (UltraPyc 1200e; Quantachrome GmbH & Co. KG, Duisburg, Germany). For each density test ten consecutive volume-measurements showing a standard deviation less than 0.02 cm^3 were performed with less than 0.07% deviation achieved. Obtained results were averaged to report 5% LUM formulation density, and compare with calculated density based on X-ray CT.

5.2.2.9 Data analysis

The data are presented as mean ± SD, and the differences between groups were analyzed by one-way ANOVA (MiniTab, version 17.3.1, Minitab LLC, USA) and confirmed by Fisher's test (MiniTab, version 17.3.1, Minitab LLC, USA). The statistical significance was considered at $p < 0.05$.

5.3 Results and discussion

5.3.1 Processability of hot-melt extrusion and 3D-printing

Eudragit-xylitol-maltodextrin filaments with 0-30% drug load were successfully extruded. Filaments with lumefantrine were yellowish with varying transparency as a function of drug concentration (see random sections of the filaments at Fig.5.1). Increasing concentration in the active formulations allowed for reduction of barrel temperature for the filaments production in comparison to the placebo reference (Table 5-1).

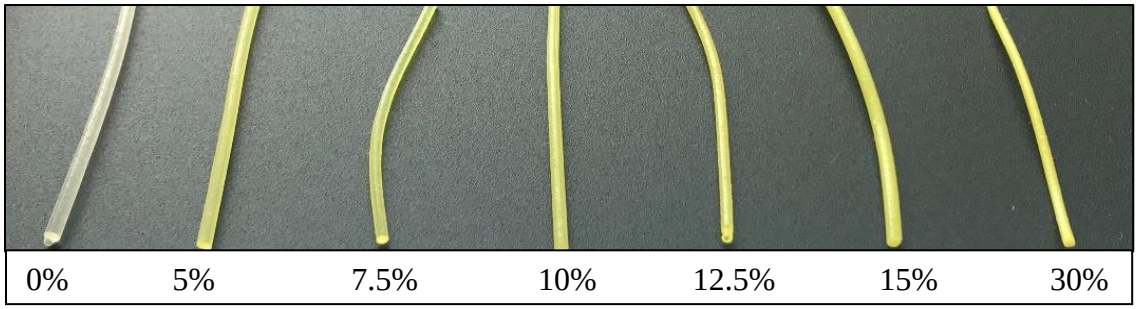

Fig.5.1. Photographs of Eudragit-based filaments with 5-30% lumefantrine following hot-melt extrusion

Table 5-1 Formulations compositions and process parameters

Formulation component (% w/w)	**EUD_0**	**EUD_5**	**EUD_7.5**	**EUD_10**	**EUD_12.5**	**EUD_15**	**EUD_30**
Lumefantrine	0.00	4.97	7.54	10.04	12.50	14.99	30.01
Eudragit E PO	75.78	72.01	70.07	68.17	66.31	64.42	53.04
Maltodextrin	10.02	9.53	9.27	9.02	8.77	8.52	7.02
Xylitol	14.19	13.49	13.12	12.77	12.42	12.07	9.93
Process parameters							
T zone 2 (°C)	43	38	39	40	40	41	40
T zone 3 (°C)	80	60	61	80	62	60	62
T zone 4 (°C)	140	120	120	100	120	120	120
T zone 5 (°C)	140	135	130	130	130	125	120
T zone 6(°C)	140	135	130	130	130	125	120
T zone 7 (°C)	140	135	135	130	130	130	120
T zone 8 (°C)	141	135	135	131	132	130	120
Tdie (°C)	142	138	134	131	132	128	120

extrusion speed (rpm)	15	22	22	20	22	27	23
Torque (%)	17	30	33	23	28	26	35
Pressure (bar)	2	3	7	1	7	2	3
Appearance after extrusion	whitish translucide	yellow translucide	yellow translucide	yellow translucide	yellow translucide	yellow translucide	yellow opaque

Besides placebo filament, the formulation with 5% drug load was the only one compatible with FDM 3D-printing due to the increased brittleness of higher drug load filaments. The further experiments were concentrated on 5% lumefantrine filaments, manufacturing tablets with 65%-100% infill density (Fig.5.2, one median section cross-section within x, y, z axis is presented).

5.3.2 Weight uniformity and morphological characteristics of 3D-printed tablets

Manufacture of lumefantrine 3D-printed tablets was achieved with size and shape being in agreement with the preset dimensions (see Table 5-2). Tablets programmed with 80% and 100% infill density demonstrated more uniform weight than those with 65%. As infill density designates only the interior while an identical outer layer (altitude shell) constituting a considerable part of the weight of the tablet, average weight of tablets with various infill densities was very similar, especially for 100% and 80%.

Qualitative assessment of tomography images for all specimens evaluated in this study, revealed the 3D-printed tablets to be of oval conformation within relatively flat top and bottom aspects. Examples are shown in (Fig.5.2). A level of inner structural void demarcated by the interweaving polymer filaments was also evident however gradually diminishing vertically towards the hot plate contact aspect. Evaluation of 3D-virtual constructs showed the precision multi-layered nature of the 3D-printed tablets when viewing their side aspects (see 3D-reconstruction within Fig.4.2).

A non-destructive automated CT morphometry analytical approach, based on the application of appropriate binary threshold, was developed in this study to evaluate 3D-printed tablet surface area, solid volume and open/close pores volume. The density values established based on correlating CT volume of specimens with their weight yielded an average of 1.19 ± 0.032 g/cm^3 (11 tablets with 3 infill densities 3D-printed from formulation 5% lumefantrine: 72% Eudragit E PO: 13.5% xylitol:9.5% maltodextrin). This fully corresponded to measured density by He-pycnometry 1.19 ± 0.011 g/cm^3 for the same formulation.

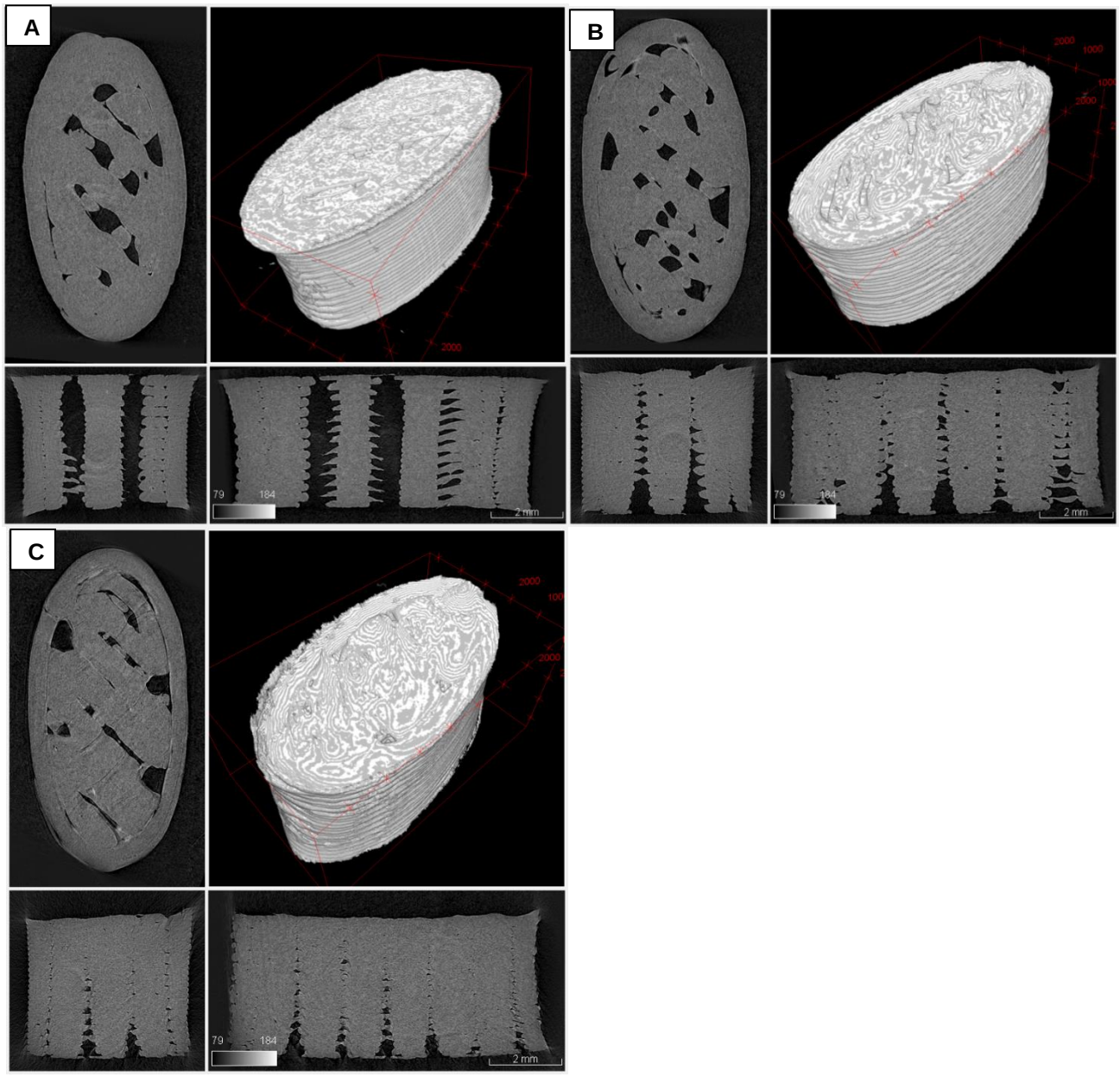

Fig.5.2. X-ray cross-sections of 5% lumefantrine 3D-printed tablets with (A) 65%, (B) 80% and (C)100% infill density. Top left is the view the cross-section perpendicular to z axis, bottom-left is parallel cross-sections in x and y directions. The upper right is the reconstructed view of the 3D-printed tablet. The upper plane of 3D-reconstruction and the cross-sections corresponds to the bottom of 3D-printed tablet

Significant increase in surface area and open pore volume was observed when decreasing infill density from 100% to 65% (Fig.5.3). The more material deposited, more confluence happens between the deposited strings and this leads to less exposed surface. Formulations with programmed 80% and 100% infill showed very similar morphological characteristics. This is likely due to the identical for all designs outer layer, occupying significant part of the tablet volume and lowering effect of programmed infill density on actual porosity. It is possible, that

confluence between the strings in 80% and 100% is similar (overlapping), however 65% we start to have less confluence. Measured relative density (Vsolid/Vtotal) of the formulations was found to be 0.8 for 65% infill density; and slightly above 0.9 for both 80% and 100% infill densities. Due to grid design and the omission of top and bottom solid layer, actual available surface area was higher than reported previously for cylinder-shaped FDM tablets with smaller size [154].

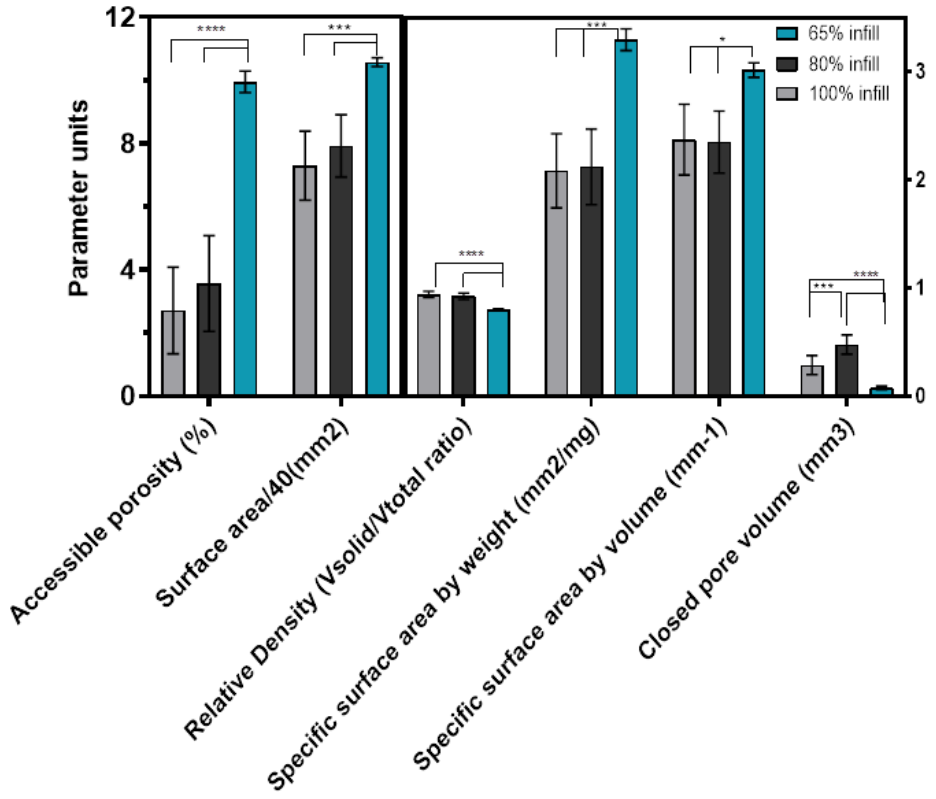

Fig.5.3. Morphological characteristics of 3D-printed 5% lumefantrine tablets, ****P<0.0001, ***P<0. 001, **P<0. 01, *P<0. 05

Table 5-2 Morphological characteristics of 5% lumefantrine 3D-printed tablets

Programmed infill density	**Weight** (mg)**	**x dimension* (mm)**	**y dimemsion* (mm)**	**z dimension * (mm)**	**Surface area* (mm^2)**	**Closed pore volume* (mm^3)**	**Open pore volume*(mm^3)**	**Measured relative density*100 (%)**
65%	108±21	9.2±0.3	4.9±0.1	3.9±0.05	422.9±5.4	0.08±0.02	13.96±0.40	80.0±0.7

80%	142±11	8.9±0.2	4.5±0.1	4.0±0.01	316.9±39.5	0.48±0.09	4.80±2.06	92.5±3.1
100%	139±13	9.2±0.3	4.9±0.1	3.9±0.05	291.8±43.8	0.29±0.09	3.33±1.72	94.3±2.8

Data presented as mean±std, based on average of *n=3 or **n=6

5.3.3 Drug load and degradation products

Lumefantrine appeared to degrade during hot-melt extrusion (no stabilizer/anti-oxidant was added), resulting in 92-97.5% assay depending on drug load and process parameters (see Table 5-3). Decreasing HME temperature from 138°C to 120°C resulted in closer values to nominal for higher concentrations of lumefantrine in 7-month-old filaments. For FDM-processable formulation, assay and by/degradation (BDP) products values in 3D-printed tablets after 2 months from manufacturing and filaments were similar, demonstrating no additional degradation during FDM 3D-printing process.

Table 5-3 Assay and degradation products in selected lumefantrine formulations

Product type	Drug load (%)	Assay (%)	BDP1 (%product)	BDP2 (%product)	BDP3 (%product)	HME temperature (°C)	3D-printing temperature (°C)	Age (months)
Filaments	5	**92.2±0.11**	not detected	0.42±0.02	0.11±0.12	138	n.a.	7
Filaments	15	**96.7±0.77**	0.14±0.005	0.50±0.02	0.16±0.001	128	n.a.	7
Filaments	30	**97.5±0.02**	0.20±0.005	0.87±0.02	0.16±0.02	120	n.a.	7
3D-printed tablets	5	**93.1±0.34**	not detected	0.26±0.24	0.07±0.05	138	160	2*

*3D-printed from 5-months' old filaments

5.3.4 Solid state analysis

DSC analysis showed a melting temperature of about 130°C for pure drug, with absence of a melting peak for lumefantrine in powder blends, filaments and 3D-printed tablets (Fig.5.4A). This lack of melting peak might be attributed to dissolution of lumefantrine in molten Eudragit EPO or peak below limit of detection due to low concentration of drug in blend. No melting peak characteristic to crystalline drug was observed in 5-15% lumefantrine in physical mixtures- initial powder blends (Fig.5.4A), with a weak peak around 130°C appearing only when drug concentration was increased to 30%, which is in line with both proposed explanations. XRPD analysis of 5% LUM 3D-printed tablets and 5-15% filaments demonstrated that the drug substance (DS) was in the amorphous state ,as opposed to pure DS and powder blend showing diffraction peaks at 18°,19°,20° and 23° 2θ characteristic to

crystalline lumefantrine (Fig.5.4B). For filaments with drug load of 30% the drug crystalline content was visible in the XRPD.

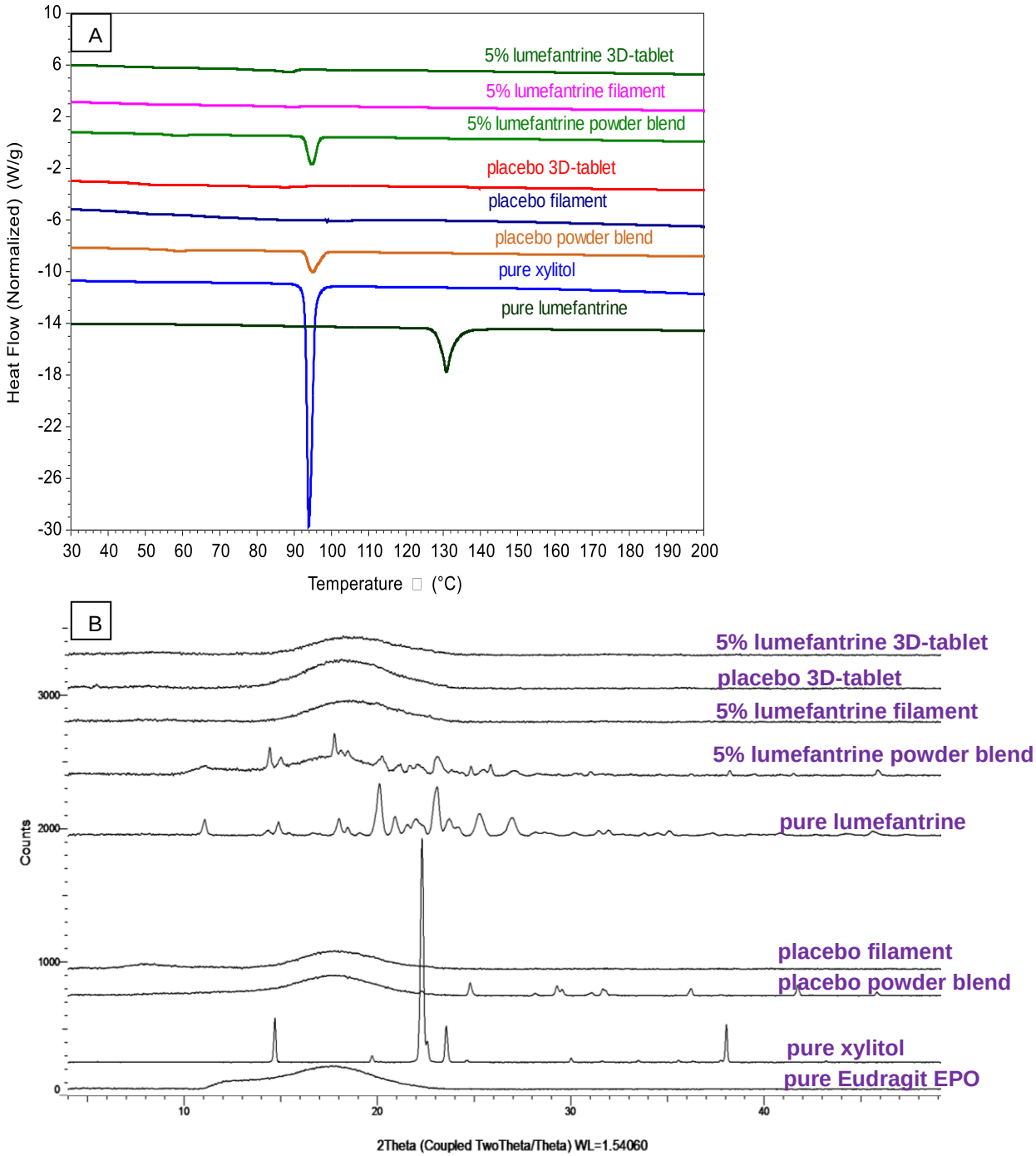

Fig.5.4. (A) DSC thermograms and (B) XRPD diffractograms of 5% lumefantrine formulation (5% lumefantrine: 72% Eudragit E PO: 13.5% xylitol: 9.5% maltodextrin) and corresponding placebo throughout manufacturing steps from powder blends to 3D-printed tablets

Raman mapping confirmed that lumefantrine was fully amorphous in 5% drug load 3D-printed tablets (Fig.5.5A,B). In all filaments the presence of crystalline lumefantrine (characteristics peaks within 1634-1636 cm^{-1}) was detected in Raman (Fig.5.5D,E), although it was undetectable with XRPD due to its lower limit of detection. In addition, Raman analysis demonstrated evidence of crystallinity for all filaments with higher drug load (Fig.5.5D,E,F), in agreement with XRPD for 30% LUM filament. Spatially, Eudragit EPO was fully miscible with lumefantrine in the amorphous solid state and not detected as single entities (Fig.5.5A-E). For 30% lumefantrine filament (Fig.5.5F) polymer matrix was seen due to its weak signal-to-noise ratio, as crystals have much better scattering properties than polymers or amorphous material and signal of the highly concentrated crystals was significantly stronger than of the matrix .The drug products were stored at room temperature. The tablets were analyzed 16 weeks after manufacturing (Raman), and filaments from 10 to 30 weeks after manufacturing (Raman) and 8 weeks (XRPD). There could be two possibilities to achieve the detected solid state: i) obtaining an amorphous 3D-printed tablet from the filament, which was still amorphous at the moment of production but recrystallized later (16 weeks vs 30 weeks from the hot-melt process); ii) re-melting of lumefantrine crystals (undetected with XRPD) in the filament, which could be an interesting option to create ASD during decentralized printing. These findings highlight importance of more precise than XRPD techniques for substances crystallinity determination, which solid state is critical for *in-vivo* bioavailability (i.e BCS class IV drugs).

To conclude, all tested filaments showed some levels of lumefantrine crystallinity whilst 3D-printed tablets were entirely amorphous after 10-30 weeks at room temperature. Hence, the process for creation in 3D-printed tablets an amorphous form of lumefantrine, which is a bioenhanced formulation type [107, 108] . Lumenfantrine was fully amorphous in the 3D-printed drug product 16 weeks after production, which could be promising for decentralized production and reduction risk of recrystallization on storage for traditional ASDs.

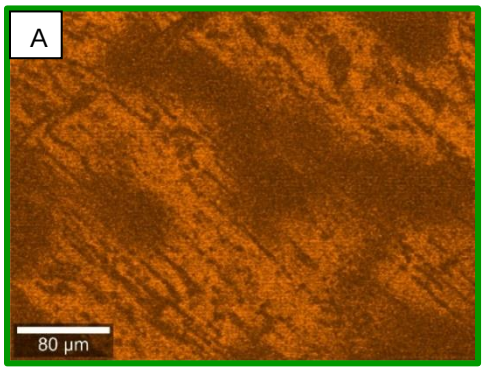

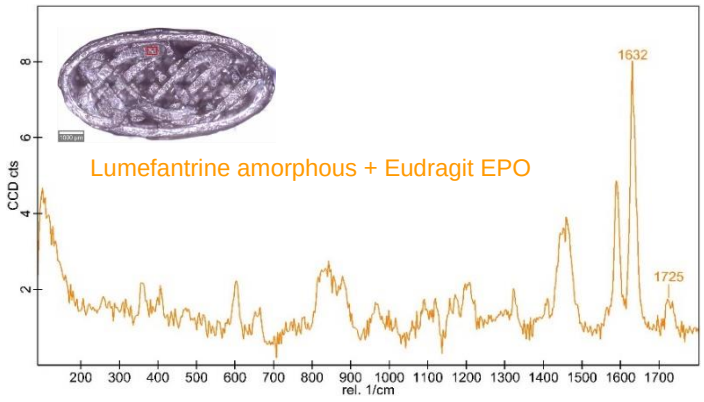

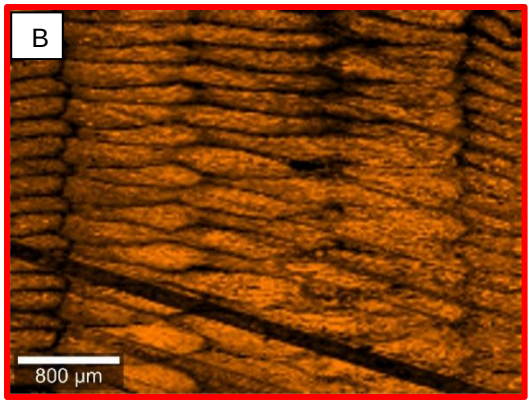
B
800 µm

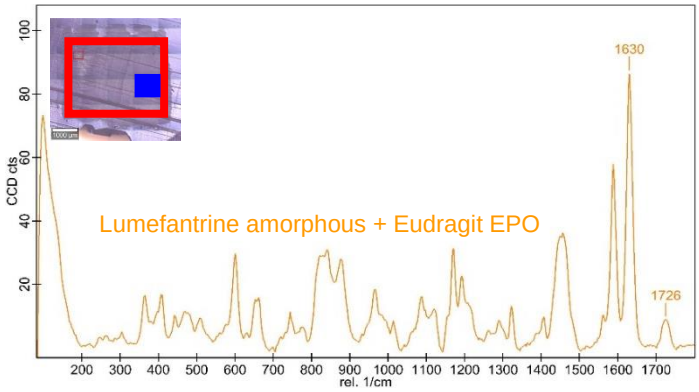
Lumefantrine amorphous + Eudragit EPO
1630
1726
CCD cts
rel. 1/cm

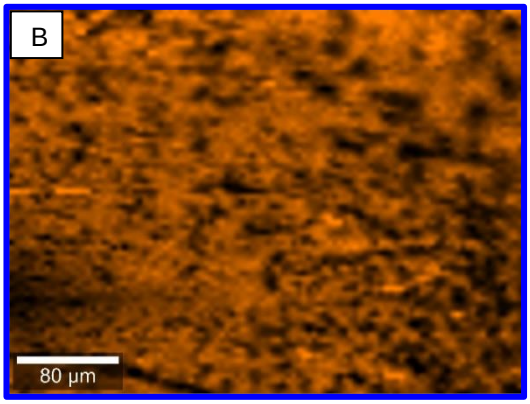
B
80 µm

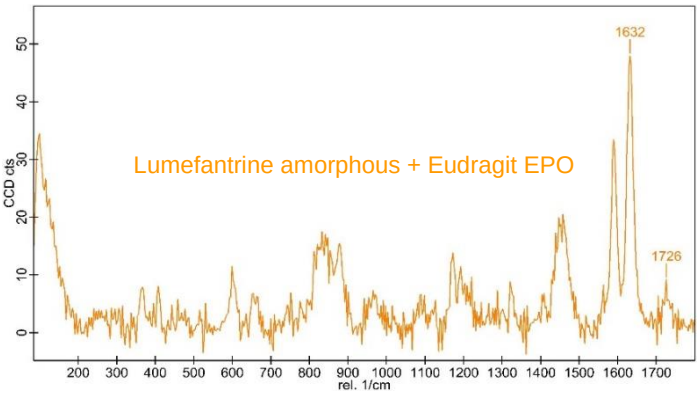
Lumefantrine amorphous + Eudragit EPO
1632
1726
CCD cts
rel. 1/cm

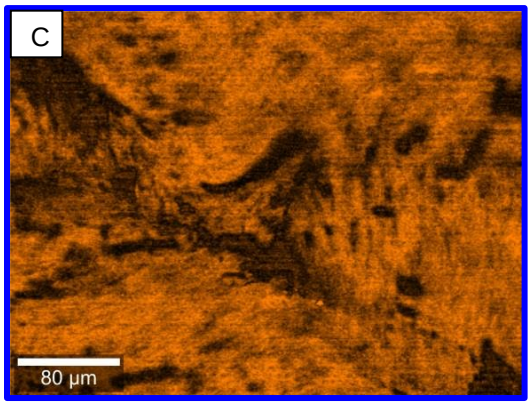
C
80 µm

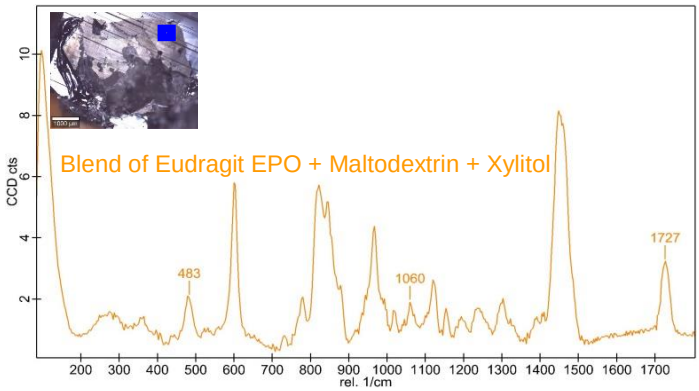
Blend of Eudragit EPO + Maltodextrin + Xylitol
483
1060
1727
CCD cts
rel. 1/cm

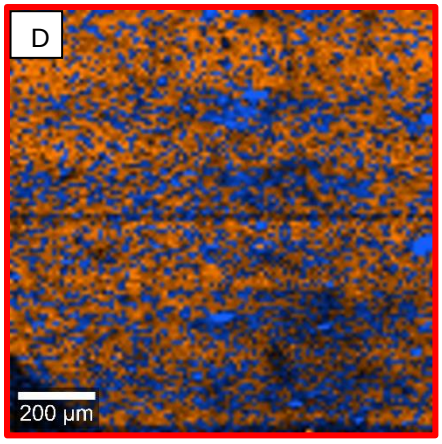
D
200 µm

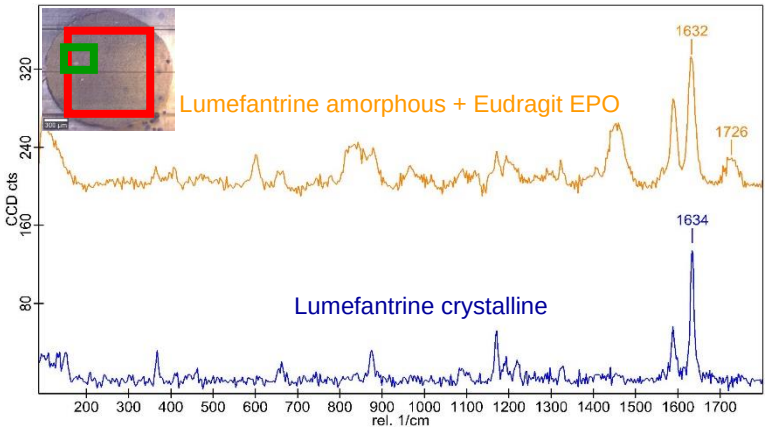
Lumefantrine amorphous + Eudragit EPO
1632
1726
1634
Lumefantrine crystalline
CCD cts
320
240
160
80
200 300 400 500 600 700 800 900 1000 1100 1200 1300 1400 1500 1600 1700
rel. 1/cm

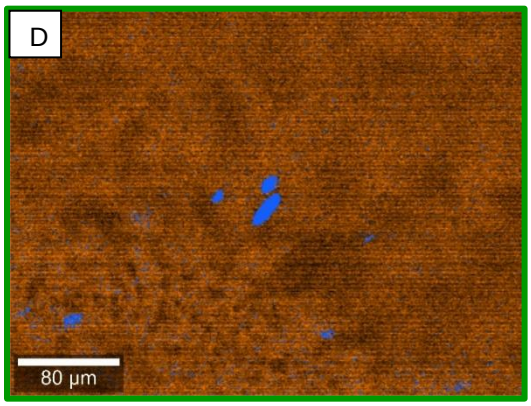
D
80 µm

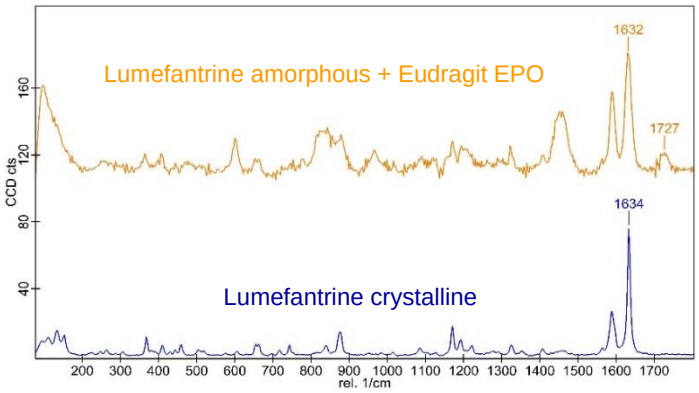
Lumefantrine amorphous + Eudragit EPO
1632
1727
1634
Lumefantrine crystalline
CCD cts
160
120
80
40
200 300 400 500 600 700 800 900 1000 1100 1200 1300 1400 1500 1600 1700
rel. 1/cm

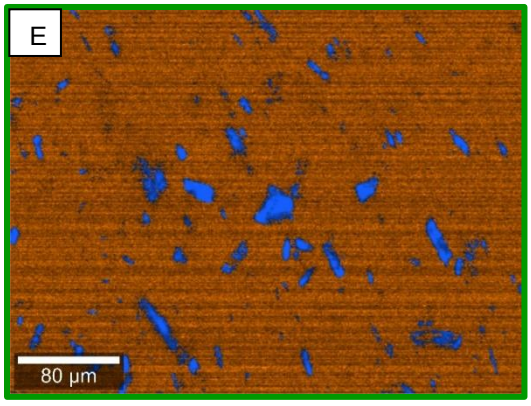
E
80 µm

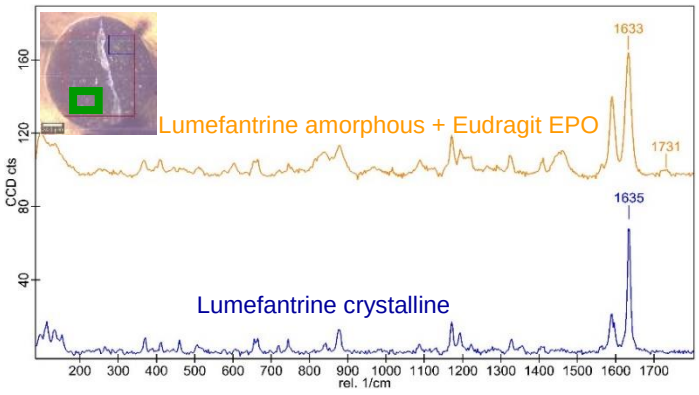
Lumefantrine amorphous + Eudragit EPO
1633
1731
1635
Lumefantrine crystalline
CCD cts
160
120
80
40
200 300 400 500 600 700 800 900 1000 1100 1200 1300 1400 1500 1600 1700
rel. 1/cm

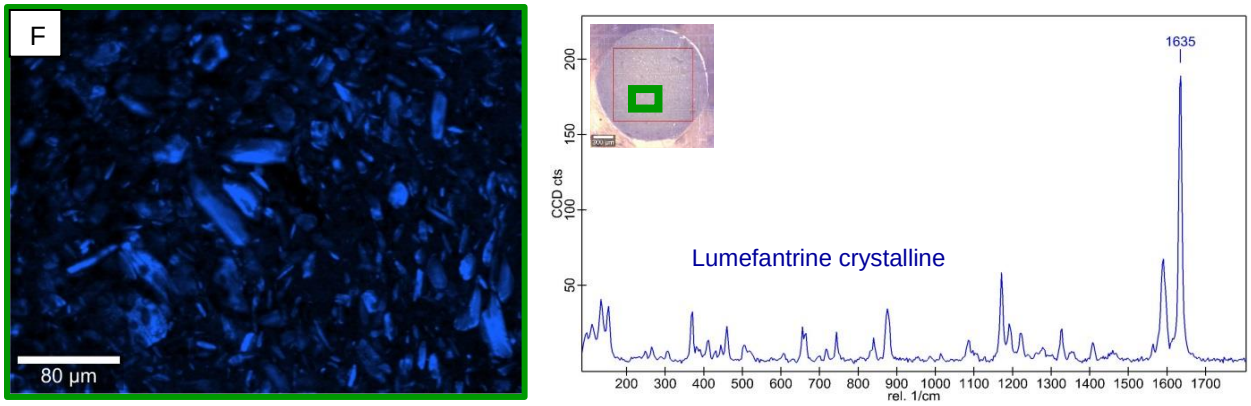

Fig.5.5. Raman spectral map (left hand side panels) and extracted spectra including representative reflection optical micrograph (right hand side panels) for: (A) surface of 5% lumefantrine 3D-printed tablet; (B) cross-sections of 5% lumefantrine 3D-printed tablet at low and high magnification, (C) corresponding placebo tablet, (D) 5%, (E) 15% and (F) 30% lumefantrine filament cross-sections. Crystalline lumefantrine is shown in blue, amorphous lumefantrine is shown in orange. Images (A), (B), (C) are typical of all infill densities

5.3.5 Dissolution studies and morphology-dissolution relationship

Dissolution tests of 5% lumefantrine 3D-printed tablets with the different infill densities in 0.1 N HCl with 0.5% CTAB are shown in Fig.5.6. Formulating lumefantrine with Eudragit EPO as primary matrix former and Xylitol/Maltodextrin combination was demonstrated as promising approach to achieve Immediate Release .FDM printed tablets with 65% density demonstrated rapid dissolution, as about 90% model BCS IV drug was released in 30 min. Increase in infill density to 80% resulted in slower API release with about 78% dissolved in 30 min, followed by further release rate decrease for 100% infill density (about 69% dissolved after 30 min).The faster drug release from lower infill tablets is consistent with previous findings [24, 90], which is usually attributed to their higher surface area to volume ratio as compared to higher infill tablets. The fact that infill density of the tablets affected the drug dissolution rate suggests that water penetrated freely through the pores of FDM 3D-printed lumefantrine tablets. Drug relative dissolved amount from reference compressed tablets were similar to the result of 3D-printed tablets with 65% and 80% infill. However, biorelevance could not be claimed as amorphous solid dispersion (in 3D-printed tablets) is known to have higher bioavailability[107, 108] than crystalline drug (in standard tablets). However, reduced infill density allowing faster dissolution rate would be expected to be beneficial *in-vivo* in comparison to denser matrix.

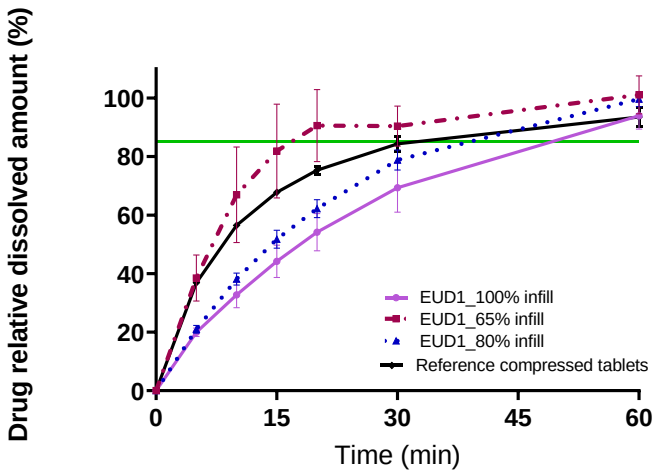

Fig.5.6. Dissolution profiles of 3D-printed tablets (5% lumefantrine, 72% Eudragit E PO, 13.5% xylitol, 9.5% maltodextrin) with 100%, 65% and 80% infill density; and of reference compressed 120 mg lumefantrine tablets. Points and bars depict mean and standard deviation of n=3 measurements

With the aim to bridge between printed morphology and dissolution performance, the drug relative amount dissolved at early time points as function of various structural parameters was studied. Effects of measured density, total and specific surface area, closed and open pore volume were explored. Accessible porosity (open pore volume), surface area, were identified as key parameters responsible for dissolution rate acceleration. 3D-tablets with 65% infill density, the only variant which met rapid release criteria, showed statistically significant increase in surface area, accessible porosity, specific surface area by weight and by volume, as well as decrease in relative density, but not in closed pores volume (Fig.5.7).

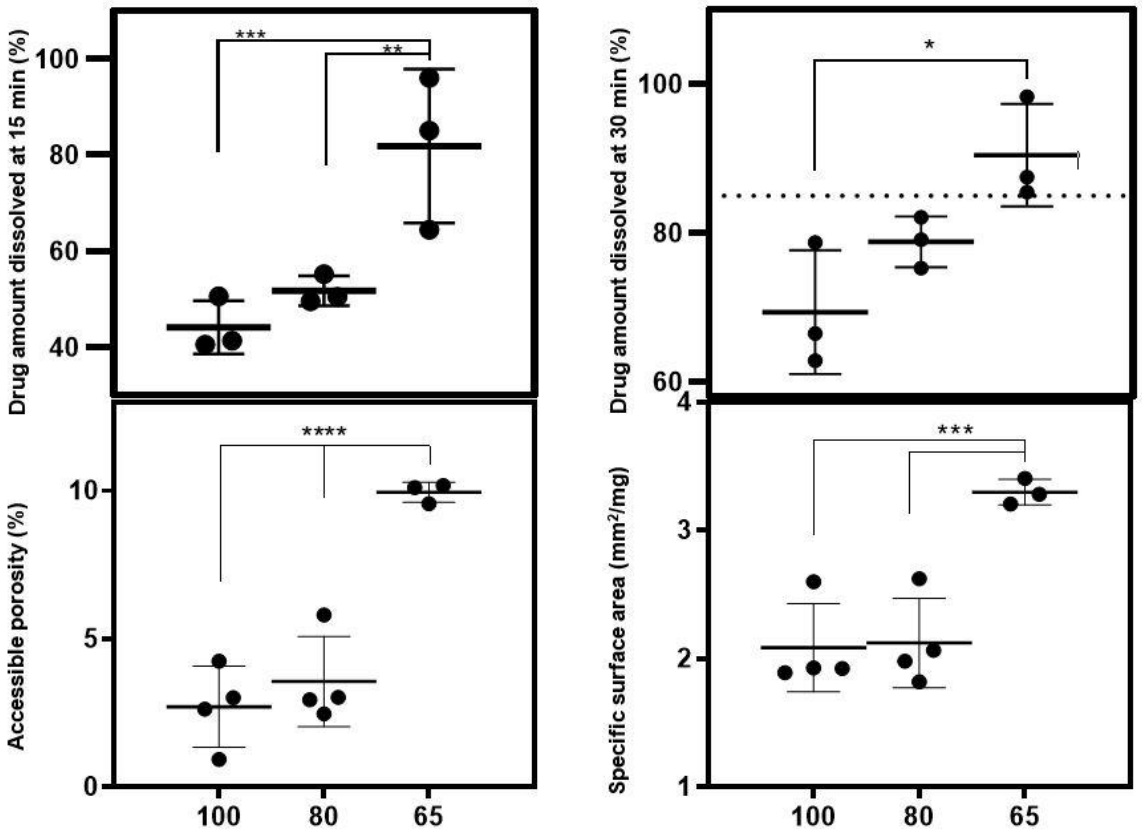

Fig.5.7. Statistical analysis of morphological characteristics and dissolution performance of 3D-printed 5% lumefantrine tablets for three infill densities shown in the x-axis, *P<0.05, **P<0.01, ***P<0.001, ****P<0.0001

Therefore, lumefantrine-Eudragit system was responsive to an increase in surface area that allowed greater water access and faster dissolution [130].Complete lumefantrine dissolution from 65% and 80%infill densities occurred at 60 min time point, however for 100% infill density full dissolution occurred at 120 min only

5.4 Conclusions

Immediate Release Eudragit EPO-based 3D-printed tablets with BCS class IV model compound were successfully developed via structural design modification. Incorporation of programmed infill density of 65%, was needed to meet rapid release criteria (at least 85% drug dissolved after 30 minutes). Moreover, achieved via 3D-printing full amorphous solid dispersion was stable for the time reasonable for decentralized manufacturing.

The observed weight deviation points necessity of in-built monitoring of melt flow and/or viscosity added by equipment manufacturers for better control of critical quality attributes of the processed objects in order to meet the regulatory requirements for weight uniformity.

Raman mapping detected evidence of crystallinity in filaments undetectable with XRPD.

The developed non-destructive microCT-based analytical methodology provided accurate morphological quantification, which was linked to dissolution behavior. Accessible porosity, surface area, relative density and

specific surface area by weight and by volume of 3D-printed tablets were identified as significant parameters responsible for dissolution rate acceleration in 65% infill density tablets. Similar morphological characteristics between 80% and 100% infill densities were reflected in dissolution performance. For the future development of IR FDM-printed dosage forms one could reduce closed pores volume, embrace open pores, as well as optimize balance between shape/size and dissolution. With regards to IR dosage forms with poorly-water-soluble compounds, combinational approach to formulation, process and morphology might be required.

The developed precise non-destructive morphological analytical method provided accurate morphological quantification and structure-dissolution relationship by using X-ray computed microtomography. The approach was crucially based on the application of appropriate binary threshold and verified by correlation to established density measurement analysis whereby, and unlike previous reports, resulting in establishing an extended range of representative morphometry parameters. Open pore volume, surface area, relative density and specific surface area by weight and by volume of 3D-printed tablets were identified as key parameters responsible for dissolution rate acceleration. For the future development of IR FDM-printed dosage forms one could reduce closed pores volume, embrace open pores, as well as optimize balance between shape/size and dissolution.

Understanding of formulation critical design and quality attributes could facilitate dose and release profile adjustments of solid dosage forms according to patient needs. This could pave the way to a new paradigm of decentralized manufacturing at hospital and community pharmacy, where one filament could be a drug formulation to deliver range of dosage strengths and release profiles.

6 Chapter 6

Simplification of Fused Deposition Modeling 3D-Printing Paradigm: Feasibility of 1-step Direct Powder Printing for Immediate Release Dosage Form Production[5]

Summary

Direct powder three-dimensional (3D)-printing (DPP) of tablets to simplify fused deposition modelling (FDM) was explored. The FDM paradigm involving hot-melt extrusion for making 3D-printable drug-loaded filaments as intermediate products for tablet manufacturing has been gaining attention for the decentralized on-site production of personalized dosage forms. For direct 3D-printing, powder blends were loaded into a cartridge-like head and were successfully printed with honeycomb design following heating of the extrusion cartridge. This 1-step DPP with incorporation of in-built porosity providing higher surface area served as proof of concept for manufacture of rapid release dosage forms. Water soluble hydroxypropylcellulose SSL was chosen as matrix former and caffeine as model drug. The effect of PEG4000 as plasticizer/pore former and Kollidon VA64 as rapidly dissolving polymer on DPP processability and dissolution rate was investigated. Directly 3D-printed tablets with low (30%) infill density showed rapid dissolution independently of the formulation, whereas for high (80%) infill density a combination of PEG4000 and Kollidon VA64 was required to achieve rapid release. The obtained tablets demonstrated good uniformity of percent drug content but had variable weight. Caffeine was present in crystalline state and in the stable polymorph in the tablets. Hence, DPP feasibility for immediate release dosage form manufacture was demonstrated. This technique might create an opportunity to avoid hot-melt extrusion allowing 3D-printing independently of mechanical properties of a filament and potentially prolonging product shelf life by reducing thermal stress.

[5] Fanous, M, Gold, S, Muller, S, Hirsch, S, Ogorka, J, Imanidis G, *Simplification of fused deposition modeling 3D-printing paradigm: Feasibility of 1-step direct powder printing for immediate release dosage form production.* Int J Pharm, 2020. **578**: p.119124

6.1 Introduction

Recent studies indicate opportunities to improve safety and efficacy for some medications via application of flexible and personalized dosage strengths [3] [4]. However, current large-scale manufacturing of dosage forms with a few fixed strengths is limited for dose individualization. Development of 3D-printing technology could bring a potential solution for on demand manufacturing of dosage units [67] [135]. Moreover, installation of small desktop 3D-printers in hospitals and pharmacies might create an opportunity for decentralized dosage forms manufacturing on-site [80]. Complex designs and geometries, multiple APIs and tailored release profiles might enable pharmaceutical 3D-printing to fulfil as yet unmet clinical needs [16].

3D-printing technology allows creation of solid objects of various designs, which are fabricated through layer-by-layer addition of materials based on a digital model. Several 3D-printing technologies exist such as selective laser sintering, powder based, inkjet printing, fused deposition modelling (FDM) and semi-solid extrusion [71] [17] [147]. These vary with respect, e.g., to process parameters such as temperature, spatial resolution of fabrication, processability of dedicated raw materials, versatility, and applicability to pharmaceutical systems in clinical settings. FDM 3D-printing in particular, involves melting of a thermoplastic filament, which is deposited in ultrafine threads along the extrusion path through the print head nozzle. For on-site manufacturing, such as in hospital or pharmacy, manufacturing of dosage forms via low-cost FDM 3D-printers might be advantageous as no powder or solvents [92] are involved in the printing process, post-processing could be avoided and mechanically strong tablets are produced [93]. The main challenges though are 3D-printability linked to mechanical properties of the filament [16], possible API degradation caused by exposure to heat [84] and tendency for slow dissolution [26].

Pharmaceutically applicable polymers, explored for FDM included cellulosic derivatives, polymethacrylates, polyurethanes and polyvinyl alcohols [85]. A variety of extended release formulations were developed for FDM 3D-printing [84] [85] [79] [86], whereas development of immediate release (IR) dosage forms appears to be more challenging [78]. Attempts to accelerate drug release included addition of non-melting fillers [126] or building fragmented tablet geometries [90] or employing polymers yielding filaments that could not be 3D-printed independently [91]. Rapid release tablets were further reported [32] yet not fulfilling the pharmacopeia criteria for immediate release products. As IR formulations represent 70% of total oral tablet market share [87] [88], availability of IR formulations is a major need towards the future of personalized dosage form production.

Moreover, the current FDM 3D-printing is a multi-step process, involving powder blending as a first step, followed by hot-melt extrusion to obtain the filament, prior 3D-printing of the filament. This may affect chemical stability for heat sensitive compounds starting a drug product shelf life countdown much earlier than the actual 3D-printing of the final dosage form. Further, formulation development needs to consider mechanical properties of the obtained filaments to allow FDM processability. This leads to materials limitation, incorporation of excipients purely to achieve 3D-printable filaments and potentially compromising drug load and release profile. Hence, potential IR formulations might be prematurely discarded as incompatible with FDM in terms of mechanical properties. Removal of the hot-melt extrusion step and reliance on filaments as intermediate products for 3D-tablets manufacturing, presents an opportunity to speed up formulation development, and focus the formulation on the needs of 3D-printing

process and release profile and enrich available design space for pharmaceuticals. Recently Goyanes et al. reported for the first-time direct powder printing feasibility for sustained release itraconazole tablets production at throughput comparable to FDM printing [27].

The objective of this study was to simplify current FDM paradigm to obtain rapid release 3D-tablets with high spatial infill resolution, by removing the step of hot-melt extrusion and reliance on filaments as intermediate products for 3D-tablets manufacturing. The difference of the employed direct powder printing technique to that reported in [23] is discussed. Emphasis of the current study was to test feasibility of direct powder 3D-printing for immediate release dosage form production.

6.2 Materials and methods

6.2.1 Materials

Caffeine (Sigma–Aldrich, UK), molecular weight 194.19 g/mol, was used as a model API. Powder mixtures of hydroxypropylcellulose (HPC SSL, Nisso Chemical, Tokyo, Japan) with or without vinylpyrrolidone-vinyl acetate copolymer (Kollidon VA64, BASF, Ludwigshafen, Germany) and Polyethylene glycol (PEG4000, Clariant, Sulzbach, Germany) with 10% caffeine were prepared. HPC SSL polymer served as hydrophilic matrix, PEG4000 as pore former and hydrophilic plasticizer, and Kollidon VA64, a rapidly dissolving polymer as possible dissolution facilitator.

6.2.2 Methods

6.2.2.1 Direct powder printing (DPP)

Powders were accurately weighed into 0.5 L bottles to make a total batch weight of 45 g and were mixed via diffusion blending for 10 min at 32 upm by T2 Turbula™ mixer.

A RegenHU Bioprinter (RegenHU, Villaz-St-Pierre, Switzerland) was used for direct powder 3D-printing experiments. About 5 g of the powder blend was directly loaded into the DDI135 head comprising a stainless steel cartridge with a volume of 10 cm^3 that was equipped with a piston and had a 0.3 mm nozzle. Printing was performed in a layer-by-layer manner following heating. Cartridge interior was neither stirred nor degassed, and pre-heating took place for approximately 10 minutes before printing commenced. A printing temperature of 155°C - 180°C was used depending on the formulation and adjusted empirically when necessary to facilitate printing. Pneumatic pressure of 1.6-3.0 bar was applied through the piston to achieve an acceptable layer deposition.

The template used to print the dosage form was designed with FreeCAD 0.13 software. The selected geometry was an oval tablet (see Fig.6.1). The tablet size was set to 8 x 16 x 4 mm (width x length x height) with one continuous outer layer (altitude shell) and no continuous bottom/top layers. The continuous outer layer enclosed the perimeter of the structure which had no bottom or top layer. Printing was performed at an ambient temperature (approx. 20-22°C) on glass surface at 8 mm/sec speed with layer height 0.15 mm using honeycomb infill pattern as determined by FreeCAD software. The maximal programmed infill density, feasible with the available set up was 80%. Two infill densities were printed, a high (80%) and a low (30%) one, the latter been chosen arbitrarily. After printing, the manufactured tablets were weighed and their dimensions were measured manually with a caliper.

Table 6-1 Formulations compositions and process parameters

Formulation component (% w/w)	**10% Caffeine HPC0**	**10% Caffeine HPC7**	**10% Caffeine PEG1**	**10% Caffeine HPC0**	**10% Caffeine HPC7**	**10% Caffeine PEG1**
Caffeine	10	10	10	10	10	10
HPC SSL	90	45	76.5	90	45	76.5
Kollidon VA64		31.5			31.5	
PEG4000		13.5	13.5		13.5	13.5
Process parameters						
Infill density (%)	30	30	30	80	80	80
T printing (°C)	170	155-158	160	180	158	160-165
Pressure (bar)	3.0	2.5	1.3-1.4	3.0	2.2-2.5	1.6

6.2.2.2 Drug load and uniformity of percent drug content

A tablet (n=3 for each formulation) was dissolved in 100 mL water, and the drug concentration was determined by HPLC (Agilent, UK) with Zorbax Eclipse plus 1.7µm, 50 x 2.1mm column (Agilent Technologies, UK), maintained at 15°C. The injected volume was 1µl. The mobile phase consisted of two components: water and methanol, starting with the former at 95% and decreasing gradually to 60% after 4 min, and increasing back to 95% after 9 min. The flow rate was 0.5 ml/min and the UV detection was carried out at a wavelength of 272 nm. All measurements were performed in triplicate. Values of separately analyzed samples (n=3) randomly selected from the two infill densities available of each formulation were normalized by weight to calculate the average percent drug content.

6.2.2.3 Dissolution test conditions

A semi-automatic tablet dissolution system Sotax AT7 (Sotax AG, Aesch, Switzerland) fulfilling requirements for USP2 dissolution method was used to perform the studies. *In vitro* release profiles of the tablets (n=3 for each formulation) were studied at pH=2 (0.01N HCl) [122] [160]. The medium was degassed with helium for 30 min on the day of experiment. Each tablet was pre-weighed and placed in the dissolution vessel containing 1000 mL 0.01 N HCl. Dissolution was carried out with a paddle speed of 50 rpm at 37 °C for 2 hours. The paddle speed was then increased to 150 rpm for a further 0.5 h to ensure full dissolution, and obtain an “infinity” value. Samples (10 ml each) were collected at time points 0, 5, 10, 15, 20, 30, 45, 60, 120 and 150 min. The dissolution medium was replenished after each sampling with an equivalent amount of 0.01N HCl solution. The drug concentration of the

samples was analyzed for concentration as above using Perkin Elmer Lambda 25 UV spectrophotometer at 272 nm. Expected 100% dissolution value was calculated based on the average drug content of the formulation. Dissolution profiles were visualized by plotting percentage of drug dissolved against time. At least 85% of drug relative dissolved amount (average n=3) after 30 min was set as rapid release criteria.

6.2.2.4 X-ray powder diffraction (XRPD)

Powders were analyzed on a quartz sample holder. Powder blends were directly dispensed on the holder surface, 3D-printed tablets were gently/manually ground with mortar and pestle. XRPD analyses were performed on a diffractometer using a K430 X-ray generator with a copper anode (voltage: 40 kV, current: 40 mA). XRD patterns in temperature were recorded in transmission mode using quartz capillaries 1.5 mm diameter (GLASS W. Müller, Berlin, Germany). The X-ray generator was a long line focus sealed tube (Siemens; Germany, Cu anode with a Kα line at 1.54 Å, operating at voltage of 40 kV and current of 20 mA). One 2D VÅNTEC-500 Area detector (4 channels, filled with argon-ethane mixture) were used to collect the data. With the settings used, 2θ angles were calculated, ranging from 1 to 18° and from 18 to 36°. Diffractograms were generated with the software Diffrac.EVA V4.0 from Bruker, USA.

6.2.2.5 Differential scanning calorimetry (DSC)

DSC measurements were performed using a Q2000 DSC (TA instrument, New Castle, PA) under nitrogen flow of 50 ml/min. Samples between 1 and 2.5 mg were analyzed using punctured aluminum pans, an empty pan was used as reference. A heating rate of 10°C/min was set between -20°C and 300°C. Software Trios v4.4.1 (TA Instruments, Inc., Waters Corporation, MA, USA) was used.

6.2.2.6 Hot-stage microscopy (HSM)

Hot stage Linkam LTS350 with Linkam TP 94 controller were used. HSM was conducted using Zeiss AxioPlan 2 imaging microscope equipped with Zeiss Plan-Neofluar objectives (5x, 10x, 20x, 40x). Phase transition during the heat-cool process was observed and images captured by Olympus UC30 camera under polarizing light for further analyses. Samples were placed on open glass slides, fixed on the hot stage and heated from 25 to 270°C at 10 °C/min. After achieving 270°C, cooling of the samples at room temperature was performed and images captured up to 72 minutes after the heating has been stopped.

6.2.2.7 Xray microcomputed tomography (microCT)

Internal structure of 3D-printed dosage forms was visualized using X-ray microcomputed tomography (Skyscan 1172, Skyscan, Kontich, Belgium). Samples were scanned in 2000 projections at a resolution of 11.32 μm/voxel. Acceleration voltage was 59 kV and currency 167 μA. Image reconstruction was conducted with NRecon software (Bruker, USA). For visualization of the created mesh, DataViewer software (Bruker, USA) was used.

6.2.2.8 Data analysis

The data are presented as mean ± SD, and the differences between various groups were analyzed by two-way ANOVA followed by Tukey's post hoc test (GraphPad Prism, version 7.0, GraphPad Software, San Diego, CA). The statistical significance was considered at $p < 0.05$.

6.3 Results and discussion

Manufacture of tablets by 3D-printing directly from powder was achieved with high spatial resolution of the internal structure of the tablet as shown by µCT and with size being in good agreement with the preset dimensions. Tablet length was 15.68 – 16.09 mm, width 8.02 - 8.1 mm and height 4.02 – 4.28 mm. No systematic difference of size between formulations was evident. X-Ray MicroCT scan provided evidence of highly repetitive and accurate structure (see Fig.6.1). Three formulations were directly 3D-printed with high and low infill density, with no significant difference in printing temperature and pressure between the two infill densities within the same formulation. Formulations composition affected process parameters, e.g. inclusion of plasticizer PEG4000 as reported by Desai [161] in the presence or absence of Kollidon VA64 allowed more mild processing conditions such as lower temperatures and pressures in comparison to use of HPC as single excipient (Table 6-1). Independently of formulation, direct print of one tablet required about 17 min (including preheating time).

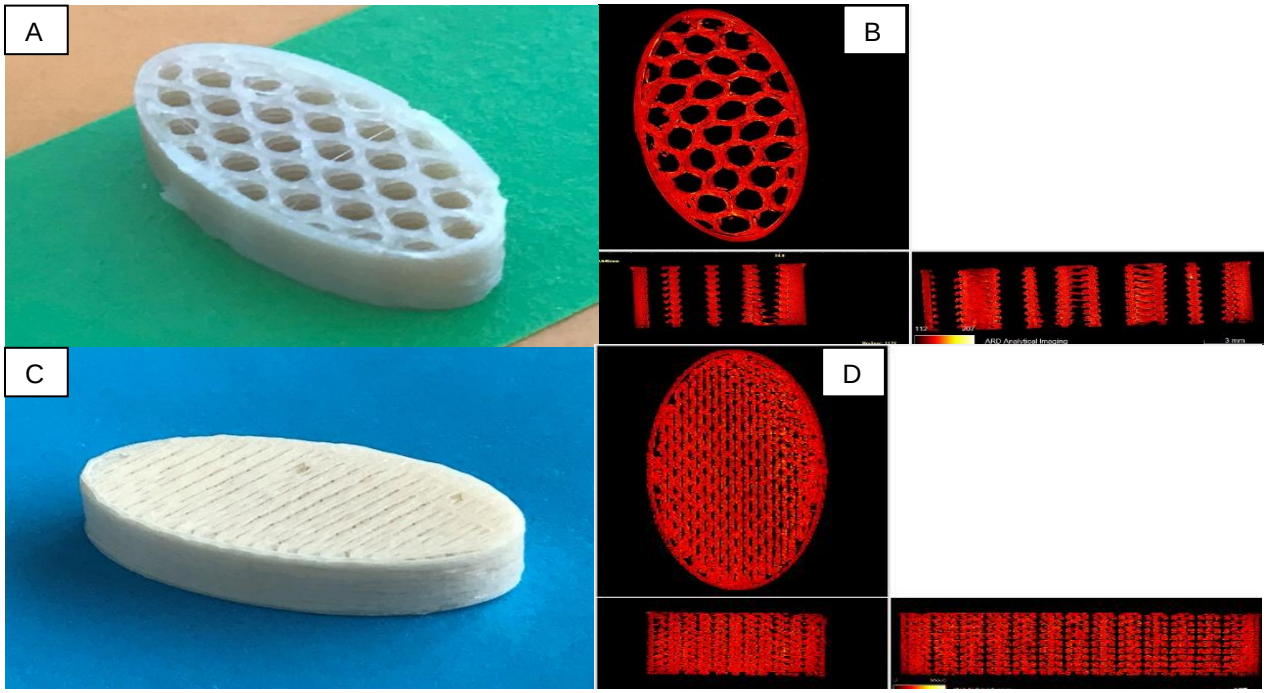

Fig.6.1. Photographs (A),(C) and mid-section microCT scans parallel (top) and perpendicular (bottom) to the plane of the tablet (B),(D) of 3D-printed tablet with 30% and 80% infill density, respectively, following direct powder 3D-printing

Overall printed tablet weight variation of 2-12% was obtained. Tablets with 80% infill density demonstrated more variable weight than those with 30% infill density (Table 6-2). Interestingly, no proportional increase in weight was caused by 50% increase in infill density. For instance, for formulations HPC0 and PEG1 increase of 50% in absolute terms, i.e. more than doubling in infill density resulted in about 25% higher weight, and for HPC7 this rise was less than 3%. The lack of proportionality between infill density and weight is in part because the infill density concerns only the interior while an identical outer layer (altitude shell) constituting a considerable part of the weight of the tablet was present for both infill densities. In addition to the effect of the outer layer, it is evident that the infill density does not directly correspond to the amount of the printed mass as reflected by the weight of the resulting tablets and the different formulations appear to respond differently to the infill density setting. The formulations,

moreover, yielded different tablet weights within the same infill density. A possible explanation might be related to different viscosity and density of the melted formulations and the different values of temperature and pressure used in the printing process. In particular, higher printing temperature used to process HPC0 formulation at the higher infill density possibly resulted in lower melt viscosity and faster flow rate of the melt, translated into more material released from the nozzle. It should be noted that the outer dimensions of the produced tablets given above were essentially the same for both infill densities. These data strongly indicate that in order to achieve accurate drug dosing by direct powder 3D-printing, extensive validation taking into account manufacturing conditions and their impact on the process characteristics of individual formulations is required.

Table 6-2 Uniformity of weight and percent drug content for DPP tablets

Formulation component (% w/w)	**10% Caffeine HPC0**	**10% Caffeine HPC0**	**10% Caffeine PEG1**	**10% Caffeine PEG1**	**10% Caffeine HPC7**	**10% Caffeine HPC7**
Infill density (%)	30	80	30	80	30	80
Finished printed tablet weight* (mg) (mean±std)	314±28.6	403±31.5	294±9.3	362±44.3	326±7.4	335±30.8
Drug content of tablets* (%) (mean±std)	9.90±0.08		10.10±0.22		9.73±0.19	
Drug content in initial blend (%)	9.98		10.59		9.91	

*Average at least n=3

Caffeine content in 3D-tablets was similar to nominal for all formulations, showing assay of 99.2% for HPC0, 98.2% for HPC7 and 95.4% for PEG1. The small variation of initial content between the blends is due to weighing error. In consequence, no difference of drug content between formulations was noted. These results demonstrate that no segregation of the components of the powder blend took place during direct powder 3D-printing likely because the small volume of the cartridge was advantageous for processability allowing uniform heating and reducing the risk of segregation. Assay values and absence of degradation products in HPLC analysis further indicated that the drug did not degrade during direct printing process. This finding is consistent with the thermostable nature of caffeine [26].

DSC of caffeine showed a melting temperature of about 238°C for pure drug, with absence of a melting peak of caffeine in powder blends and 3D-tablets. This lack of melting peak is attributed to dissolution of caffeine in molten HPC (Fig.6.2). XRPD analysis (Fig.6.3) of 3D-printed tablets provided evidence of crystalline caffeine in directly printed tablets (characteristic diffraction peaks at 12° and 27° 2θ), with single-peak characteristic for polymorph I for 3D-printed tablets as opposed to double-peak characteristic for polymorph II for pure caffeine and powder blend. This is in agreement with previously demonstrated polymorphic transformation of caffeine due to the mechanical stress that occurred during manual grinding of the sample [127]. XRPD and DSC demonstrated partial amorphization of PEG4000 in directly printed tablets.

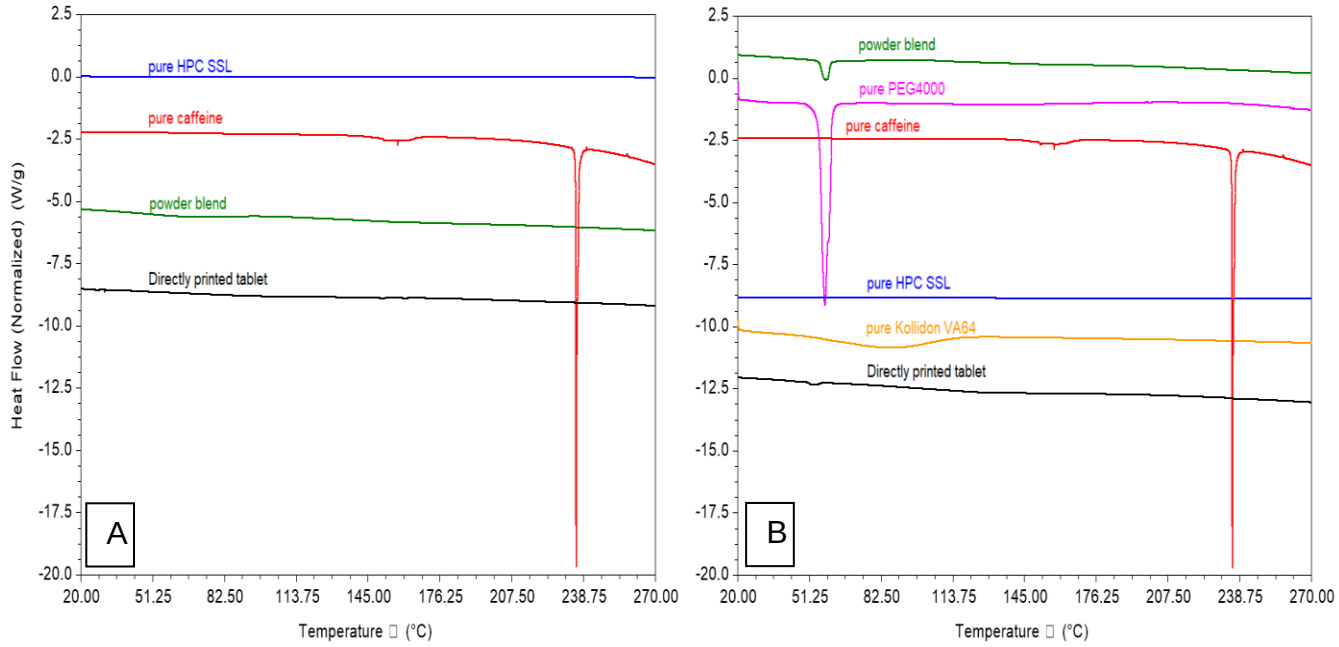

Fig.6.2. DSC thermograms of pure substances, powder blends and 3D-printed tablets for formulations (A) HPC0: 10% Caffeine - 90% HPC, (B) HPC7: 10% Caffeine - 45% HPC - 31.5% KVA64 - 13.5% PEG4000

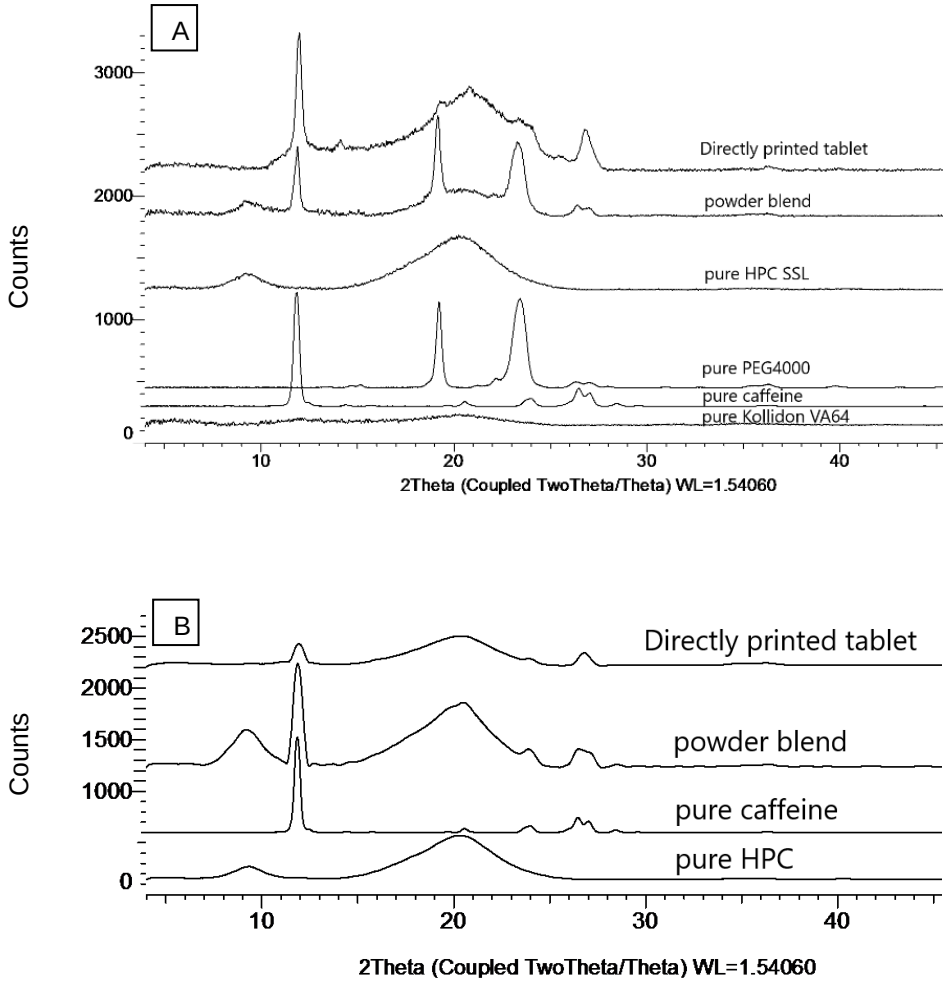

Fig.6.3. X-ray powder diffractograms of pure substances, powder blends and 3D-printed tablets for formulations (A) HPC0: 10% Caffeine - 90% HPC), (B) HPC7: 10% Caffeine - 45% HPC - 31.5% KVA64 - 13.5% PEG4000

HPC melts at lower temperature than caffeine, which allows the drug to dissolve in the molten polymer [143] [144] [145] [146]. This assumption is supported by observations during hot-stage microscopy where the caffeine looks to dissolve in the HPC at temperatures lower than its melting point (Fig.6.4). Before the experiment, caffeine was present in the powder blend as needles generally aggregated in larger particles, which is typical appearance of caffeine as a starting material [127]. Around 180°C (about 60°C below expected melting point of caffeine) caffeine crystals started to dissolve in HPC (Fig.6.4B,C). This confirmed the interaction between caffeine and HPC, which led to absence of a melting peak characteristic of caffeine at DSC, as the drug dissolved before reaching its melting point. However, caffeine appeared to recrystallize rapidly following cooling at room temperature (Fig.6.4D) forming needle-like particles characteristic to polymorph II material. Hence, caffeine was present in crystalline form associated with polymorph II in directly printed 3D-tablets while polymorph I detected in XRPD measurements of the tablets was due to manual grinding of caffeine contained in the products leading to polymorphic transformation.

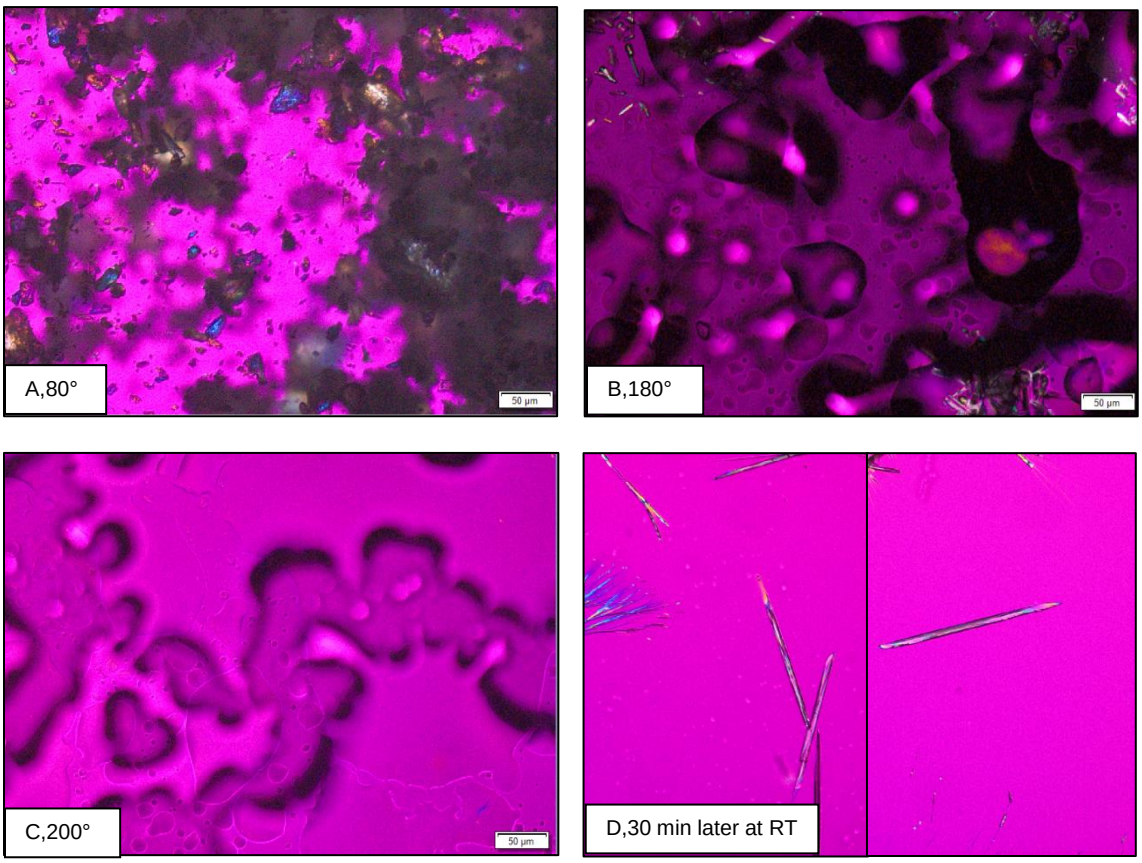

Fig.6.4. HSM images showing phase transition of powder blend components of HPC0 (10% Caffeine - 90% HPC). Sample was captured at A: 80°C, B: 180°C, C: 200°C and D: RT, 30 min after the heating was stopped. Magnification: x20 for A-C, x40 for D

Dissolution tests on the different formulations performed at pH=2 are shown in Fig.6.5. Directly printed tablets with low infill density demonstrated rapid dissolution (at least 85% drug dissolved in 30 min) independently of the formulation. Increase in infill density to 80% resulted in slower API release, with HPC7 (10% Caffeine - 45% HPC - 31.5% KVA64 - 13.5% PEG4000) being the only formulation qualifying for rapid release (Fig.6.5).

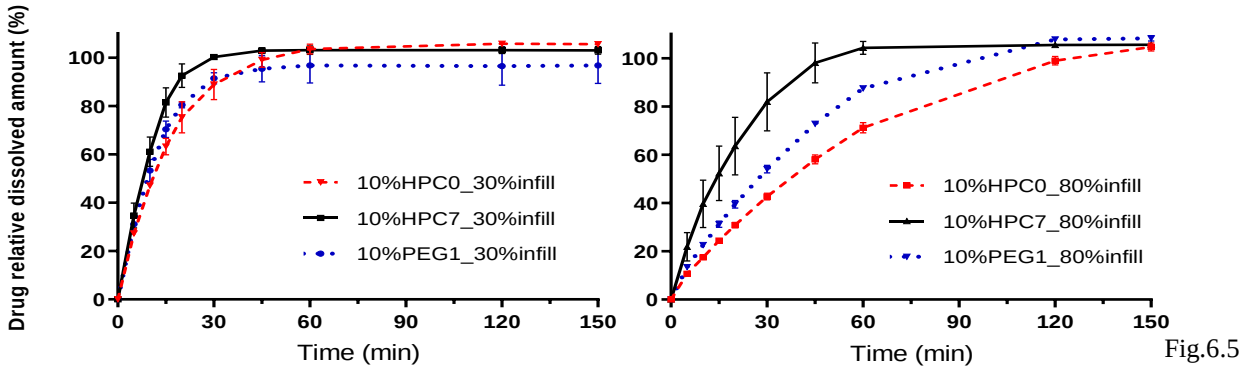

Fig.6.5

Fig.6.5.Drug dissolution profiles of directly printed 10% caffeine tablets with three formulations and low (left) and high (right) infill density

Formulation HPC7, hence, demonstrated superiority for rapid release tablets production, meeting rapid release criteria independently of infill density, with complete drug release in 0.01N HCl after 30 and 45 min for 30% and 80% infill, respectively. The difference of release rate between HPC7 and the other two formulations was for 80% infill density statistically highly significant (Fig. 6.6). Combination of rapidly dissolving polymer Kollidon VA64 as done by Solanki [24] and pore-former PEG4000, when incorporated in cellulosic matrix is herewith shown to positively affect dissolution rate.

Formulations HPC0 and PEG1 exhibited at 30% infill density a significantly faster release than at 80% infill density (Fig 6.6). The faster drug release from low infill tablets may be attributed to their higher surface area to volume ratio as compared to 80% infill tablets, as shown previously for FDM printed tablets [24]. The fact that infill density of the tablets affected the drug dissolution rate suggests that water penetrated freely through the pores of directly printed HPC-based formulations.

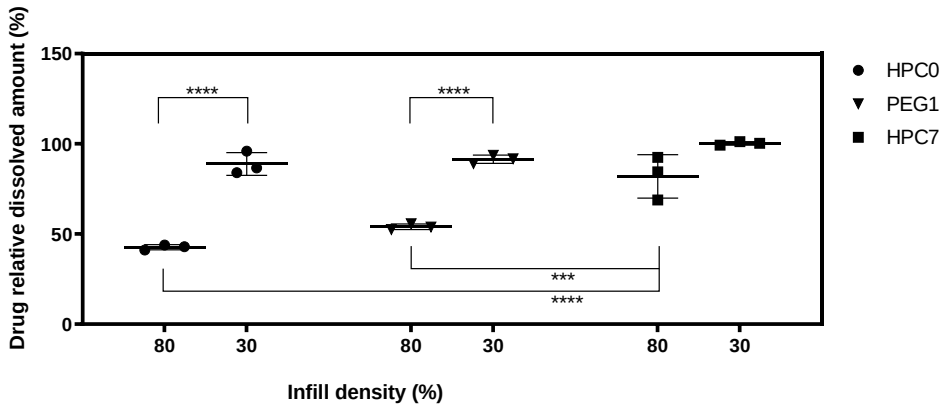

Fig.6.6 Relative dissolved amount of drug at 30 min time point, for directly printed 10% caffeine tablets with low (30%) and high (80%) infill density. P<0.0001 of 80% vs 30% for PEG1 and HPC0. P<0.0001 of 80% HPC0 vs 80% HPC7. P<0.001 of 80% HPC7 vs 80% PEG1

The effect of infill density and thus geometry on release rate is shown to be different for the three formulations. Interestingly, formulations PEG1 and HPC0, which exhibited strong reduction of drug release rate at high infill density also produced a larger increase of tablet weight at the high infill density compared to HPC7. This would translate into a smaller surface area to volume ratio compared to HPC7 for which the surface area to volume ratio would be almost the same for two infill densities based on the weight of the produced tablets. This may provide a reasonable explanation as to why the effect of infill density on release rate is dependent on the formulation. This further points out the necessity of in-built monitoring of melt flow and/or viscosity added by 3D-printer manufacturers for better control of critical quality attributes of the processed object.

Additionally, comparatively slower dissolution observed for formulations such as HPC0 at high infill density might be explained by matrix erosion being the release controlling step. [24]. Therefore, the system is responsive to an increase in surface area that allows greater water access and faster dissolution [130]. For a fast dissolving formulation such as HPC7 on the other hand, drug diffusion may become relevant for release and surface area of access plays less of a role [130]. Complete caffeine dissolution from three tested formulations occurred before 120 min time point for both infill densities.

Compared to the recently published direct powder 3D-printing technique [23] the present work operates with a similar batch size and printing temperature. However, the loading of powder material in an open hopper in [23] may be considered a disadvantage causing putative operator exposure compared to the use of prefilled cartridges introduced in the present study assuring a controlled environment. The mechanism of forward motion of the material by single screw extrusion is fundamentally different than the use of compressed air-driven piston. It is not possible at this time, however, to compare the two mechanisms with respect to robustness and reproducibility. The nozzle diameter in the present study is a lot smaller (0.3 mm) than in [23] (0.8 mm) allowing a better resolution of printing, a smaller layer height (0.15 mm versus 0.2 mm) and smaller weight variability (2-12% versus 11-15%) at the expense of speed (8 mm/s in this work versus 20 mm/s in [23]). API crystallinity in the final product in view of IR properties is out of the scope of this work as caffeine has poor glass forming ability (contrary to itraconazole in [23]) and good water solubility.

6.4 Conclusions

Single step direct powder (fusion) 3D-printing was explored and found to be feasible for manufacture of rapid release dosage forms. Directly printed tablets showed low variability of percent drug content and weight variability that depended on infill density. Decreasing infill density to 30% allowed achieving rapid release of the drug from the directly printed tablets. Infill density affected drug release profile depending on formulation. Direct powder printing technique may create an opportunity to omit the hot-melt extrusion step required for FDM allowing 3D-printing independently of mechanical properties of a filament and potentially prolonging formulation shelf life as thermal stress is applied only once, shortly before tablet production. It is difficult to assess with certainty at this time whether the thermal stress imposed by DPP is indeed smaller than the cumulative thermal stress resulting from the consecutive HME and FDM processes. Nevertheless, DPP has the clear advantage that manufacturing at a central facility requires only the preparation and packaging of the powder blend compared to hot melt extrusion required for FDM. Hence, overall degradation before application of the drug product might be reduced as DPP could be done decentralized on site, with powder blend supplied in prefilled cartridges. Additionally, no excipients are required specifically intended to impart mechanical properties to the filaments that are adequate for 3D-printing. The handling with powders on-site, seemingly a disadvantage of DPP compared to FDM, can be easily alleviated by the use of pro-filled closed cartridges containing the ready-to-print blend. Main concern still is the weight uniformity, which should be investigated with other formulations and model compounds. Flow rate and ideally melt viscosity during the printing should be monitored to validate dose accuracy. In addition, equipment needs to be optimized for pharmaceutical applications as current equipment has long residence time in the melt and continuous stream of air

including oxygen that impact stability. Clinical sites, finally, could potentially benefit from the use of similar 3D-printers to fabricate implants, tablets and even tissues and organs.

7 Final remarks and outlook

Oral dosage forms (ODFs) are safe and convenient, and as such present the most common drug administration route. Opportunities exist to improve safety and efficacy of some medications via personalization of dosage strengths. In order to take advantage of this opportunity novel decentralized manufacturing concepts need to be developed which can be carried out, for example, at hospitals or pharmacies. As discussed in this work, an automated dispensing technique such as 3D-printing presents an interesting approach which could address these needs.

The present work investigated pharmaceutical application of Fused Deposition Modeling and further Direct Powder Printing for decentralized production. At the outset a number of critical quality attributes (CQAs) were defined as success criteria, including uniformity of content to deliver precise dosing, weight uniformity, desired dissolution profiles (immediate release) and physico-chemical stability. These were achieved via optimization of formulations, process parameters and tablet structures.

A toolbox approach was taken to formulation development and resulted in development of scalable hot-melt extruded formulations with a range of drug loads for both hydrophilic and lipophilic compounds. The studies described in Chapters 3 and 6 demonstrated that both DPP and FDM techniques are compatible for thermostable compounds as no API degradation was detected. Sections 4 and 5 supported the view, that careful selection of the main matrix former should be performed for thermally labile compounds, e.g. for lumefantrine Eudragit® EPO-based formulation was more compatible in terms of chemical stability than HPC/Kollicoat® IR-based formulations. Use of HPC as a single excipient for FDM resulted in lower than expected assay attributed to the adherence of powdered drug substance to the walls of the feeding hopper or inner surfaces of the extruder; this was not observed for DPP owing to a single-cartridge and reduced contact surfaces. Kollidon® VA 64 impaired mechanical properties of the filaments for both hydrophilic and poorly-water soluble model compounds, although specific effect (i.e. translated to maximal FDM-processable drug load) depended on API as showed in chapters 3 and 4. Addition of a plasticizer (PEG 4000) was demonstrated to have a positive effect on the dissolution rate and processability. Rapidly dissolving formulations developed for a hydrophilic model compound in Chapter 3 were not sufficient to meet the target dissolution criteria for a poorly water-soluble compound in Chapter 4, and a new formulation approach was applied in Chapter 5 to deliver IR. Combination of xylitol with maltodextrin positively affected processability and/or dissolution for a wide range of formulations.

Chapters 4 and 5 demonstrated a unique opportunity of (re)creating fully amorphous drug solid state from filaments containing crystalline API. FDM 3D-printing, which is a hot-melt process by design, appears to be especially promising for manufacturing of personalized dosage forms containing ASDs of poorly soluble drugs, particularly as the risk of recrystallization during the in-use period (expected to be ~30 days) is significantly lower than that of traditional manufacturing technologies which require a shelf life of typically 2-3 years.

X-ray microcomputed tomography (μCT), used as a non-destructive quantitative characterization tool, allowed initial understanding of structure-dissolution relationship as described in in chapters 4 and 5. An increase in accessible porosity, total surface area, specific surface area by weight and by volume and decrease in relative density appeared to be critical factors for modification of lumefantrine dissolution rate, whereas increase in closed pores volume did not contribute to accelerating dissolution from Eudragit® E PO-based matrix. For HPC/Kollicoat® IR dissolution was overall much slower than for Eudragit® E PO-based tablets, as expected for cellulosic/polyvinyl-alcohol derivatives versus basic methacrylate-derivative. No difference in dissolution rate between tablets with 80% and 100% programmed infill density was observed despite the significant difference in relative density and accessible porosity. Therefore, for the future development of IR FDM-printed dosage forms in addition to the suitable polymeric matrix selection, one could reduce closed pores volume, increase open pores, as well as optimize the balance between shape/size and dissolution. Chapters 4 and 5 show, that actual density for Eudragit® EPO-based formulation was higher than programmed, whereas for HPC- and Kollicoat® IR- lower than the programmed one. This could be because the formulations were printed at similar temperatures, although the polymers used have different melting/Tg temperatures leading to more/less material dispensed as a function of melt viscosity and post-process shrinkage.

As an outlook for the future studies, Direct Powder Printing technology described in Chapter 6 was applied on non-FDM-printable Eudragit EPO-based formulations appearing in Chapter 4. Lumefantrine formulations with 15% and 30% lumefantrine load were showed to be DPP-printable in a standalone feasibility study (Fig.7.1). Hence, DPP demonstrated to be not only independent of mechanical properties of the filament, but also allowed to reduce the number of process steps, as well as expanding the formulation space and improve the portfolio applicability. Moreover, Raman mapping confirmed full amorphous solid dispersion 3-months after manufacturing for both high drug loads. Direct Powder Printing appears to be promising technique for future personalized dosage forms development.

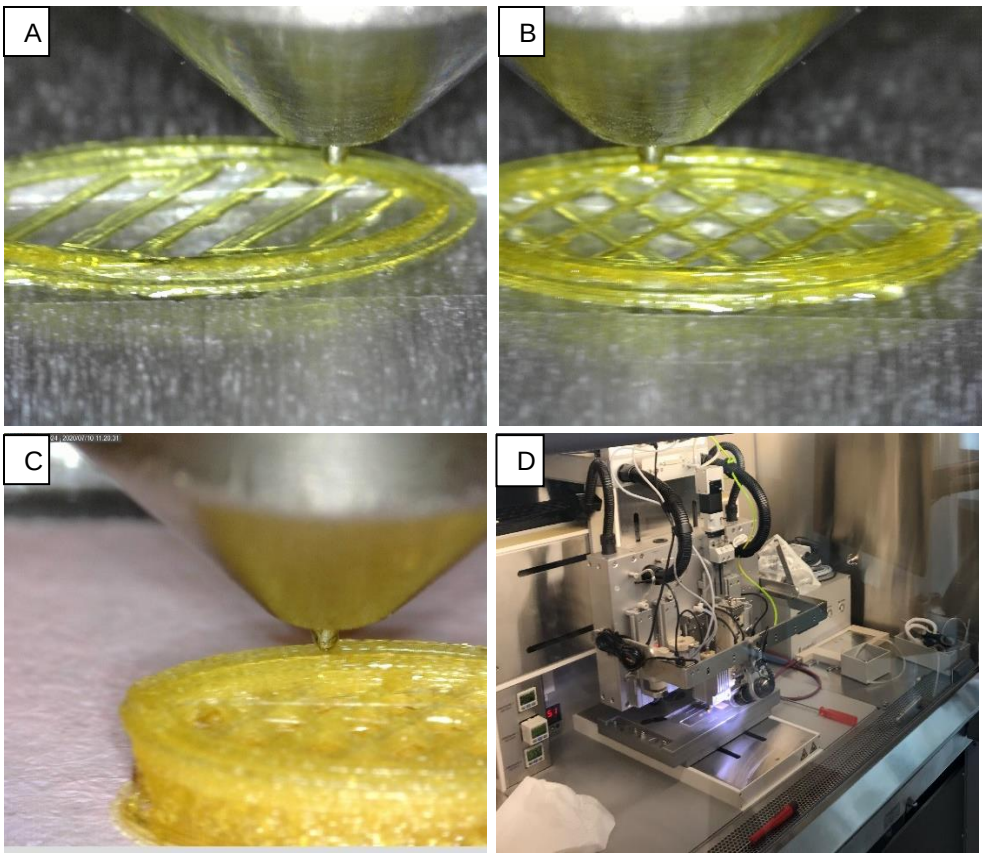

Fig.7.1. Representative example of 15% lumefantrine Direct powder printing with 50% grid infill density (A-C) with RegenHU Bioprinter set up (D)

For the clinical implementation of the technology, Quality Control and real-time-release-testing (RTRT) strategy from filament to finished product is required. For example, content uniformity, microbiological testing, as well as physicochemical compatibility and stability studies, could be examined on the filament. A concept of verification of the process parameter impact on the critical quality attributes (CQAs) would need to be developed such that process monitoring and automated in-process control (IPC) could be applied for real time release. The developed RTRT could be applied for many of the CQAs (i.e. temperature discussed in Chapters 3 and 5; uniformity of content discussed in Chapters 4, 5 and 6; dissolution behaviour), allowing minimal end product testing such as weight and/or optical control. Possibility of "recreating" amorphous solid dispersion in 3D-printed tables shown in Chapters 4 and 5 is promising for improving bioavailability of poorly-soluble drugs, however difference of solid state between the intermediate product and final ODF highlights the need in QbD principles.

The complete healthcare ecosystem should be modified accordingly in order to allow better drug personalization, including sharing of properly cleaned personalized data with regards to medicinal treatments between hospitals/insurance companies and drug manufacturers. This includes the need for a coordinated effort between pharma companies to make the implantation realistic and allow a common regulatory landscape to be developed. GMP-qualified 3D-printers with validated and verified software, including risk management of the algorithms,

should be used. In the future, drugs might be printed based on the approaches developed in this work at the local pharmacies, hospitals or even 3D-printing hubs following personalization of the dose based on the patient's biomarkers, questionnaires or interactive artificial intelligence (AI) interface.

The presented approaches of hydrophilic polymeric matrices combined with designed CAD structures for 3D-printing hold much promise in future personalized pharmaceutical development. Based on the real-world needs for flexible and personalized medicines, this thesis presented the concept of FDM/DPP for pharmaceutical manufacturers and hospital/community pharmacists to broaden their current capabilities in delivering individualized ODFs in a decentralized manner.

8 Bibliography

1. Homayun B, Lin X, Choi HJ, *Challenges and Recent Progress in Oral Drug Delivery Systems for Biopharmaceuticals.* Pharmaceutics, 2019. **11**(3): p. 129.
2. Sastry SV, Nyshadham JR, Fix JA, *Recent technological advances in oral drug delivery—a review.* Pharm Sci Technol Today, 2000. **3**: p. 138-145.
3. Vogenberg F, Isaacson Barash C, Pursel M, *Personalized medicine: part 1: evolution and development into theranostics* P & T, 2010. **35**(10): p. 560–576.
4. NHS, *Improving outcomes through personalized medicine*, in *https://www.england.nhs.uk/wp-content/uploads/2016/09/improving-outcomes-personalised-medicine.pdf.* 2016.
5. Cohen J, *Ways to Minimize Adverse Drug Reactions. Individualized doses and common sense are key.* Postgraduate Medicine, 1999. **106**(3): p. 163-72.
6. Hanning SM, Lopez FL, Wong ICK, Ernest TB, Tuleu C, Orlu Gul M,, *Patient centric formulations for paediatrics and geriatrics: Similarities and differences.* Int J Pharm, 2016. **512**(2): p. 355-359.
7. Topić E, *Pharmacogenomics and Personalized Medicine.* EJIFCC, 2008. **19**(1): p. 31-41.
8. Administration, U.F.a.D. *Table of Pharmacogenomic Biomarkers in Drug Labeling*. 2020 ,cited 17th September 2020.
9. Administration), F.U.F.D. *FY2015 Regulatory Science Research Report: Narrow Therapeutic Index Drugs*. 2017 17th September 2020].
10. Polasek T, Shakib S, Hodjegan AR, *Precision Dosing in Clinical Medicine: present and future.* Expert Review of Clinical Pharmacology, 2018. **11**(8): p. 743-746.
11. Griessmann K, Breitkreutz J, Schubert-Zsilavecz M, Abdel-Tawab M, *Dosing accuracy of measuring devices provided with antibiotic suspensions.* Paediatr Perinat Drug Ther 2007. **8**(61-70).
12. Desai D, Wang J, Wen H, Li X, Timmins P, *Formulation design challenges, and development considerations for fixed Dose combination (FDC) of oral solid dosage forms.* Pharm Dev Technol, 2013. **18**: p. 1265-1276.
13. Liu F, Ranmal S, Batchelor HK, Orlu-Gul M, Ernest TB, Thomas IW, Flanagan T, Tuleu C, *Patient-Centered Pharmaceutical Design to Improve Acceptability of Medicines: Similarities and Differences in Paediatric and Geriatric Populations.* Drugs, 2014. **74**: p. 1871–1889.
14. Goyanes A, Madla CM, Umerji A, Piñeiro GD, Giraldez Montero JM, Lamas Diaz MJ, Gonzalez Barcia M, Taherali F, Sánchez-Pintos P, Couce M, Gaisford S, Basit AW, *Automated therapy preparation of isoleucine formulations using 3D printing for the treatment of MSUD: First single-centre, prospective, crossover study in patients.* International Journal of Pharmaceutics, 2019. **567**(118497).
15. Gibson I, Rosen D, Stucker B, *Additive Manufacturing Technologies: 3D Printing,Rapid Prototyping,and Direct Digital Manufacturing*. 2nd edition ed. 2015, New York: Springer.
16. Alhnan M, Okwuosa, TC, Sadia, Muzna, WK, Ahmed, W, and Arafat, B, *Emergence of 3D Printed Dosage Forms: Opportunities and Challenges.* Pharmaceutical Research, 2016. **33**(8): p. 1817-832.
17. Rahman Z, Barakh Ali AF,Ozkan T, Charoo NA,Reddy IK, Khan MA, *Additive Manufacturing with 3D Printing: Progress from Bench to Bedside.* The AAPS Journal 2018. **20**: p. 101.
18. Fanous M, Gold S, Muller S, Hirsch S, Ogorka J, Imanidis G, *Simplification of fused deposition modeling 3D-printing paradigm: Feasibility of 1-step direct powder printing for immediate release dosage form production.* Int J Pharm, 2020. **578**: p. 119124.
19. Rantanen J, Sandler N, *Printing and Additive Manufacturing.* AAPS PharmSciTech 2019. **20**: p. 261.
20. Okwuosa TC,Stefaniak D, Arafat B, Isreb A, Wan K-W, Alhnan MA, *A Lower Temperature FDM 3D Printing for the Manufacture of Patient-Specific Immediate Release Tablets.* Pharmaceutical Research, 2016. **33**(11): p. 2704-2712.
21. Wei C, Solanki NG, Vasoya JM, Shah AV, Serajuddin ATM, *Development of 3D Printed Tablets by Fused Deposition Modeling Using Polyvinyl Alcohol as Polymeric Matrix for Rapid Drug Release.* Journal of Pharmaceutical Sciences, 2020.
22. Fanous M, Gold S, Hirsch S, Ogorka J, Imanidis G, *Development of Immediate Release (IR) 3D-printed oral dosage forms with focus on industrial relevance.* Eur J Pharm Sci, 2020. **155**: p. 105558.
23. Korte C, Quodbach J, *Formulation development and process analysis of drug-loaded filaments manufactured via hot-melt extrusion for 3D-printing of medicines.* Pharm Dev Technol, 2018. **10**: p. 1117-1127.

24. Solanki, N, Tahsin M, Shah AV, Serajuddin ATM, *Formulation of 3D Printed Tablet for Rapid Drug Release by Fused Deposition Modeling: Screening Polymers for Drug Release, Drug-Polymer Miscibility and Printability*. Journal of Pharmaceutical Sciences, 2018. **107**(1): p. 390-401.
25. Nasereddin JM, Wellner N, Alhijjaj M, Belton P, Qi S, *Development of a Simple Mechanical Screening Method for Predicting the Feedability of a Pharmaceutical FDM 3D Printing Filament.* Pharm Res, 2018. **59**: p. 151.
26. Goyanes A, Buanz ABM, Basit AW, Gaisford S, *Fused-filament 3D printing (3DP) for fabrication of tablets.* International Journal of Pharmaceutics, 2014. **476**(1-2): p. 88-92.
27. Goyanes A, Allahham N, Trenfield SJ, Stoyanov S, Gaisford S, Basit AW, *Direct powder extrusion 3D printing: Fabrication of drug products using a novel single-step process.* International Journal of Pharmaceutics, 2019. **567**(118471).
28. Ong JJ, Awad A, Martorana A, Gaisford S, Stoyanov E, Basit AW, Goyanes A, *3D printed opioid medicines with alcohol-resistant and abuse-deterrent properties.* Int J Pharm, 2020. **579**: p. 119169.
29. European Medicines Agency, *Personalised medicines – focus on patients and healthcare professionals*. 2017.
30. European Medicines Agency, *Personalised medicine*. https://www.ema.europa.eu/en/glossary/personalised-medicine Visited on September 11th, 2020.
31. Breitkreutz J, Boos J, *Paediatric and geriatric drug delivery.* 37-45 2007. **4**(1): p. 37-45
32. Kearns GL, Abdel-Rahman SM, Alander SW, Blowey DL, Leeder JS, Kauffman RE, *Developmental pharmacology-drug disposition, action, and therapy in infants and children.* N Engl J Med, 2003. **349**(12): p. 1157-1167.
33. Williams K, Thomson D, Seto I, Contopoulos-Ioannidis DG, Ioannidis JPA, Curtis S, Constantin E, Batmanabane G, Hartling L, Klassen T, *Standard 6: Age Groups for Pediatric Trials.* Pediatrics, 2012. **129**(Supplement 3): p. S153-S160.
34. Agunod M, Yamaguchi N, Lopez R, Luhby AL, Glass GB, *Correlative study of hydrochloric acid, pepsin, and intrinsic factor secretion in newborns and infants.* Am J Dig Dis 1969. **14**: p. 400-14.
35. Rodbro P, Krasilnikoff PA, Christiansen PM, *Parietal cell secretory function in early childhood.* Scand J Gastroenterol, 1967. **2**: p. 209-13.
36. Munro AW, *Cytochrome P450 1A1 opens up to new substrates.* J Biol Chem, 2018. **293**(50): p. 19211–19212.
37. Takahashi H, Ishikawa S, Nomoto S, Nishigaki Y, Ando F, Kashima T, Kimura S, Kanamori M, Echizen H, *Developmental changes in pharmacokinetics and pharmacodynamics of warfarin enantiomers in Japanese children* Clin Pharmacol Ther, 2000. **68**: p. 541-55.
38. Marshall JD, Kearns GL, *Developmental pharmacodynamics of cyclosporine*. Clin Pharmacol Ther, 1999. **66**: p. 66-75.
39. Drenth-van Maanen AC, Wilting I, Jansen PAF, *Prescribing medicines to older people—How to consider the impact of ageing on human organ and body functions.* Br J Clin Pharmacol, 2019. **10.1111**: p. bcp.14094
40. Wynne HA, Cope LH, Mutch E, Rawlins MD, Woodhouse KW, James OF, *The effect of age upon liver volume and apparent liver blood flow in healthy man.* Hepatology, 1989. **9**: p. 297–301.
41. Mangoni A, Jansen PAF, Jackson S, *Prescribing for elderly patients*. 2009, Wiley-Blackwell.
42. Jansen PA, Brouwers JR, *Clinical pharmacology in old persons.* Scientifica (Cairo), 2012. **2012**: p. 723678.
43. Morgan E, *Impact of infectious and inflammatory disease on cytochrome P450-mediated drug metabolism and pharmacokinetics.* Clin Pharmacol Ther, 2009. **85**: p. 434–438.
44. Cusack B, *Pharmacokinetics in Older Persons.* The American Journal of Geriatric Pharmacotherapy, 2004. **2**(4): p. 274-302.
45. Masters JC, Wiernik PH, *Are we ready to include organ-impaired patients in oncology trials? A clinical pharmacology perspective on recent recommendations.* J Clin Pharmacol, 2018. **58**(6): p. 701.
46. Huss M, Duhan P, Gandhi P, Chen C, Spannhuth C, Kumar V, *Methylphenidate dose optimization for ADHD treatment: review of safety, efficacy, and clinical necessity.* Neuropsychiatric Disease and Treatment, 2017. **13**: p. 1741–1751.
47. Dücker CM, Brockmöller J, *Genomic Variation and Pharmacokinetics in Old Age: A Quantitative Review of Age- vs. Genotype-Related Differences.* Clin Pharmacol Ther, 2019. **105**(3): p. 625-640.

48. Titova N, Chaudhuri KR, *Personalized Medicine in Parkinson's Disease: Time to Be Precise.* Movement Disorders, 2017. **32**(8): p. 1147-1154.
49. Pai M, Bearden DT, *Antimicrobial Dosing Considerations in Obese Adult Patients.* Pharmacotherapy, 2007. **27**(8): p. 1081-1091.
50. Balwani M, Burrow TA, Charrow J, Goker-Alpan O, Kaplan P, Kishnani PS, Mistry P, Ruskin J, Weinreb N, *Recommendations for the use of eliglustat in the treatment of adults with Gaucher disease type 1 in the United States.* Molecular Genetics and Metabolism, 2016. **117**(2): p. 95-103.
51. Wernicke JF, Dunlop SR, Dornseif BE, *Low-dose fluoxetine therapy for depression.* Psychopharmacol Bull, 1988. **24**(1): p. 183-8.
52. Tamargo J, Le Heuzey J, Mabo P, *Narrow therapeutic index drugs: a clinical pharmacological consideration to flecainide.* Eur J Clin Pharmacol, 2015. **71**: p. 549–567.
53. Strickley R, *Pediatric Oral Formulations: An Updated Review of Commercially Available Pediatric Oral Formulations Since 2007.* 108, 2019. **4**: p. 1335-1365.
54. American Academy of Pediatrics, Committee on drugs, *"Inactive" ingredients in pharmaceutical products: Update (subject review).* Pediatrics 1997. **99**: p. 268-278.
55. World Health Organization, *Flexible Solid Oral Dosage: Dispersible formulations of amoxicillin*, in *Revised WHO Classification and Treatment of Pneumonia in Children at Health Facilities: Evidence Summaries*. 2014: Geneva.
56. Wening K, Breitkreutz J, *Oral drug delivery in personalized medicine: unmet needs and novel approaches.* Int J Pharm, 2011. **404**: p. 1-9.
57. Roberts M, Vellucci D, Mostafa S, Miolane C, Marchaud D, *Development and evaluation of sustained-release Compritol® 888 ATO matrix mini-tablets.* Drug Dev Ind Pharm, 2008. **38**(9): p. 1068-1076.
58. Roy P, Shahiwala A, *Multiparticulate formulation approach to pulsatile drug delivery: current perspectives.* J Control Release, 2009. **134**(2): p. 74-80.
59. World Health Organization, *https://www.who.int/selection_medicines/committees/expert/17/application/paediatric/Dosage_form_report DEC2008.pdf.* 2008 25th September 2020].
60. Hanning SM, Muhamed J, Orlu-Gul M, *Investigation into the dosage form attributes of currently UK licensed cardiovascular and Parkinson's disease drug products.* Int J Pharm, 2015. **479**: p. 159-162.
61. British National Formulary, *Joint Formulary Committee*. 66th Edition ed. 2013, London: BMJ Group and Pharmaceutical Press.
62. George J, Majeed W, Mackenzie IS, MacDonald TM, Wei L, *Association between cardiovascular events and sodium-containing effervescent, dispersible, and soluble drugs: nested case-control study.* BMJ, 2013: p. 347.
63. Manrique YJ, Lee DJ, Islam F, Nissen LM, Cichero JAY, Stokes JR, Steadman KJ, *Crushed tablets: does the administration of food vehicles and thickened fluids to aid medication swallowing alter drug release?* J Pharm Pharm Sci, 2014. **17**: p. 207-219.
64. Frattarelli D, Galinkin J, Green T, Johnson T, Neville K, Paul I, Van Den Anker J, *Off-label use of drugs in children.* Pediatrics, 2014. **133**: p. 563-567.
65. Breitkreutz J, *European perspectives on pediatric formulations.* Clin Ther, 2008. **30**: p. 2146-2154.
66. Office, U.S.G.A. *3D Printing:Opportunities, Challenges,and Policy Implications of Additive Manufacturing*. 2015 [cited last retrieved 18h September 2020.
67. Norman J, Madurawe RD, Moore CMV, Khan MA, Khairuzzaman A, *A new chapter in pharmaceutical manufacturing: 3D-printed drug products.* Advanced Drug Delivery Reviews, 2017. **108**: p. 39-50.
68. Sculpteo (a brand of BASF), *The History of 3D Printing: 3D Printing Technologies from the 80s to Today*. 2020 23rd Sept 2020].
69. Ventola CL, *Medical applications for 3D printing: current and projected uses.* Pharmacy and Therapeutics, 2014. **39**: p. 704–11.
70. PA: ASTM International, *ISO/ASTM52900-15: Standard terminology for additive manufacturing—general principles—terminology*, in 2015: West Conshohocken.
71. Jacobs P, *Rapid prototyping and manufacturing: Fundamentals of Stereolithography by Society of Manufacturing Engineers*. 1993, Mcgraw-Hill New York.
72. Fina F, Goyanes A, Gaisford S, Basit AW, *Selective laser sintering (SLS) 3D printing of medicines.* Int J Pharm, 2017. **529**(1-2): p. 285-293.

73. Gaisford S, *8- 3D printed pharmaceutical products*, D. Kalaskar, Editor. 2017: Woodhead Publishing. p. 155-166.
74. Konta AA, García-Piña M, Serrano DR, *Personalised 3D Printed Medicines: Which Techniques and Polymers Are More Successful?* Bioengineering 2017. **4**(79).
75. Algahtani MS, Mohammed AA, Ahmad J, *Extrusion-Based 3D Printing for Pharmaceuticals: Contemporary Research and Applications.* Curr Pharm Des, 2018. **24**(42): p. 4991-5008.
76. Ibrahim M, Otsubo T, Narahara H, Koresawa H, Suzuki H, *Inkjet printing resolution study for multi-material rapid prototyping.* JSME Int. J. Ser. C, 2006. **49**: p. 353-360.
77. Kyobula M, Adedeji A, Alexander MR, Saleh E, Wildman, R, Ashcroft I, Gellert PR, Roberts CJ, *3D inkjet printing of tablets exploiting bespoke complex geometries for controlled and tuneable drug release.* Journal of Controlled Release, 2017. **261**: p. 207-215.
78. Arafat B, Wojsz M, Isreb A, Forbes RT, Isreb M, Ahmed W, Arafat T, Alhnan MA, *Tablet fragmentation without a disintegrant: A novel design approach for accelerating disintegration and drug release from 3D printed cellulosic tablets.* European Journal of Pharmaceutical Sciences, 2018. **11**(2): p. 191-99.
79. Skowyra J, Pietrzak K, Alhnan MA, *Fabrication of Extended-release Patient-tailored Prednisolone Tablets via Fused Deposition Modelling (FDM) 3D Printing.* European Journal of Pharmaceutical Sciences, 2015. **11**(2): p. 11-17.
80. Alomari M, Mohamed FH, Basit AW, Gaisford S, *Personalised dosing: Printing a dose of one's own medicine.* International Journal of Pharmaceutics, 2015. **494**(2): p. 568-577.
81. Khaled SA, Burley JC, Alexander MR, Yang J, Roberts CJ, *3D printing of five-in-one dose combination polypill with defined immediate and sustained release profiles.* Journal of Controlled Release, 2015. **217**: p. 308-314.
82. Goyanes A, Kobayashi M, Martínez-Pacheco R, Gaisford S, Basit AW, *Fused-filament 3D printing of drug products: Microstructure analysis and drug release characteristics of PVA-based caplets.* International Journal of Pharmaceutics, 2016. **514**(1): p. 290-295.
83. Elbadawi M, Muñiz Castro B, Gavins FKH, Jie Ong J, Gaisford S, Pérez G, Basit AW, Cabalar P, Goyanes Á, *M3DISEEN: A Novel Machine Learning Approach for Predicting the 3D Printability of Medicines.* Int J Pharm, 2020: p. 119837.
84. Goyanes A, Buanz AB, Hatton GB, Gaisford S, Basit AW, *3D printing of modified-release aminosalicylate (4-ASA and 5-ASA) tablets.* Eur J Pharm Biopharm, 2014. **89**: p. 157–62.
85. Ilyés K, Kovács NK, Balogh A, Borbás E, Farkas B, Casian T, Marosi G, Tomuță I, Nagy ZK, *The applicability of pharmaceutical polymeric blends for the fused deposition modelling (FDM) 3D technique: Material considerations–printability–process modulation, with consecutive effects on in vitro release, stability and degradation.* European Journal of Pharmaceutical Sciences,, 2019. **129**: p. 110-123.
86. Goyanes A, Chang H, Sedough D, Hatton GB, Wang J, Buanz A, Gaisford S, Basit AW, *Fabrication of controlled-release budesonide tablets via desktop (FDM) 3D printing.* International Journal of Pharmaceutics, 2015. **496**(2): p. 414-420.
87. Marketsandmarkets, *Drug delivery technology market.* https://www.marketsandmarkets.com/ResearchInsight/drug-delivery-technologies-market.asp, 2013.
88. GBIResearch, *Oral drug delivery market report*. 2012: http://www.gbiresearch.com/, last retrieved 07th August 2020.
89. Kollamaram G, CrokerDM, WalkerGM, GoyanesA, Basit AW, Gaisford S, *Low temperature fused deposition modeling (FDM) 3D printing of thermolabile drugs.* International Journal of Pharmaceutics, 2018. **545**(1-2): p. 144-152.
90. Alhnan M, *Solid forms and methods of preparing the same* in *WO 2017/072536 A1*. 2017.
91. Kempin W, Domsta V, Grathoff G, Brecht I, Semmling B, Tillmann S, Weitschies W, Seidlitz A, *Immediate Release 3D-Printed Tablets Produced Via Fused Deposition Modeling of a Thermo-Sensitive Drug.* Pharm Res, 2015. **35**: p. 124.
92. Zema L, Melocchi A, Maroni A, Gazzaniga A, *Three-Dimensional Printing of Medicinal Products and the Challenge of Personalized Therapy.* Journal of Pharmaceutical Sciences, 2017. **106**(7): p. 1697-705.
93. Pietrzak K, Isreb A, Alhnan MA, *A flexible-dose dispenser for immediate and extended release 3D printed tablets.* Eur J Pharm Biopharm, 2015. **96**: p. 380–7.
94. Chiou W, Riegelman S, *Pharmaceutical Applications of Solid Dispersion Systems* J. Pharm. Sci., 1971. **60**: p. 1281–1302.
95. Chiou WL, Riegelman S, *Preparation and dissolution characteristics of several fast-release solid dispersions of griseofulvin.* J. Pharm. Sci, 1969. **58**(12): p. 1505-10.

96. Goldberg A, Gibaldi M, Kanig JL, *Increasing Dissolution Rates and Gastrointestinal Absorption of Drugs via solid Solutions and Eutectic mixtures.* J. Pharm. Sci, 1966. **55**: p. 482-487.
97. Horter D, Dressman JB, *Influence of physicochemical properties on dissolution of drugs in the gastrointestinal tract.* Advanced Drug Delivery Reviews, 2001. **46**: p. 75–87.
98. Chiou WL, Riegelman S, *Preparation and dissolution characteristics of several fast-release solid dispersions of griseofulvin.* J Pharm Sci, 1969.
99. Jaiswar DR, Jha D, Amin PD, *Preparation and characterizations of stable amorphous solid solution of azithromycin by hot melt extrusion.* J Pharm Invest, 2016. **46**: p. 655–668
100. Sandhu H, Shah N, Chokshi H, Malick A, *Overview of Amorphous Solid Dispersion Technologies*, in *Amorphous Solid Dispersions. Advances in Delivery Science and Technology*, S.H. Shah N, Choi D, Chokshi H, Malick A, Editor. 2014, Springer: New York.
101. Zhang J, Han R, Chen W, Zhang W, Li Y, Ji Y, Chen L, Pan H, Yang X, Pan W, Ouyang D, *Analysis of the Literature and Patents on Solid Dispersions from 1980 to 2015.* Molecules., 2018. **23**(7): p. 1697.
102. PharmaCircle Database, *Search: "Marketed oral amorphous solid dispersions"*. 2020 28th September 2020].
103. Repka M, BandariS, KallakuntaVR, Vo AQ, McFall H, Pimparade MB, Bhagurkar AM, *Melt extrusion with poorly soluble drugs – An integrated review.* Int J Pharm, 2018. **535**(1-2): p. 68-85.
104. Verma S, Rudraraju VS, *A Systematic Approach to Design and Prepare Solid Dispersions of Poorly Water-Soluble Drug.* AAPS PharmSciTech, 2014. **15**: p. 641–657.
105. Shah S, Maddineni S, Lu J, Repka MA, *Melt extrusion with poorly soluble drugs.* Int J Pharm, 2013. **453**(1): p. 233-252.
106. Vasconcelos T, Sarmento B, Costa P, *Solid dispersions as strategy to improve oral bioavailability of poor water soluble drugs.* Drug Discovery Today, 2007. **12**: p. 1068–1075.
107. Jain J, Leong FJ, Chen L, Kalluri S, Koradia V, Stein DS, Wolf M-C, Sunkara G, Kota J, *Bioavailability of lumefantrine is significantly enhanced with a novel formulation approach, an outcome from a randomized, open-label pharmacokinetic study in healthy volunteers.* Antimicrob Agents Chemother 2017. **61**: p. e00868-17.
108. Jain J, Leong FJ, Winnips C, Wolf M-C, *Therapeutic regimen*, in *Patent Application* 20180303837, Editor. 2018.
109. Gupta P, Chawla G, Bansal AK, *Physical stability and solubility advantage from amorphous celecoxib: the role of thermodynamic quantities and molecular mobility.* Mol Pharm, 2004. **1**: p. 406–413.
110. Hancock B, Shamblin SL, *Molecular mobility of amorphous pharmaceuticals determined using differential scanning calorimetry.* Thermochim Acta, 2001. **380**: p. 95–107.
111. Hancock B, Parks M, *What is the true solubility advantage for amorphous pharmaceuticals?* Pharm Res, 2000. **17**: p. 397–404.
112. Muzna S, Sośnicka A, Arafat B, Isreb A, Ahmed W, Kelarakis A, Alhnan MA, *Adaptation of Pharmaceutical Excipients to FDM 3D Printing for the Fabrication of Patient-tailored Immediate Release Tablets.* International Journal of Pharmaceutics, 2016. **513**: p. 659-68.
113. Govender R, Abrahmsén-Alami S, Folestad S, Larsson A, *High Content Solid Dispersions for Dose Window Extension: A Basis for Design Flexibility in Fused Deposition Modelling.* Pharm Res 2020. **37**(9).
114. Maniruzzaman M, Boateng JS, Snowden MJ, Douroumis D, *A review of hot-melt extrusion: process technology to pharmaceutical products.* ISRN Pharm, 2012. **2012**(2): p. 436763–9.
115. Iyer RM, Hegde S, DiNunzio J, Singhal D, Malick W, *The impact of roller compaction and tablet compression on physicomechanical properties of pharmaceutical excipients.* Pharm Dev Technol, 2014. **19**(5): p. 583–92.
116. Sigma-Aldrich, Inc. *3D-printing filaments: PVA filaments*. 2020 29th September 2020].
117. Evonik Industries, A. *Evonik launches RESOMER® Filaments for the 3D printing of bioresorbable medical implants*. 2020 29th September 2020].
118. Okwuosa, T.C., et al., *A Lower Temperature FDM 3D Printing for the Manufacture of Patient-Specific Immediate Release Tablets.* Pharmaceutical Research, 2016. **33**(11): p. 2704-2712.
119. Kadry H, Al-Hilal TA, Keshavarz A, Alam F, Xu C, Joy A, Ahsan F, *Multi-purposable filaments of HPMC for 3D printing of medications with tailored drug release and timed-absorption.* International Journal of Pharmaceutics, 2018. **544**(1): p. 285-296.
120. Robnik B, Naumoska K, Casar Z, *Thermal oxidation of poly(ethylene oxide–propylene oxide–ethylene oxide) triblock copolymer: Focus on low molecular weight degradation products.* Polym. Degrad. Stab, 2002. **77**(55–66).

121. Robnik B, Naumoska K, Casar Z, *A Novel Testing Approach for Oxidative Degradation Dependent Incompatibility of Amine Moiety Containing Drugs with PEGs in Solid-State.* Macromol. Chem. Phys, 2020. **202**: p. 2273–2280.
122. Vertzoni M, Augustijns P, Grimm M, Koziolek M, Lemmens G, Parrott N, Pentafragka C, Reppas C, Rubbens J, Van Den Abeele J, Vanuytsel T, Weitschies W, Wilson CG, *Impact of regional differences along the gastrointestinal tract of healthy adults on oral drug absorption: An UNGAP review*,. European Journal of Pharmaceutical Sciences, 2019. **134**: p. 153-175.
123. CDER, *Dissolution Testing of Immediate Release Solid Oral Dosage Forms Guidance for Industry*, F.a.D.A. U.S. Department of Health and Human Services, Editor. 1997: U.S. Government Printing Office: Washington, DC.
124. Younes M, Aggett P, Aguilar F, Crebelli R, Dusemund B, Filipic M, Frutos MJ, Galtier P, Gundert-Remy U,Kuhnle GG, Lambre C, Leblanc J-C, Lillegaard IT, Moldeus P, Mortensen A, Oskarsson A, Stankovic I,Waalkens-Berendsen I, Woutersen RA, Wright M, Herman L, Tobback P, Pizzo F, Smeraldi C, Tard A,Papaioannou A, Gott D, *Safety of low-substituted hydroxypropyl cellulose (L-HPC) to be used as a food additive in food supplements in tablet form.* EFSA Journal, 2018. **16**(1): p. 5062.
125. Puri, V., Brancazio,D, Desai,PM, Jensen,KD, Chun,JH, Myerson,AS, and Trout,BL, *Development of Maltodextrin-Based Immediate-Release Tablets Using an Integrated Twin-Screw Hot-Melt Extrusion and Injection-Molding Continuous Manufacturing Process.* Journal of Pharmaceutical Sciences, 2017. **106**(11): p. 3328-3336.
126. Sadia M, Sośnicka A, Arafat B, Isreb A, Ahmed W, Kelarakis A, Alhnan MA, *Adaptation of pharmaceutical excipients to FDM 3D printing for the fabrication of patient-tailored immediate release tablets.* Int J Pharm, 2016. **513**(1-2): p. 659-668.
127. Mazel V, Delplace C, Busignies V, Faivre V, Tchoreloff P, Yagoubi N, *Polymorphic transformation of anhydrous caffeine under compression and grinding: a re-evaluation.* Drug Development and Industrial Pharmacy 2011. **37**(7): p. 832-40.
128. Sigma-Aldrich Inc, *Caffeine anhydrous product information.* 1999: p. https://www.sigmaaldrich.com/content/dam/sigma-aldrich/docs/Sigma-Aldrich/Product_Information_Sheet/c0750pis.pdf.
129. Korte C, Quodbach J, *3D-Printed Network Structures as Controlled-Release Drug Delivery Systems: Dose Adjustment, API Release Analysis and Prediction.* AAPS PharmSciTech, 2018. **19**: p. 3333.
130. Fernández-Hervás M, Vela MT, Arias MJ, Rabasco AM, *Modeling and comparison of dissolution profiles.* European Journal of Pharmaceutical Sciences, 2001. **13**(2): p. 123-133.
131. F Fernández-Hervás M, Vela MT, Arias MJ, Rabasco AM, *Percolation theory: Evaluation and interest of percolation thresholds determination in inert matrix tablets.* Pharmaceutica Acta Helvetiae, 1996. **71**(4): p. 259-264.
132. Roots Analysis, *HPAPIs and Cytotoxic Drugs Manufacturing Market, (2nd Edition)*. 2016.
133. Pandit S, Kundu S, *Optical and structural behaviors of crosslinked polyvinyl alcohol thin films.* AIP Conference Proceedings, 2018. **1942**(1): p. 080029.
134. Lang B, McGinity JW, Williams RO, III, *Hot-melt extrusion – basic principles and pharmaceutical applications.* Drug Development and Industrial Pharmacy, 2014. **40**(9): p. 1133-1155.
135. Trenfield S, Awad A, Goyanes A, Gaisford S, Basit AW, *3D Printing Pharmaceuticals: Drug Development to Frontline Care.* Trends in Pharmacological Sciences, 2018. **39**(5): p. 440-451.
136. Thakkar R, Pillai AR, Zhang J, Zhang Y, Kulkarni V, Maniruzzaman M, *Novel On-Demand 3-Dimensional (3-D) Printed Tablets Using Fill Density as an Effective Release-Controlling Tool.* Polymers (Basel), 2020. **12**(9): p. 1872.
137. Newman A, Knipp G, Zografi G, *Assessing the performance of amorphous solid dispersions.* J Pharm Sci, 2012. **101**: p. 1355–1377.
138. Fanous M, Malak B, Gold S, Sobczuk A, Hirsch S, Ogorka J, Imanidis G, *Development of Immediate Release 3D-Printed Dosage Forms for Poorly Water-Soluble Drugs by Fused Deposition Modeling: Study of Morphology, Solid State and Dissolution* Int J Pharm, 2021, *submitted*.
139. Karl M, Nalawade S, Maschke A, Djuric D, Kolter K, *Suitability of pure and plasticized polymers for hot melt extrusion*, in *The 37th Annual Meeting and Exposition of the Controlled Release Society*. 2010: Portland, Oregon,USA.
140. US Pharmacopoeial Convention, *The USP 26-National Formulary* 2003, 21 Rockville MD

141. Hall Z, Allan EL, van Schalkwyk DA, van Wyk A, Kaur H, Am J Trop Med Hyg. 2016;94(5):993-1001. doi:10.4269/ajtmh.15-0665, *Degradation of Artemisinin-Based Combination Therapies Under Tropical Conditions.* Am J Trop Med Hyg, 2016. **94**(5): p. 993-1001.
142. Marques MBF, Araujo BCR, Fernandes C,Yoshida MI, Mussel WN, and Sebastião RCO, *Kinetics of Lumefantrine Thermal Decomposition Employing Isoconversional Models and Artificial Neural Network.* J Braz Chem Soc, 2020. **31**(3): p. 512-522.
143. Abu-Diak O, Jones DS, Andrews GP, *An investigation into the dissolution properties of celecoxib melt extrudates: understanding the role of polymer type and concentration in stabilizing supersaturated drug concentrations.* Mol Pharm, 2011. **8**: p. 1362–71.
144. Albers J, Alles R, Matthée K, Knop K, Nahrup JS, Kleinebudde P, *Mechanism of drug release from polymethacrylate-based extrudates and milled strands prepared by hot-melt extrusion.* Eur J Pharm Biopharm, 2009. **71**: p. 387–94.
145. Nakamichi K, Nakano T, Yasuura H, Izumi S, Kawashima Y, *The role of the kneading paddle and the effects of screw revolution speed and water content on the preparation of solid dispersions using a twin-screw extruder.* Int J Pharm, 2002. **241**: p. 203–11.
146. Song Y, Wang L, Yang P, Wenslow RM Jr, Tan B, Zhang H, Deng Z, *Physicochemical characterization of felodipine–kollidon VA64 amorphous solid dispersions prepared by hot-melt extrusion.* J Pharm Sci, 2013. **102**: p. 1915–23.
147. Kyobula M, Adedeji A, Alexander MR, Saleh E, Wildman R, Ashcroft I, Gellert PR, Roberts CJ, *3D inkjet printing of tablets exploiting bespoke complex geometries for controlled and tuneable drug release.* J Control Release, 2017. **261**: p. 207-215.
148. Azad MA, Olawuni D, Kimbell G, Badruddoza AZM, Hossain MS and Sultana T, *Polymers for Extrusion-Based 3D Printing of Pharmaceuticals: A Holistic Materials-Process Perspective.* Pharmaceutics, 2020. **12**(2): p. E124.
149. Curti C, Kirby DJ, Russell CA, *Current formulation approaches in design and development of solid oral dosage forms through three-dimensional printing.* Prog Addit Manuf 2020. **5**: p. 111-123.
150. Lobenberg R, Amidon GL, *Modern bioavailability, bioequivalence and biopharmaceutics classification system. New scientific approaches to international regulatory standards.* European Journal of Pharmaceutics and Biopharmaceutics, 2000. **50**: p. 3-12.
151. Kawabata Y, Wada K, Nakatani M, Yamada S, Onoue S, *Formulation design for poorly water-soluble drugs based on biopharmaceutics classification system: Basic approaches.* Int J Pharm, 2011. **420**(1): p. 1-10.
152. Boyd B, Bergström CAS, Vinarov Z, Kuentz M, Brouwers J, Augustijns P, Brandl M, Bernkop-Schnürch A, Shrestha N, Préat V, Müllertz A, Bauer-Brandl A, Jannin V, *Successful oral delivery of poorly water-soluble drugs both depends on the intraluminal behavior of drugs and of appropriate advanced drug delivery systems.* European Journal of Pharmaceutical Sciences, 2019. **137**: p. 104967.
153. Huang LF, Tong, WQ, *Impact of solid state properties on developability assessment of drug candidates.* Advanced Drug Delivery Reviews, 2004. **56**: p. 321–334.
154. Goyanes A, Martinez PR, Buanz A, Basit AW, Gaisford S, *Effect of geometry on drug release from 3D printed tablets.* International Journal of Pharmaceutics, 2015. **494**(2): p. 657-663.
155. Meier C, Nollenberger N, Gryczke A, Petereit H-U, Dressman J, *Pharmaceutical compositions containing mixtures of polymers and active agents poorly soluble in water* 2008, Evonik Roehm GmbH.
156. Song Y, Zemlyanov D, Chen X, Su Z, Nie H, Lubach JW, Smith D, Byrn S, Pinal R, *Acid-base interactions in amorphous solid dispersions of lumefantrine prepared by spray-drying and hot-melt extrusion using X-ray photoelectron spectroscopy.* International Journal of Pharmaceutics, 2016. **514**: p. 456-464.
157. Kapur N, Sahoo PK, Wong AKC, *A new method for gray-level picture thresholding using the entropy of the histogram.* Computer vision, graphics, and image processing, 1985. **29**(3): p. 273–285.
158. Ollion J, Cochennec J, Loll F, Escudé C, Boudier T, *TANGO: A Generic Tool for High-throughput 3D Image Analysis for Studying Nuclear Organization.* Bioinformatics, 2013. **29**(14): p. 1840-1.
159. Lorensen W, Cline HE, *Marching cubes: A high resolution 3D surface construction algorithm.* ACM SIGGRAPH Computer Graphics, 1987. **21**(4): p. 163–169.
160. Marieb EN, Hoehn K, *Human anatomy & physiology*. 2010, San Francisco:: Benjamin Cummings

161. Desai D, Sandhu H, Shah N, Malick W, Zia H, Phuapradit W, Vaka SRK, *Selection of Solid-State Plasticizers as Processing Aids for Hot-Melt Extrusion.* Journal of Pharmaceutical Sciences, 2018. **107**(1): p. 372 - 379.

List of abbreviations

ADHD	Attention deficit hyperactivity disorder
AI	Artificial Intelligence
API	Active pharmaceutical ingredient
ASD	Amorphous solid dispersion
BCS	Biopharmaceutics classification system
CAD	Computer-aided design
CYP	Cytochrome P450
DCP	Dibasic calcium phosphate
DDI	Drug-drug interactions
DPD	Dihydropyrimidine dehydrogenase
DPP	Direct Powder Printing
DSC	Differential scanning calorimetry
EXT	Extrusion
GMP	Good manufacturing practice
HPC	Hydroxypropylcellulose
HPMC	Hydroxypropyl methylcellulose
HPMCAS	Hydroxypropyl methylcellulose acetate succinate
FDA	Food and Drug Administration
FDM	Fused deposition modeling
HPLC	High performance liquid chromatography
HME	Hot-melt extrusion
HSM	Hot stage microscopy
IR	Immediate release
NAT	N-Acetyltransferase
NTI	Narrow therapeutic index
OAT	Organo-Anion-Transporter
OCT	Organic cation transporter
OTC	Over-the-counter
QbD	Quality by design
PD	Pharmacodynamics
PEG	Polyethylene glycol
PEO	Polyethylene oxide
PG	Pharmacogenomics
PK	Pharmacokinetics
SHS	Selective heat sintering
SLA	Stereolithography
SLS	Selective laser sintering
TPMT	Thiopurin-Methyltransferase
UGT	Uridine diphosphoglucuronosyltransferase
USP	United States Pharmacopeia
UV	Ultraviolet
XRPD	X-ray powder diffraction

List of figures

List of symbols

2D	Two-dimensional
3D	Three-dimensional
α	Relative crystallinity
k	Rate constant
Tg	Glass transition temperature
Tm	Melting temperature

List of tables

Marina Fanous (Gurina)

curriculum vitae

PROFESSIONAL EXPERIENCE

Since 02.2021	Senior Global Trial Manager, Global Drug Development, Novartis Pharma AG
02.2018 – 01.2021	Doctoral Candidate, Global Drug Development, Novartis Pharma AG
10.2020– 01.2021	Temporary job shadowing as Trial Operations Manager, Trial Management (TM), GDO
03.2017 – 01.2018	Principal Scientist (Contract), Global Drug Development, Novartis Pharma AG
08.2015 – 02.2017	Relocated to Basel, attended German A1-B2 TELC Certified language courses
09.2012 – 07.2015	Pharmacist (from 03.2014) and Pharmacy Assistant (09.2012– 02.2014), Super-Pharm Ltd, Israel
04.2013 – 10.2013	Hospital and Clinical Trials Pharmacist-Intern, Assaf aRofe Medical Center, Israel
11.2010 – 03.2011	Medicinal Chemistry Lab Technician (project), HUJI, Israel
09.2009 – 10.2010	First Aid Instructor, HomeAid, Israel
04.2007 – 04.2009	Military Medic (04-09.2007) and Clinic Manager (10.2007-04.2009), Home Front Command, Israeli Defense Forces, Gaza Strip Area, Israel

EDUCATION

2018 - 2021	PhD (Doctor) in Pharmaceutical Sciences Faculty of Science, University of Basel, Switzerland
2013 – 2015	MSc in Pharmaceutical Sciences Institute of Drug Research, The Hebrew University of Jerusalem (HUJI), Israel
2009 – 2013	BSc in Pharmacy, Medicinal Sciences Excellence Program, School of Pharmacy, The Hebrew University of Jerusalem, Israel
2003 – 2006	High School Diploma, Mevoot aNegev Experimental High School, Israel

SELECTED VOLUNTEERING EXPERIENCE

2010 – 2015	Team Lead, Ach Gadol (Big Brother) non-profit organization, Israel
2009 – 2014	Students Representative and Coordinator, Medicinal Sciences Excellence program, HUJI, Israel

SELECTED PUBLICATIONS

M. Fanous, M. Bitar, S. Gold, A. Sobczuk, S. Hirsch, J. Ogorka, G. Imanidis. Development of Immediate Release 3D-Printed Dosage Forms for Poorly Water-Soluble Drugs by Fused Deposition Modeling: Study of Morphology, Solid State and Dissolution. Int J Pharm, 2021, 120417.

M. Fanous, S. Gold, S. Hirsch, J. Ogorka, G. Imanidis. Development of immediate release (IR) 3D-printed oral dosage forms with focus on industrial relevance. Eur J Pharm Sci, 2020, (155), 105558

M. Fanous, S. Gold, S. Muller, S. Hirsch, J. Ogorka, G. Imanidis. Simplification of fused deposition modeling 3D-printing paradigm: Feasibility of 1-step direct powder printing for immediate release dosage form production. Int J Pharm, 2020, (578) 119124

P. Wessels, H. Tiemessen, P. De Marco, M. Larabi, C. Schiedel, **M. Gurina**. Liposomal formulation for use in the treatment of cancer. Patent WO2018078064A1, filed 27-10-2017, first grant 02-05-2018

LANGUAGES

English (fluent), Hebrew (fluent), Russian (mother tongue), German (business proficiency-B2 TELC), Arabic(basic), Italian(basic)